4-24-2015

Electrochemical Based Detection of Cancer Biomarker Proteins using Multi-labeled Magnetic Particles in Microfluidic Systems

Colleen Ellen Krause
University of Connecticut - Storrs, colleen.krause@uconn.edu

Electrochemical Based Detection of Cancer Biomarker Proteins using Multi-labeled Magnetic Particles in Microfluidic Systems

Colleen Ellen Krause, Ph.D.

University of Connecticut, 2015

Time is measured as a moment, hour, day or year as indicated by a clock or calendar. To someone facing cancer it seems to count backwards from a date determined by an incurable disease. Even with the advances in research and technology cancer is still a leading cause of death in the United States as no cure exists. Biomedical research is constantly struggling with cancer detection, diagnosis, treatment, and prevention. Currently, cancer detection is expensive, diagnoses are sometimes erroneous, treatment is invasive, and prevention is a challenge.

The primary goal of the cancer detection is to develop simple non-invasive tests that indicate cancer risk, allow early cancer detection, classify tumors so that the patient can receive the most appropriate therapy and monitor disease progression, regression and recurrence. Currently cancer is often diagnosed though imaging technologies or through invasive procedures often after the cancer has formed a sizable tumor, or already metastasized. Methods that rely on measurements of alterations or abnormalities in certain protein concentrations are promising alternatives for diagnosis and improving patient care. Since significant interpersonal variation of single protein expression levels are often observed in patients within a given disease, simultaneous measurement of a collection of

protein biomarkers may help to lead to more accurate and early diagnosis and offer more insights to the disease state and characteristics, thereby potentially improving patient care.

The objectives of this thesis are to develop protein sensors that are inexpensive, sensitive, rapid, use minimal sample volume, have multiplex capabilities, and are technically simple to use for applications with real cancer patient samples in a point-of-care setting. Such methods may make cancer diagnoses possible without locating the tumor, or even before a tumor has formed.

Electrochemical Based Detection of Cancer Biomarker Proteins using Multi-labeled Magnetic Particles in Microfluidic Systems

Colleen Ellen Krause

B.S. Chemistry, Salve Regina University, 2009

A Dissertation

Submitted in Partial Fulfillment of the

Requirements for the Degree of

Doctoral of Philosophy

At the

University of Connecticut

2015

APPROVAL PAGE

Doctor of Philosophy Dissertation

Electrochemical Based Detection of Cancer Biomarker Proteins using Multi-labeled Magnetic Particles in Microfluidic Systems

Presented by

Colleen Ellen Krause, B.S.

Major Advisor _____

James F. Rusling

Associate Advisor _____

Mark W. Peczuh

Associate Advisor _____

Bernard S. Munge

University of Connecticut

2015

Dedicated to

My Parents

Loreen and Michael Krause

2015

Acknowledgements

I have been very blessed throughout my academic career to have several mentors, teachers, and friends, as well as an amazingly supportive family. I am dedicating my thesis to my parents Loreen and Michael Krause who gave me strength, support, and encouragement to pursue my dreams. To my Dad, I think about you everyday you were taken from me far too early.

I would like to thank my major research advisor and mentor Prof. James Rusling for teaching me the importance of collaboration as well as how to conduct research independently. In addition, I would like to thank my second advisor Prof. Bernard Munge who taught me what research is all about. To you both, thank you for your constant guidance and support in the many projects we have undertaken. Thank you Prof. Mark Peczuh for your continual guidance and support throughout my academic career here at the University of Connecticut. A special thanks to Dr. Susan Meschwitz and Dr. Edward Neth for teaching me how to become an excellent instructor you both have been and continue to be excellent mentors.

I would also like to thank colleges /peers who became friends. To my partner in crime Brunah Otieno, thank you we have been though a lot together. Thank you Dana, and Dhanuka together we came in and have faced this journey along side each other. Thank you Gary, Linlin, Sadagopan, Yun, and Naimish for my introduction into the Rusling research lab. Thank you Gayatri, Chi, Amit, Mohamed, Spundana, Abhay, Di, Snehasis, Abby, Boya, Jen, Karteek, Islam, Mohammed, and Greg for your dedication to research as

well as for your assistance and support in and out of the laboratory. Thank you to my undergraduate research partners and friends Lines, Lindsay, Dave.

I would like to give a big thanks to my collaborators. Thank you Prof. Ronaldo Faria, and Dr. Alina Latus for the projects that we have undertaken and the special friendships we formed. Thank you Dónal Leech and the Leech research group members especially Peter Ó Conghaile, and Conan Mercer at the National University of Ireland, Galway. I had an amazing time that I will never forget. Thank you Douglas Peterson and group from the University of Connecticut Health Center for work on the oral mucositis project.

My thanks also goes out to Emilie, Charlene, Adam and all other staff in the chemistry department for assisting with all things administrative, orders, and teaching labs.

Many thanks to my awesome friends and amazing family. Thanks to both the Ackley's and Krause's who have surrounded me with love and support. I was very blessed to have amazing grandparents early in life who helped me become the person I am today. Thank you to my brothers Matt and Dan who put up with me. Thank you to my friends Christa, Matt, Allison, Caitlin, Amanda, Jaci, Ellen, Justin, and Christian we have had some good times together and will continue to do so. To Christopher you make me so happy and I am so lucky that I have you in my life.

Table of Contents

List of Schemes

List of Figures

List of Tables

Chapter One

Introduction

1.1 Goals and Significance

In 1971, US President Nixon declared a war on cancer.[1] This was an effort to raise public awareness of the devastating disease that posed/poses a serious threat on the human race.[2] Since the declaration over 40 years ago we have discovered that cancer can manifest in hundreds of types and subtypes, affecting almost all organs and tissues.[2,3] We have also learned that cancer cells are extremely complex.[2,3] Cancer cells are derived from instrumental mutations and rearrangements of the human genome.[2,3,4,5] These transformations cause cells to promote the extensive growth of cancer through genetic and epigenetic reprogramming of regulatory circuits, which corrupt normal cells to become proliferating cancer cells. [2,3,4,5] However, despite all the progress that has been made in understanding the nature of cancer the question remains are we winning this war? According to the World Oncology Forum that met in late 2012 the answer is No.[2]

Cancer remains a leading cause of death in the United States and through out the world. It is second only to heart disease.[6] More than 1.6 million people are diagnosed with cancer each year, and this year alone over 585,000 Americans will die because of cancer, corresponding to 1,600 deaths per day.[6] It is evident that as diagnoses are delayed, the survival rate decreases significantly. The 5-year relative survival rates among patients who are diagnosed with either advanced lung, colorectal, or breast cancer are only 3%, 10%, and 27%.[6] However, survival rates among patients diagnosed with

localized lung, colorectal, or breast cancers are significantly higher at 50%, 90%, and 98%.[6] In light of these statistics, diagnosing cancer at an early stage before they metastasize and become incurable will have a significant impact on cancer survival.

Current methods of cancer detection are often based on imaging technology such as magnetic resonance imaging (MRI), positron emission tomography (PET), and computed tomography (CT), which use contrast materials that can distinguish between different anatomical features.[7,8,9,10,11] However, each of these are limited to imaging giving no quantification of cancer and limited information of the onset of cancer. Furthermore these imaging techniques may be unavailable in limited resource settings.[7,8,9,10,11] Other techniques are based on cell morphology and microscopy which involve invasive biopsies to observe cancerous cells in tissue samples.[12,13] These tests are not individually conclusive as tissue removal can often miss cancerous cells especially at early onset of the disease.[12,13] Alternatively, patients may be screened for cancer without undergoing any invasive procedure by assaying bodily fluids to test for levels of cancer biomarker proteins.[14, 15]

In general biomarkers are chemical, physical, or biological parameters that can be used to indicate a biological or disease state.[16] They can be used to develop target therapies, predict risk, help in early screening, forecast how well a patient will respond to treatment, and monitor disease progression.[16] Specifically, a tumor marker is any molecule produced by a tumor or by a host in response to a cancer cell that can be objectively measured as an indicator of a cancerous process.[16,17] These biomarkers can be grouped into a multitude of categories including proteins, glycoproteins, oncofetal antigens, horomones, receptors, genetic markers and RNA molecules. [16,17]

Overall, most biomarker studies are aimed at understanding the pathobiology of the disease.[18,19] In the case of cancer we know that as normal cells evolve to cancer cells they acquire a succession of hallmark capabilities that enable them to become tumorigenic and ultimately malignant.[4,5,18] These "Hallmarks of Cancer" as described by Hanahan and Weinberg include sustaining proliferative signaling, genome instability and mutation, insensitivity to growth inhibitory (antigrowth) signals, avoiding immune destruction, limitless replicative potential, tumor promoting inflammation, sustained angiogenesis, evasion of programmed cell death, deregulating cellular energies, and tissue invasion and metastasis.[4,5] These capabilities are shared in most if not all types of human tumors and are a result of genetic alterations that include gene rearrangements, point mutations, and gene amplifications.[2,4,5,19] However, it is evident that the functional endpoint of these genetic alterations lies at the protein level.[20,21] Genetic mutations can modify protein signaling pathways and various protein interactions that make up the circuitry within the cell (Figure 1.1).[20,21] Therefore, it is clear that mining of biological samples at the protein level will provide useful protein candidates that can serve as markers for disease states. [20]

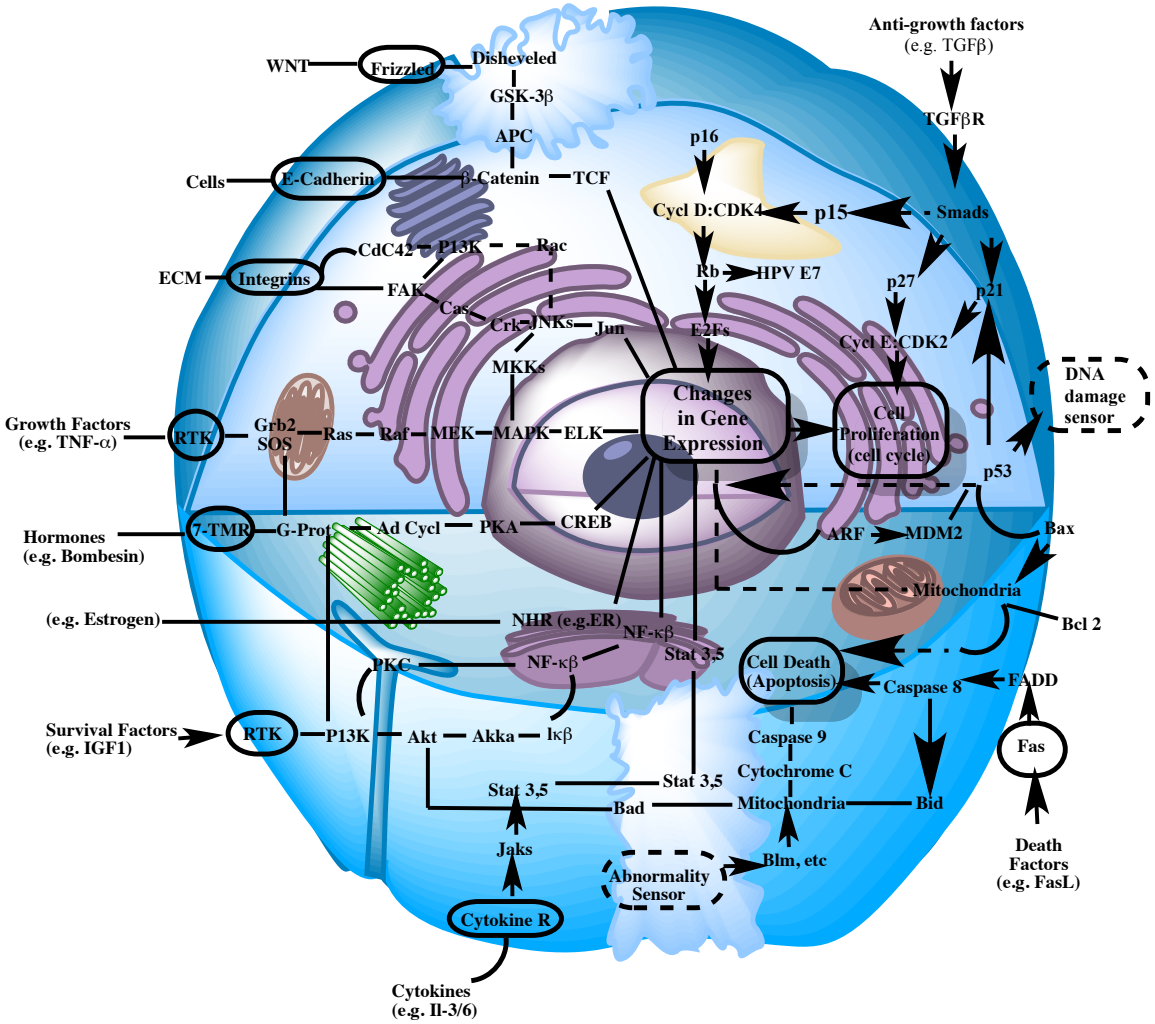

Figure 1.1 Protein Circuit of the Cell. Adapted from reference (4).

Advancements in the field of proteomics have lead to the detection of hundreds to thousands of protein cancer biomarkers through the use of both 2-D gel electrophoresis and mass spectrometry.[17,20,22] However, despite the tremendous efforts that have been made there are less than two dozen cancer proteomic biomarkers approved by the FDA in

the United States for clinical use.[17,23] Furthermore, these biomarkers have significant limitations. Many biomarkers can be indicative of more than one disease such as serum PSA which is elevated in conditions such as benign prostatic hypertrophy, prostatitis, or even with excess levels of testosterone.[19,24] Therefore, efforts have been focused on development of panels of biomarker proteins that are specific to the disease.[14,19,22,24,25,26] Assaying panels of these specific protein biomarkers would further minimize false positives and negatives predicted values. In addition, measurement of multiple protein biomarkers holds enormous potential in simplifying disease diagnosis and guiding personalized patient care strategies.[19,26]

Once protein biomarkers are identified, the next step is to develop an assay with suitable for point-of-care diagnosis.[17,19] In order for these assays to be effectively used in a clinical setting they must be inexpensive, multiplexed, require minimal sample volume, reduced turnaround times (shorter assay times), require little to no expertise to operate, and exhibit a wide dynamic range in complex media, such as serum.[17,19,27] Therefore, the goal of this dissertation is to address the aforementioned difficulties in production of a POC sensor. In order to achieve these objectives efforts will be focused on development of ultrasensitive multiplexed electrochemical immunoassay systems that combine nanostructured sensor electrodes and massively multi-labeled detection microparticles into simple modular microfluidic devices.

1.2 Point of Care Protein Detection Systems

The capability to measure the levels of individual proteins in cells tissues, extracts and biological fluids has been a long-standing and critical component in the progress of

both life science research and clinical practice.[28] Currently, most cancer biomarker protein testing for clinical diagnoistics takes place in dedicated centralized laboratories using large, automated analyzers.[27,29] This requires samples to be transported to a testing site, thereby increasing on wait times, increased administration as well as medical cost.[27,29] Development of point of care devices are hoping to change these facts by providing rapid and reliable quantitative results anytime and anywhere, for example in clinics and hospital emergency departments.[27,29] However, in order for a device to be used in the clinical setting current biological testing systems must be reduced to the size of a handheld devices that require only minimal amounts of sample and reagents, while maintaining a multi-analyte, high-throughput, specific and sensitive assay.[27,29]

There are numerous assay formats that exist to measure proteins in solutions (enzyme-linked immunosorbent assays, ELISAs, on cell surfaces (flow cytometry), within cells (immunohistochemical and immunoflorescent microscopy), and within organs (invivo imaging with labeled antibodies).[28] However, for nearly forty years ELISAs, have served as the workhorse for protein detection.[30] Today they are still the most widely used clinical protein detection systems, and have been labeled as the gold standard for single-protein measurement. ELISAs employ the use of a sandwich immunoassay.[19,31,28] In this format, a primary antibody (Ab_1), which is specific to its antigen (target protein), is attached to the bottom of a well plate. After antigen is bound to these antibodies, a second enzyme labeled detection antibody (Ab_2) attaches which provides both a detection and amplification. Once detection antibodies are in place a substrate chemical is applied which is converted by the enzyme label, causing a change in color of solution, which produces a visible signal that are typically read by a

chromogenic reporter (Scheme 1.1).[30] ELISA's are commercially available, have low detection limits in pgmL^{-1} range, and are highly specific for their targeted protein.[19,31,28] However, ELISAs are timely, labor intensive, and require large sample volumes. Additionally, ELISA lack high sensitivity needed to detect multiple biomarkers.

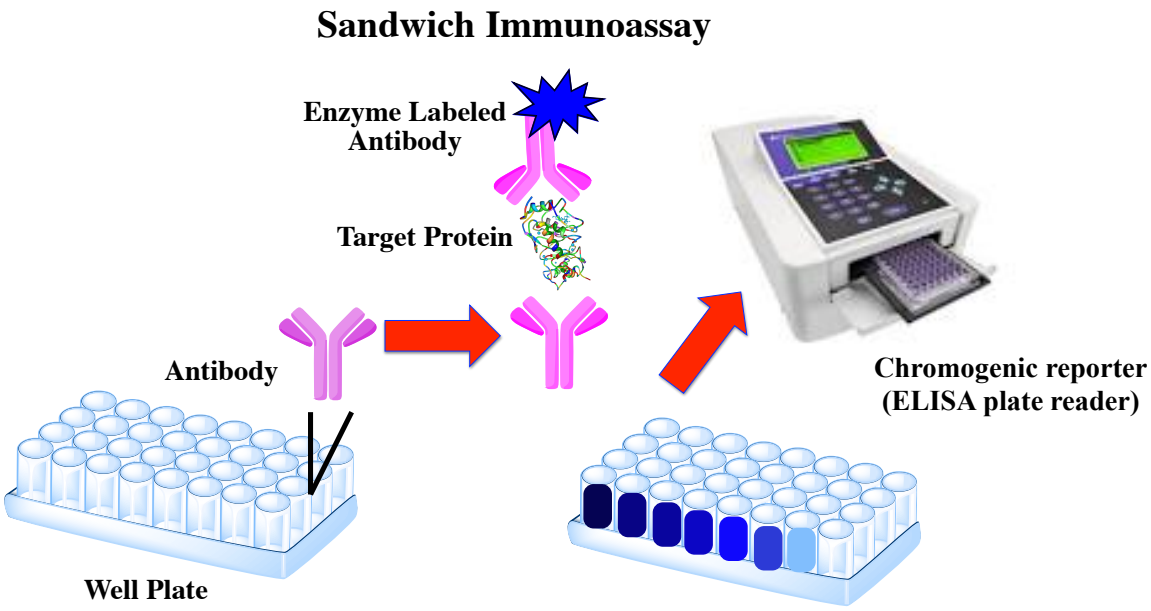

Scheme 1.1 Full sandwich immunoassay protocol for ELISA based assays.

Advancements in the field of mass spectrometry based proteomics have enabled multiple biomarker mesurements to be achieved with good sensitivity.[14,22] Nevertheless, they are currently too expensive and technically complex for routine clinical diagnosis. Alternatively, there are several commercially available analyzers for multiplex

determination of up to 10 selected target proteins, that can reach low detection limits for 1-100 pg mL^{-1} in serum.[19,32] These systems are based on fluorescence (Luminex, Myriad RBM), electrochemiluminescence (Roche Diagnostics, Mesoscale Discovery), or surface plasmon resonance (Horiba Inc, BIO-RAD).[32,29,33] However, each of these commercial instruments require specialized consumables and sometimes equipment, such as sample well plates, chips, laser sources and reagent kits which are expensive and therefore limit their usefulness for point of care applications where resources are limited.[32,29,33] Electrochemical detection strategies on the other hand offer robust and quantitative measurements using low-cost and simple instrumentation with the ability to be incorporated into a portable device.[32,34] The glucose meter, which currently has control over 85% of the entire POC biosensor market is based on electrochemical detection.[27] In addition the coupling of electrochemical devices with nanomaterial's offers unique multiplexing capability for multiplex detection of multiple analytes.[19,35,36]

1.3 Electrochemical based Protein Detection

Electrochemical based biosensors determine the level of protein analyte of interest by detecting changes in either potential, current, capacitance, conductance or impedance caused by a specific biorecognition reaction.[29,34,37] The biosensor intimately couples a biological recognition element to an electrode transducer, which converts the biological recognition event into a useful electrical signal.[29,34] There are several common electrode transducers such as impedance, conductometric, protentiometric, and amperometric that are used in biological electrochemical sensing.[29,34,37] Impedance transducers rely on measuring resistive and capacitive changes that are in response to a biorecognition

event.[38] Typically, a biorecognition element is bound to the surface of an electrode and the frequency is varied to obtain an impedance spectrum.[38] The resistive and capacitive components of impedance are determined from an in phase and out of phase current responses.[38] The interfacial impedance is a result of analyte binding to the biorecognition element.[38] Conductometric transduction involves measuring the change of conductive properties of a sample solution.[37] This usually involves AC potential to be applied across two metal electrodes causing a current flow.[37] In the event of biorecognition of an analyte the ionic composition changes, using a resistance meter the change in conductance can be observed.[37] Potentiometric sensors on the other hand generate their signals by concerting the biorecognition reaction into a potential signal through the use of ion selective electrodes.[34,37] These ion selective electrodes feature a membrane that exclusively binds with the charged ion of interest, this then causes an accumulation of a charge potential that can be read by a impedance voltmeter.[34,37] However, despite the obvious advantages of using these unlabeled electrochemical biosensors they still require significant future development in terms of both cost and in sensitivity to test clinical samples.[19] Alternatively, amperometric biosensors function by applying a constant potential and monitoring the current associated with the redox (reduction or oxidation) of an electroactive species that is involved in the recognition process. Amperometric sensors offer high sensitivity and wide linear dynamic ranges making them highly attractive candidates for clinical protein detection.[29,34,37]

Nearly thirty years ago Heineman and Halsall pioneered the electrochemical detection of proteins based on applying enzyme-linked immunosorbent assays to an electrode surface.[39] Such protocols rely on labeling the antibody or antigen with an

enzyme that instead of causing a change of color as in ELISA based methods generates an electroactive product that can be detected amperometrically.[39,40,41] The enzyme label applied by the Heineman group was alkaline phosphatase, which produces electroactive products.[39,40,41] Using this approach, the capture antibodies dwell in a flow system upstream of the detector. [39,40,41] Products from the enzyme label are then transported to the electrode by fluidics. [39,40,41] They are able to obtain excellent detection limits in the pg/mL to ng/mL range for small molecules and proteins. [39,40,41]

As time progressed significant efforts were made to develop self-contained single analyte enzyme-linked electrochemical immunosensors.[42,43,44] These sensors predominately feature antibodies being attached directly to the electrode surface, these antibodies are able to capture their target protein of interest (Scheme 1.2). [42,43,44] Once the protein target is captured, an enzyme labeled secondary antibody binds and detection is carried out all on the same surface. This sandwich immunoassay format is the most selective and sensitive for protein detection. [42,43,44]

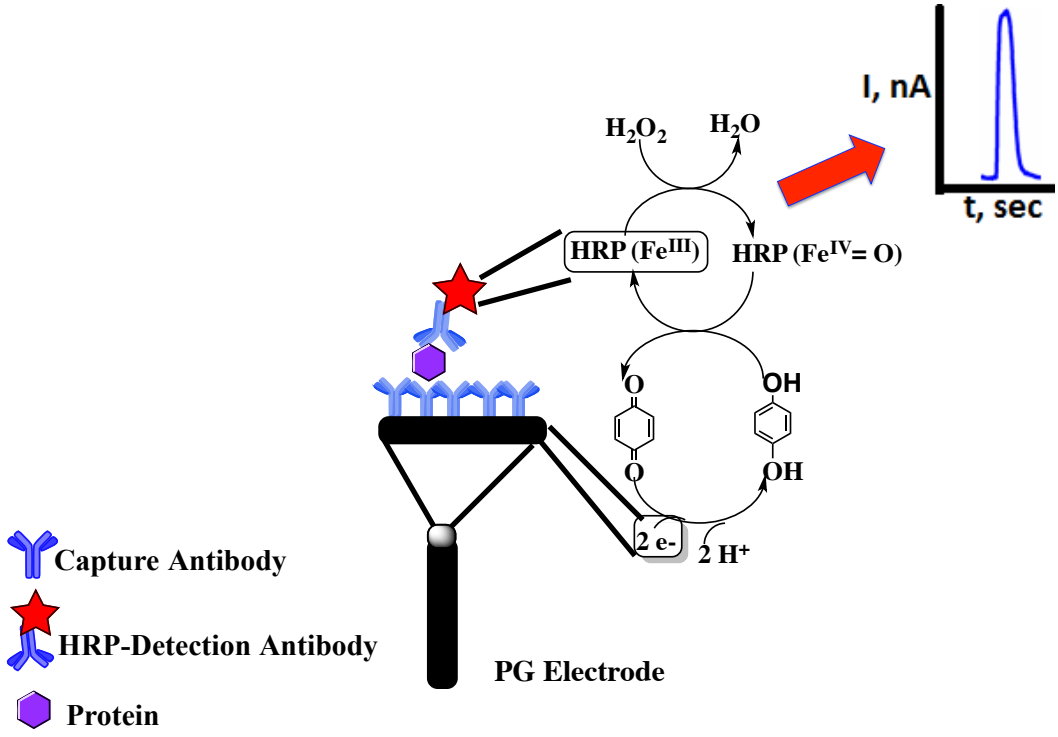

Scheme 1.2 Full sandwich immunoassay built upon the surface of a single electrode. Amperometric signal generation carried out by Horserasish peroxidase.

Alternative enzymes labels such as horseradish peroxidase (HRP) are widely used for ELISAs and for electrochemical based immunosensors.[19,45] Horseradish peroxidase (HRP) is a member of the ferroprotoporphyrin group of peroxidase.[46,47] It is a single chain polypeptide containing a central iron heme group. The heme group is capable of catalytic oxidation/reduction by hydrogen peroxide (Scheme 1.2).[46,47] Once activated by hydrogen peroxide the iron heme is converted to its oxidized form (Fe^{IV}= O) that can be

reduced on electrodes at low potentials.[47] Almost all electrochemical based protein detection within this dissertation will be carried out using this paramount enzyme label.

In addition to both horseradish peroxidase and alkaline phosphatase many other labels for electrochemical detection of proteins have been used such as glucose oxidase, conductive polymers, electroactive metal ions and complexes, and liposomes that are loaded with electroactive compounds.[48,49,50,51] However, the most sensitive of detection schemes have employed strategies including dissolvable nanoparticles, and nanoparticles with multiple enzyme labels or multiple redox probes.[36,49,50,52,53,54,55,56] Employing these approaches investigators are able to achieve high signal amplification by providing many signal generating species for each analyte that is captured on to the sensor surface.

1.4 Nanoparticle labeled Immunoassays

The ability to amplify your detection single is critical to the sensitive detection of proteins. The first reports of dissolvable nanoparticle labels employed in electrochemical based immunoassays were by Dequaire et al.[57] Here, gold nanoparticles were bound to detection antibodies to amplify the electrochemical signals using a sandwich immunoassay approach within microwells.[57] Once particle were bound to their target analytes, an acid solution is applied to the microwells and the metal ions are released and detected by anodic stripping voltammetry.[57] Similar strategies were further developed by Wang et al to achieve even greater sensitivity using gold nanoparticles to catalyzed silver precipitation enhancing the release of ions.[49] In addition to gold and silver, CdS quantum dots decorated on magnetic beads were also used as labels in electrochemical stripping analysis.[49] Alternatively, detection antibodies labeled with either nanoparticles or

polymer beads loaded with electroactive labels such as ferrocene derivatives can be used as labels (Figure 1.2).[49,54,56]

As previously discussed both horseradish peroxidase and alkaline phosphatase can serve as excellent enzyme electrochemical labels.[19,39,45] Attaching multiple copies of these enzyme labels to nanoparticles can greatly enhance the sensitivity of the electrochemical detection (Figure 1.2).[58,59] Wang et al was the first to report the use of nanoparticle labeled with multiple enzyme labels for the ultrasensitive detection of DNA (Figure 1.2) .[60] Multiwall carbon nanotubes were decorated with thousands of copies of alkaline phosphatase and detection antibodies (or probe DNA) to achieve fM detection of IgG in buffer (Figure 1.2).[60] Further enhancements to sensitivity of these protocol were achieve by using layer-by-layer film deposition of alkaline phosphatase with oppositely charged polyions to the surface of carbon nanotubes resulting in extremely low detection limits of 70 aM for IgG in butter.[61]

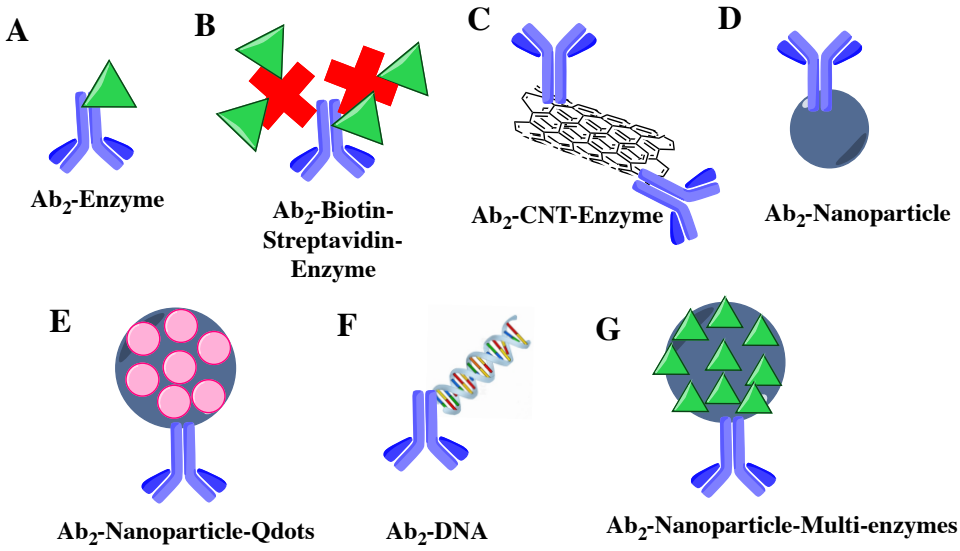

Figure 1.2 Amplification approaches for electrochemical immunosensor using nanoparticles or other moieties attached to a secondary antibody (Ab_2). Adapted from references (19,35).

Our own research team has employed the use of multiple enzyme labels in designing immunosensor protocols for a library of known cancer biomarker proteins.[19,51,52,62,63,64,65] Initially conventional detection antibodies labeled with horseradish peroxidase were employed, this was quickly replaced by more sensitive detection schemes using streptavidin-biotin complexes.[64] Here, biotinlyated detection antibodies are conjugated to streptavidin labeled HRP which can provide 14-16 horseradish peroxidase labels to each detection antibody increasing the sensitivity of the electrochemical detection.[64] Further enhancements to signal amplification were achieved

by conjugating horseradish peroxidase to carbon nanotubes and eventually to magnetic beads, which enable up to half a million HRPs to be bound.[19,51,52,62,63,65]

Magnetic bead based amplification strategies offer many advantages over non-magnetic nanoparticle in terms of the ease of manipulation for labeling, antibody attachment, and purification of bead bioconjugates with simple and inexpensive magnets.[35,66,67] Typically, paramagnetic beads are employed for magnetic separation and transport as they become magnetized in an applied magnetic field, yet have zero magnetization in the absence of a magnetic field.[68] These beads have high surface areas per unit volume, good stability which enable effective antibody attachment.[66,67,68] In addition these beads are commercially available with sizes ranging from 100 nm to 50 μm, and with coatings of either organic functional groups or precoated biomolecules that can bind to specific partners.[59] Using these commercially available magnetic particles we have been able to achieve ultra low detection limits down to the aM range in sensitivity for the electrochemical detection of clinically relevant proteins.[69] Further enhancements to sensitive electrochemical detection of proteins can be achieved by employing nanoparticles at the sensor surface.

1.5 Nanoparticle Platforms for Electrochemical Detection

Due to the fact that reactions are generally carried out in close proximity to the electrode surface, the electrodes themselves play critical roles in performance of an electrochemical biosensor.[37] Therefore, the detection ability of each sensor is based on selected function of a specific electrode, electrode material, its surface modification and/or its dimensions.[37] Tailoring electrode surfaces to achieve unique properties has

expanded tremendously with advent in nanofabrication.[70] Here scientist are controlling the electrode surface architecture on the nanoscale whether it be through nanomaterials, organic monolayer modification, or using combination of both modification of layers involving organic monolayers and nanomaterials.[70] These nanoparticle based surfaces offer large surface areas that enable attachment of multitudes of capture antibodies and offer intricate surface structures that provide better access of proteins analytes to the capture antibodies.[71] Methodologies for production of nanostructured immunosensors include attaching films of carbon nanotubes, gold nanoparticles, or even controlled electrodeposition of noble metals to obtain porous nanostructured surfaces.[19,52,62,72,73,74]

Development of nanoparticle platforms on electrode surfaces began in the early 1990s.[75,76,77] These platforms were initially used to increase their electrochemical signals via their high surface-to-volume ratios. By increasing the electroactive surface area investigators are able to reach lower detection limits and higher sensitivity to analytes.[75] Gradually, efforts were focused on their application to bioconjugated systems.[70] However, in order to bioconjugate a nanoparticle to say an antibody the particles themselves need to possess a means of attachment such as coatings of either organic functional groups or precoated biomolecules that can bind to specific partners.

Carbon nanotubes are commonly functionalized by treatments with strong acids such as HNO_3 and H_2SO_4.[78,79,80] These treatments shorten the length of the carbon nanotubes and add terminal carboxylate groups, which can then be used for conjugation with biomolecules (Figure 1.3).[78,79,80] Our own research team has employed shortened single wall carbon nanotubes, in an upright format, called SWCT forests for sensitive detection of PSA.[52,53,63] To develop these films, end-carboxylated SWNTs are self-

assembled from DMF solutions onto thin iron oxide-Nafion underlayers to an electrode surface.[52,53,63] Antibody attachment is accomplished through standard amide coupling using 1-(3-(dimethylamino)propyl)-3ethylcarbodiimide hydrochloride (EDC) and N-hydrosulfosuccinimide (NHSS).[52,53] Using the aforementioned protocols and combining SWCT forest sensors with multilabeled CNT-HRP-Ab_2 particles were able to accomplish up to a 10-15 fold increase in surface concentrations of attached antibodies compared to flat carbon surfaces, which lead to a 10-fold signal enhancement in electrochemical based immunoassays.[63,65]

Alternative strategies for achieving nanoparticle-based platforms for ultrasensitive detection of proteins employed by our research group were to use densely packed films of 5nm gold nanoparticles (AuNP).[62] The AuNPs used here are protected by a monolayer of glutathione molecules that analogous to the SWNT provide carboxylate groups to the sensor surface allowing for antibody attachment.[62] Films were fabricated on electrode surfaces by depositing a 0.3-0.5 nm under-layer of cationic poly(diallydimethylammonium) PDDA, washing, and then depositing 5 nm glutathione-decorated gold nanoparticles (GSH-AuNPs) (Figure 1.3).[62] Similarly, antibodies were attached to glutathione-protected AuNPs using EDC/NHSS amidization.[62] High sensitivity of these sensor electrodes was further obtained by using 1μm magnetic bead-Ab_2-HRP bioconjugates with 7500 HRP labels.[62] These sensors delivered both high sensitivity and low detection limits for PSA in serum, which was eight fold lower than that obtained by our previously mentioned SWCNT forest sensor.[62] Further comparison between both the SWCNT and AuNP platforms were accomplished for the determination of IL-6, a clinically relevant biomarker protein in serum (Figure 1.3).[64] Here,

immunoassays featured biotinlyated detection antibodies conjugated to streptavidin labeled HRP.[64] Again, the AuNP platform was able to achieve lower detection limit of 10 pg mL^{-1}, a 3-fold better than achieved by the SWCNT sensor.[64] Furthermore, the AuNP sensors delivered a large linear dynamic range of 20-4000 pg mL^{-1}, covering almost of the clinically relevant range for this cancer biomarker.[64] These current strategies of combing nanostructured electrodes with massively labeled detection particles were expanded further for multiplex determination of proteins on sensor arrays.

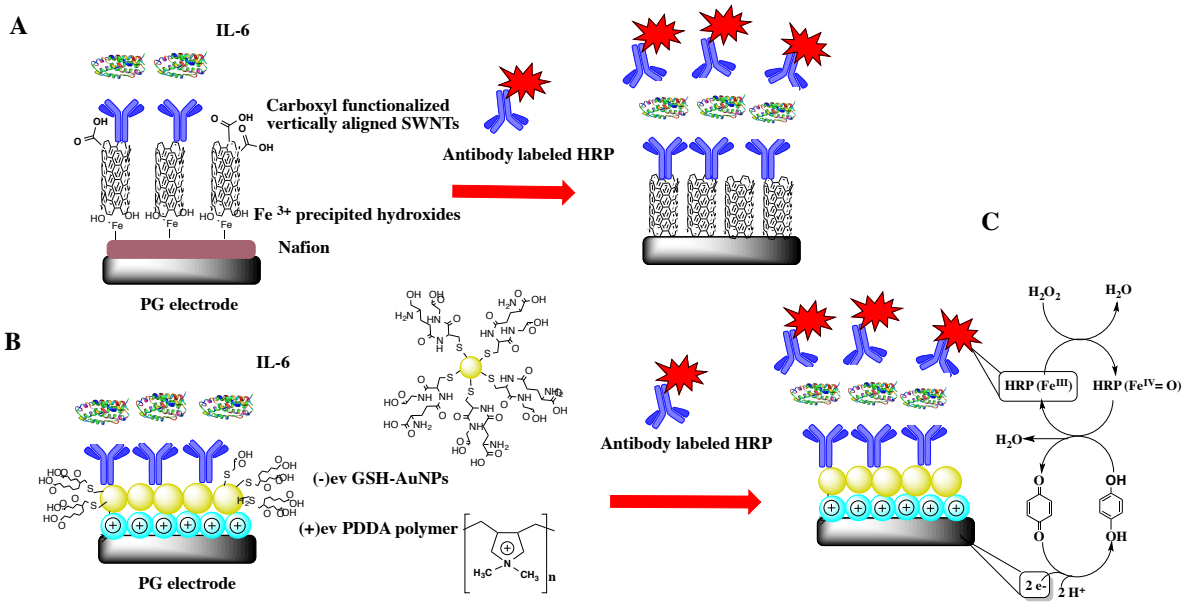

Figure 1.3 The development of the immunosensor for IL-6 on both A) the surface of SWNTs and B) GSH-AuNPs. C) The catalytic mechanism for HRP's electrochemical detection. (The image of IL-6 was created with Protein Workshop from Xu, G. Y.; Yu, H. A.; Hong, J.; Stahl, M.; McDonagh, T.; Kay, L. E.; Cumming, D. A. *J. Mol. Biol.* **1997**, *268*, 468–481).

1.6 Electrochemical Multiplex Protein Arrays

Multiplex protein measurement is vital to understanding the pathobiology of disease states. Proteins constantly function with networks pathways, complexes and families (Figure 1.1).[28] Consequently, actions of individual proteins are not only reliant on their abundance, but also on the results of interacting, antagonistic and synergistic proteins.[28] The pathobiology of oral mucositis is an excellent example of the complex behavior of proteins that will be discussed in later chapters of this thesis. Measurements of single biomarkers are thus not very advantageous to understanding the pathobiological state. Therefore, research efforts in the field of electrochemical protein measurement are focused on multiplexing.

Two of the most common approaches used for multiplex electrochemical protein detection are the bar code labeling and secondly multi-electrode arrays.[19,81,82] The bar code approach employs a series of nanoparticles or quantum dots generating dissolvable metals that posses' different reduction potentials using similar approaches to Dequaire et al.[57,83] Liu et al employed an example of this multiplexing approach for the simultaneous electrochemical detection of β_2-microglobulin, IgG, bovine serum albumin, and C-reactive protein.[83] Here, lead sulfide, cadmium sulfide, zinc sulfide and copper sulfide colloidal crystals were conjugated to antigen specific antibodies, which when dissolved yielded Pb^{2+}, Cd^{2+}, Zn^{2+}, and Cu^{2+} ions.[83] High sensitivity detection of each of these proteins was achieved using stripping voltammetry.[83] Extensions of these bar code labels were further developed by the use of striped microrods, alloy nanowires and multiple metal spheres.[49] However, these multiplex strategies are restricted by the number of

different metals available and by resolution of each of the metal oxidations within the electrochemical potential scale.[81]

The second approach to multiplex electrochemical detection involves using multi-electrode arrays where each electrode has a different antibody attached (Figure 1.4).[19,81,82] Wilson et al using arrays of iridium oxide electrodes applied an early example of this array format. The pair of iridium oxide electrodes using alkaline phosphatase as the enzyme label achieved simultaneous detection of two-cancer biomarkers α-fetoprotein and carcinoembryonic antigen with a detection limit of 1 ng mL^{-1}.[84] This approach was further extended to an 8-electrode array for the simultaneous detection of seven cancer biomarkers with detection limits down to 2 ng mL^{-1}.[85] While this method showed good correlations with standard ELISAs for proteins in serum they stilled lacked the sensitivity to reach clinically relevant ranges for many biomarker proteins.[81] Alternatively, Wei et al was able to achieve detections limits down to the fg mL^{-1} for detection of oral cancer protein biomarkers using a 16-sensor electrochemical chip coated with a DNA dendrimer/ conducting polymer film.[86]

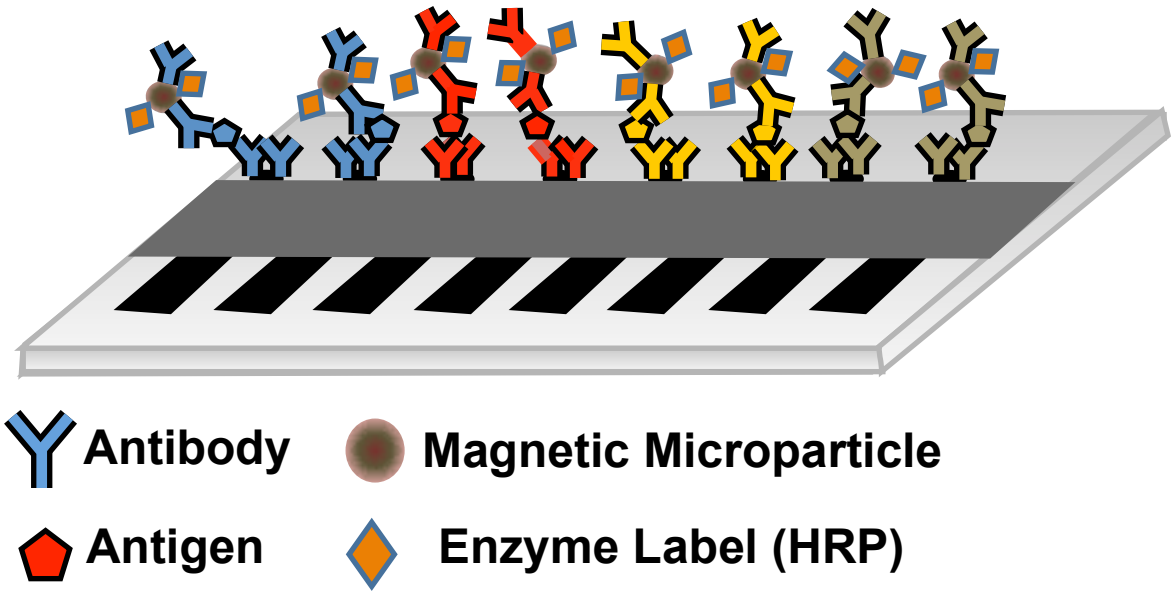

Figure 1.4 The multiplexed 8-electrode array with attachment of multiple proteins (in this case 4, shown in different colors) with duplication, each electrode being measured simultaneously.

In order to demonstrate these ultralow detection limits for multiplex detection of a collection of proteins our own reach team as previously described combines the use of nanostructured electrodes with massively labeled detection particles. Chikkaveeriah et al demonstrated an early example of our own array format consisting of 4 bundled electrodes for the simultaneous detection of four prostate biomarkers.[87] Clinically relevant ranges for each biomarker were achieved using these electrode arrays coated with SWCT forest and multiply labeled with streptavidin-HRP conjugates.[87] Further extensions of these protocols were carried out using AuNP films on commercially available carbon screen printed arrays as well as low cost in house fabricated inkjet

printed 8-electrode microfluidic arrays that will be discussed in later chapters of this thesis.

1.7 Microfluidic Electrochemical Detection

Microfluidic immunosensors offer many remarkable features for point of care detection such as requiring minimal sample volumes (often only in nanoliters), high surface to volume ratios which enables for shorter assay times, and degrees of automation.[88,89] Moreover, these microfluidic immunosensors have the ability to be integrated with other microanalytical functions such as mixers, valves, as well as detections that greatly enhance its analytical performance to development of a total micro-analysis system.[88,89] In addition to pioneering electrochemical immunosensing the Heinemann group was among the first to integrate microfluidics with electrochemical protein detection.[90] Using their alkaline phosphatase enzyme label, Heinemann and co-workers developed a magnetic bead based immunoassay system within a glass microfluidic device to achieve detection limits of 50 ng mL^{-1} within 20 min assays.[90]

Microfluidic devices in addition to being fabricated by glass may also be fabricated using polymers such as poly(dimethylsiloxane), or PDMS.[91,92] PDMS is a soft elastomer that is optically transparent.[91,92] The soft elastomer is the most widely used material in academic microfluidics as it easy to fabricate by replication of molds, highly flexible, and biocompatible.[91,92] In addition to its easy fabrication it has the ability to be sealed to itself or other substrates both reversible or irreversibly without an adhesive.[91,92] Substrates such as silicon, glass, or plastics for PDMS have been widely used for easy fabrication of lap on chip devices.[91,92] Ko and co-workers demonstrated an early example

of lab on chip featuring PDMS devices with integrated electrodes.[93] Here, Ko and co-workers develop their electrochemical microfluidic device by placing their patterned PDMS ontop a poly(dimethyl methacrylate) PMMA substrate containing gold electrodes.[93] In a similar format our research team produces our microfluidic electrochemical devices.

Our first microfluidic electrochemical detection system was fabricated using a machine molded 63 μL PDMS channel that was sandwiched between 2 hard PMMA plates, connected by PEEK tubing to a pump and sample injector (Figure 1.5A).[94] This detection chamber easily houses our 8-electrode sensor immuno-arrays as well as both a platinum (Pt) wire counter, and silver/silver chloride (Ag/AgCl) reference, electrodes (Figure 1.5A).[94] Prior to being incorporated in the microfluidic device these arrays were coated with sequential layers of the polycation PDDA and GSH-AuNPs as previously described to attach antibodies through primary amine groups to each electrode surface.[94] Protein analytes were captured offline in microcentrifuge tubes using antibody conjugate magnetic beads coated with tosyl groups that allowed for the attachment an estimated 200,000 HRP labels per bead.[94] Once protein analytes were captured the beads were washed, magnetically separated, and injected into the microfluidic detection system (Figure 1.5B). [4] Employing this microfluidic device along with offline capture of protein analytes interleukin-6 and prostate specific antigen Chikkaveeraiah et al was able to achieve detection limits in the sub $pgmL^{-1}$ range in 1-hour assays.[94] This system was further extended to the multiplex detection of four protein biomarkers, including interleukin-6, interleukin-8, VEGF, and VEGF-C for clinical diagnostics of oral cancer.[95] Using streptavidin-derivatized beads and biotin-labeled HRP and Ab_2 lead to increase in

enzyme labels (400,000 HRP) enabling for ultra low detection limits to be achieved (5-50 fg mL^{-1}) in 50 min assays.[95]

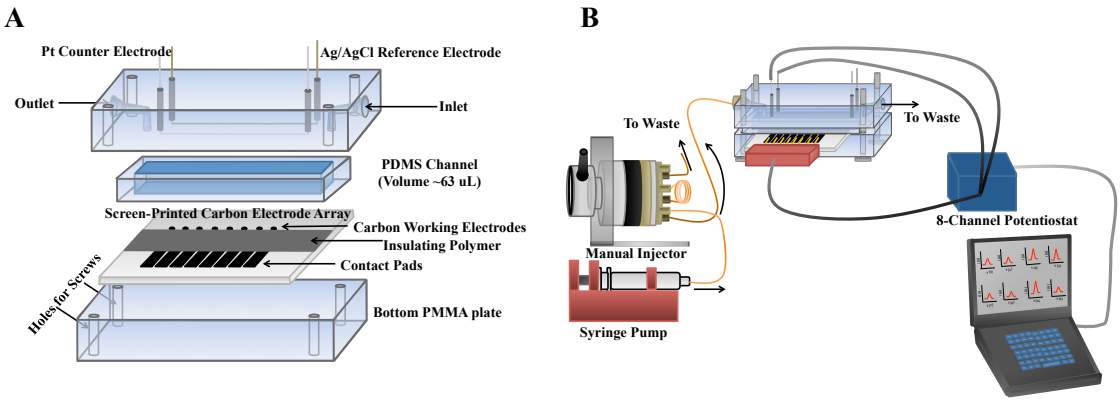

Figure 1.5 (A) The disposable 8-electrode array incorporated into the microfluidic device consisting of soft PDMS channel and to PMMA plates, the top containing ports for both inlet and outlet for fluid to flow threw. The top PMMA also contains both the Pt counter and Ag/AgCl reference electrodes. **(B)** The experimental set up for the microfluidic device containing the 8-electrode potentiostat and computer readout.

In order to achieve further degrees of automization within our microfluidic electrochemical detection we expanded our microfluidic design to include a capture chamber upstream of the detection chamber to replace the off-line capture step.[96] This new design enables most of the immunoassay steps to be incorporated into the microfluidic device, requiring only loading of reagents, samples and wash solutions by the operator.[96] Further application of this modular microfluidic device will be discussed in later chapters of this dissertation.

1.8 Summary/ Overview of Dissertation

Cancer is a very complex disease with many signal transduction pathways, and genomic alterations, not to mention the many types and sub-types there are in existence.[3] Therefore, measurement of levels of specific biomolecules, such as certain proteins, may give further insight to the origin as well as the severity of the disease state.[26,19] However, for accurate diagnosis it is essential to measure panels of these protein biomarkers.[19,36,97] Thus, there is a great need for simple high throughput sensors that address all the needs of a point-of-care setting (i.e. low-cost, multiplex, high sensitivity, minimal sample consumption, technical simplicity).[19] This dissertation aims to address these aforementioned requirements through the development ultrasensitive microfluidic electrochemical immunoassay systems that are based on simple analytical instrumentation in order to achieve high sensitivity and low detection limits for protein detection.

Chapter 1 provides an introduction to point of care sensor designs, electrochemical based protein detection strategies, and the important links between advancements in the field of nanomaterial science and electrochemistry. Furthermore, this chapter highlights the importance of microfluidics in the translation of these sensor designs to portable point of care detection systems. Discussions of the pioneering research on these various topics described in this chapter provide a concrete foundation to the further work that will be presented in this dissertation.

Chapter 2 describes the fabrication of a low cost sensor array. Thin film electronic devices hold enormous potential for the fabrication of low cost sensors that may be incorporated into next generation microfluidic devices. We employed a non-contact

fabrication method of inkjet printing to produce gold nanoparticle (AuNP) electrochemical arrays on plastic, with a unit cost of only 20 cents per array. These arrays were fabricated from ink made of dodecane thiol-protected gold nanoparticles synthesized in-house and were soluble in toluene. This AuNP ink was then printed on to a flexible, heat resistant polyimide Kapton substrate. Once printed the arrays were then annealed and insulated with a Kapton precursor layer, poly(amic acid) (PAA). These results demonstrated that an elegant, cheap, and simple technique for fabricating AuNP arrays by direct inkjet printing is capable of being incorporated into a next generation microfluidic device for the electrochemical detection of proteins.

Chapter 3 explains the integration of these low cost inkjet printed sensor arrays into a simple microfluidic device for low sample volume detection of two cancer biomarker proteins, interleukin-6 (IL-6) and interleukin-8 (IL-8) within 8 min (Figure 2). Conventional immunoassays often take hours to complete; however, more rapid assays are needed for point-of-care sensing and surgical applications in cancer diagnostics. Sensor arrays are fabricated as described in Chapter 2. The resulting gold sensor elements are then coated with a self-assembled monolayers providing functionality to attach capture antibodies to their surfaces. Magnetic beads of 1 μm diameter derivatized with ~300,000 horseradish peroxidase labels (HRP) and thousands of antibodies are developed to capture the biomarker proteins from serum samples off-line (outside the microfluidic device setup) to provide high sensitivity and ultralow detection limits (DLs). The results obtained in Chapter 3 indicate that this fast immunoarray protocol could be employed for rapid detection of biomarker proteins in surgical samples or to detect inflammation during cancer therapy.

Finally, Chapter 4 describes a more user-friendly microfluidic system by adding a reaction chamber for automated on-line capture and detection of three pro-inflammatory cytokines and C-reactive protein. This protein biomarker panel was designed to assess risk for oral mucositis, a painfully debilitating disease that results from high dose radiation therapy in oncology patients. These protein analytes are captured from biomedical samples in an on-line microfluidic chamber by thoroughly labeled magnetic beads, then magnetically separated, washed, and introduced into the detection chamber housing an 8-electrode screen printed carbon immunosensor coated with glutathione-gold nanoparticles (GSH-AuNP). Ultralow detection limits of 10 fg/mL were achieved for simultaneous detection of the four protein biomarkers. Accuracy and diagnostic utility of these microfluidic arrays were demonstrated by measuring the levels of the four biomarker proteins in oral mucositis patient serum samples and comparing with standard ELISA. The use of microfluidic immunosensors to measure concentrations of elevated biomarkers holds promise for accurate, low cost, and rapid determination of projected risk of OM that can be used by dentists and oncologists for patient management.

1.9 References

(1) Barker, A. D.; Jordan, H. Legislative History of the National Cancer Program, 2003.

(2) Hanahan, D. *Lancet* **2014**, *383*, 558–563.

(3) Chin, L.; Andersen, J. N.; Futreal, P. A. *Nat. Med.* **2011**, *17*, 297–303.

(4) Hanahan, D.; Weinberg, R. A. *Cell* **2000**, *100*, 57–70.

(5) Hanahan, D.; Weinberg, R. A. *Cell* **2011**, *144*, 646–674.

(6) Siegel, R.; Ma, J.; Zou, Z.; Jemal, A. *CA. Cancer J. Clin.* **2014**, *64*, 9–29.

(7) Weissleder, R. *Science* **2006**, *312*, 1168–1171.

(8) Czernin, J.; Allen-Auerbach, M.; Schelbert, H. R. *J. Nucl. Med.* **2007**, *48*, 78S – 88.

(9) Adams, S.; Baum, R. P.; Stuckensen, T.; Bitter, K.; Hör, G. *Eur. J. Nucl. Med. Mol. Imaging* **1998**, *25*, 1255–1260.

(10) Antoch, G.; Vogt, F. M.; Freudenberg, L. S.; Nazaradeh, F.; Goehde, S. C.; Barkhausen, J.; Dahmen, G.; Bockisch, A.; Debatin, J. F.; Ruehm, S. G. *JAMA* **2003**, *290*, 3199–3206.

(11) Schmidt, G. P.; Haug, A. R.; Schoenberg, S. O.; Reiser, M. F. *Eur. Radiol.* **2006**, *16*, 1216–1225.

(12) Kovács, A. F. *Br. J. Cancer* **2005**, *92*, 206–207.

(13) Ross, G. L.; Soutar, D. S.; Gordon MacDonald, D.; Shoaib, T.; Camilleri, I.; Roberton, A. G.; Sorensen, J. A.; Thomsen, J.; Grupe, P.; Alvarez, J.; Barbier, L.; Santamaria, J.; Poli, T.; Massarelli, O.; Sesenna, E.; Kovács, A. F.; Grünwald, F.; Barzan, L.; Sulfaro, S.; Alberti, F. *Ann. Surg. Oncol.* **2004**, *11*, 690–696.

(14) Hanash, S. M.; Pitteri, S. J.; Faca, V. M. *Nature* **2008**, *452*, 571–579.

(15) Kulasingam, V.; Diamandis, E. P. *Nat. Clin. Pract. Oncol.* **2008**, *5*, 588–599.

(16) Dugeshwar, K. *J. Mol. Biomark. Diagn.* **2011**.

(17) Füzéry, A. K.; Levin, J.; Chan, M. M.; Chan, D. W. *Clin. Proteomics* **2013**, *10*, 13.

(18) Ebert, M. P. A.; Korc, M.; Malfertheiner, P.; Röcken, C. *J. Proteome Res.* **2006**, *5*, 19–25.

(19) Rusling, J. F.; Kumar, C. V; Gutkind, J. S.; Patel, V. *Analyst* **2010**, *135*, 2496–2511.

(20) Rai, A. J.; Chan, D. W. *Ann. N. Y. Acad. Sci.* **2004**, *1022*, 286–294.

(21) Petricoin, E. F.; Zoon, K. C.; Kohn, E. C.; Barrett, J. C.; Liotta, L. A. *Nat. Rev. Drug Discov.* **2002**, *1*, 683–695.

(22) Hawkridge, A. M.; Muddiman, D. C. *Annu. Rev. Anal. Chem. (Palo Alto. Calif).* **2009**, *2*, 265–277.

(23) Manne, U.; Srivastava, R.-G.; Srivastava, S. *Drug Discov. Today* **2005**, *10*, 965–976.

(24) Prensner, J. R.; Rubin, M. A.; Wei, J. T.; Chinnaiyan, A. M. *Sci. Transl. Med.* **2012**, *4*, 127rv3.

(25) Oon, S. F.; Pennington, S. R.; Fitzpatrick, J. M.; Watson, R. W. G. *Nat. Rev. Urol.* **2011**, *8*, 131–138.

(26) Ludwig, J. A.; Weinstein, J. N. *Nat. Rev. Cancer* **2005**, *5*, 845–856.

(27) Gubala, V.; Harris, L. F.; Ricco, A. J.; Tan, M. X.; Williams, D. E. *Anal. Chem.* **2012**, *84*, 487–515.

(28) Kingsmore, S. F. *Nat. Rev. Drug Discov.* **2006**, *5*, 310–320.

(29) Healy, D. A.; Hayes, C. J.; Leonard, P.; McKenna, L.; O'Kennedy, R. *Trends Biotechnol.* **2007**, *25*, 125–131.

(30) Voller, A.; Bartlett, A.; Bidwell, D. E. *J. Clin. Pathol.* **1978**, *31*, 507–520.

(31) Lilja, H.; Ulmert, D.; Vickers, A. J. *Nat. Rev. Cancer* **2008**, *8*, 268–278.

(32) Chikkaveeraiah, B. V; Bhirde, A. A.; Morgan, N. Y.; Eden, H. S.; Chen, X. *ACS Nano* **2012**, *6*, 6546–6561.

(33) Elshal, M. F.; McCoy, J. P. *Methods* **2006**, *38*, 317–323.

(34) Wang, J. *Biosens. Bioelectron.* **2006**, *21*, 1887–1892.

(35) Rusling, J. F.; Bishop, G. W.; Doan, N.; Papadimitrakopoulos, F. *J. Mater. Chem. B. Mater. Biol. Med.* **2014**, *2*.

(36) Rusling, J. F. *Chem. Rec.* **2012**, *12*, 164–176.

(37) Dorothee Grieshaber, R. M. J. V. E. R. Electrochemical Biosensors - Sensor Principles and Architectures. *Sensors (Basel, Switzerland)*, 2008, *8*, 1400.

(38) Daniels, J. S.; Pourmand, N. *Electroanalysis* **2007**, *19*, 1239–1257.

(39) Heineman, W. R.; Halsall, H. B. *Anal. Chem.* **1985**, *57*, 1321A – 1331A.

(40) Ronkainen-Matsuno, N. J.; Thomas, J. H.; Halsall, H. B.; Heineman, W. R. *TrAC Trends Anal. Chem.* **2002**, *21*, 213–225.

(41) Ronkainen, N. J.; Halsall, H. B.; Heineman, W. R. *Chem. Soc. Rev.* **2010**, *39*, 1747–1763.

(42) Lu, B.; Smyth, M. R.; O'Kennedy, R. *Anal. Chim. Acta* **1996**, *331*, 97–102.

(43) Carter, R. M.; Poli, M. A.; Pesavento, M.; Sibley, D. E. T.; Lubrano, G. J.; Guilbault, G. G. *Immunomethods* **1993**, *3*, 128–133.

(44) Warsinke, A.; Benkert, A.; Scheller, F. W. *Fresenius. J. Anal. Chem. 366*, 622–634.

(45) Gorton, L.; Lindgren, A.; Larsson, T.; Munteanu, F. D.; Ruzgas, T.; Gazaryan, I. *Anal. Chim. Acta* **1999**, *400*, 91–108.

(46) Veitch, N. C. *Phytochemistry* **2004**, *65*, 249–259.

(47) Ahammad,A. J. Saleh. *J. Biosens. Bioelectron* **2013**.

(48) Wang, J. *Chem. Rev.* **2008**, *108*, 814–825.

(49) Wang, J. *Electroanalysis* **2007**, *19*, 769–776.

(50) Luo, X.; Morrin, A.; Killard, A. J.; Smyth, M. R. *Electroanalysis* **2006**, *18*, 319–326.

(51) *Bioelectrochemistry*; Bartlett, P. N., Ed.; John Wiley & Sons, Ltd: Chichester, UK, 2008.

(52) Kim, S. N.; Rusling, J. F.; Papadimitrakopoulos, F. *Adv. Mater.* **2007**, *19*, 3214–3228.

(53) Rusling, J. F.; Yu, X.; Munge, B. S.; Kim, S. N.; Papadimitrakopoulos, F. *Engineering the Bioelectronic Interface*; Davis, J., Ed.; Royal Society of Chemistry: Cambridge, 2009.

(54) Veetil, J. V; Ye, K. *Biotechnol. Prog. 23*, 517–531.

(55) Zhang, H.; Zhao, Q.; Li, X.-F.; Le, X. C. *Analyst* **2007**, *132*, 724–737.

(56) Wang, J. *Small* **2005**, *1*, 1036–1043.

(57) Dequaire, M.; Degrand, C.; Limoges, B. *Anal. Chem.* **2000**, *72*, 5521–5528.

(58) Jensen, G. C.; Yu, X.; Gong, J. D.; Munge, B.; Bhirde, A.; Kim, S. N.; Papadimitrakopoulos, F.; Rusling, J. F. *J. Nanosci. Nanotechnol.* **2009**, *9*, 249–255.

(59) Mani, V.; Chikkaveeraiah, B. V; Rusling, J. F. *Expert Opin. Med. Diagn.* **2011**, *5*, 381–391.

(60) Wang, J.; Liu, G.; Jan, M. R. *J. Am. Chem. Soc.* **2004**, *126*, 3010–3011.

(61) Munge, B.; Liu, G.; Collins, G.; Wang, J. *Anal. Chem.* **2005**, *77*, 4662–4666.

(62) Mani, V.; Chikkaveeraiah, B. V; Patel, V.; Gutkind, J. S.; Rusling, J. F. *ACS Nano* **2009**, *3*, 585–594.

(63) Yu, X.; Munge, B.; Patel, V.; Jensen, G.; Bhirde, A.; Gong, J. D.; Kim, S. N.; Gillespie, J.; Gutkind, J. S.; Papadimitrakopoulos, F.; Rusling, J. F. *J. Am. Chem. Soc.* **2006**, *128*, 11199–11205.

(64) Munge, B. S.; Krause, C. E.; Malhotra, R.; Patel, V.; Gutkind, J. S.; Rusling, J. F. *Electrochem. commun.* **2009**, *11*, 1009–1012.

(65) Malhotra, R.; Papadimitrakopoulos, F.; Rusling, J. F. *Langmuir* **2010**, *26*, 15050–15056.

(66) Franzreb, M.; Siemann-Herzberg, M.; Hobley, T. J.; Thomas, O. R. T. *Appl. Microbiol. Biotechnol.* **2006**, *70*, 505–516.

(67) Verpoorte, E. *Lab Chip* **2003**, *3*, 60N – 68N.

(68) Gijs, M. A. M.; Lacharme, F.; Lehmann, U. *Chem. Rev.* **2010**, *110*, 1518–1563.

(69) Munge, B. S.; Coffey, A. L.; Doucette, J. M.; Somba, B. K.; Malhotra, R.; Patel, V.; Gutkind, J. S.; Rusling, J. F. *Angew. Chemie Int. Ed.* **2011**, *50*, 7915–7918.

(70) *Chemically Modified Electrodes*; Alkire, R. C.; Kolb, D. M.; Lipkowski, J.; Ross, P. N., Eds.; Advances in Electrochemical Sciences and Engineering; Wiley-VCH Verlag GmbH & Co. KGaA: Weinheim, Germany, 2009.

(71) Das, J.; Kelley, S. O. *Anal. Chem.* **2011**, *83*, 1167–1172.

(72) *Engineering the Bioelectronic Interface*; Davis, J., Ed.; Royal Society of Chemistry: Cambridge, 2009.

(73) Bertram, R. *Angew. Chemie* **1970**, *82*, 820–820.

(74) Soleymani, L.; Fang, Z.; Sargent, E. H.; Kelley, S. O. *Nat. Nanotechnol.* **2009**, *4*, 844–848.

(75) Freeman, R. G.; Grabar, K. C.; Allison, K. J.; Bright, R. M.; Davis, J. A.; Guthrie, A. P.; Hommer, M. B.; Jackson, M. A.; Smith, P. C.; Walter, D. G.; Natan, M. J. *Science* **1995**, *267*, 1629–1632.

(76) Patolsky, F.; Gabriel, T.; Willner, I. *J. Electroanal. Chem.* **1999**, *479*, 69–73.

(77) Musick, M. D.; Peña, D. J.; Botsko, S. L.; McEvoy, T. M.; Richardson, J. N.; Natan, M. J. *Langmuir* **1999**, *15*, 844–850.

(78) Gooding, J. J. *Electrochim. Acta* **2005**, *50*, 3049–3060.

(79) Jacobs, C. B.; Peairs, M. J.; Venton, B. J. *Anal. Chim. Acta* **2010**, *662*, 105–127.

(80) Karousis, N.; Tagmatarchis, N.; Tasis, D. *Chem. Rev.* **2010**, *110*, 5366–5397.

(81) Rusling, J. F. *Anal. Chem.* **2013**, *85*, 5304–5310.

(82) Limoges, B.; Marchal, D.; Mavré, F.; Savéant, J.-M.; Schöllhorn, B. *J. Am. Chem. Soc.* **2008**, *130*, 7259–7275.

(83) Liu, G.; Wang, J.; Kim, J.; Jan, M. R.; Collins, G. E. *Anal. Chem.* **2004**, *76*, 7126–7130.

(84) Wilson, M. S. *Anal. Chem.* **2005**, *77*, 1496–1502.

(85) Wilson, M. S.; Nie, W. *Anal. Chem.* **2006**, *78*, 6476–6483.

(86) Wei, F.; Liao, W.; Xu, Z.; Yang, Y.; Wong, D. T.; Ho, C.-M. *Small* **2009**, *5*, 1784–1790.

(87) Chikkaveeraiah, B. V; Bhirde, A.; Malhotra, R.; Patel, V.; Gutkind, J. S.; Rusling, J. F. *Anal. Chem.* **2009**, *81*, 9129–9134.

(88) Bange, A.; Halsall, H. B.; Heineman, W. R. *Biosens. Bioelectron.* **2005**, *20*, 2488–2503.

(89) Henares, T. G.; Mizutani, F.; Hisamoto, H. *Anal. Chim. Acta* **2008**, *611*, 17–30.

(90) Choi, J.-W.; Oh, K. W.; Thomas, J. H.; Heineman, W. R.; Halsall, H. B.; Nevin, J. H.; Helmicki, A. J.; Henderson, H. T.; Ahn, C. H. *Lab Chip* **2002**, *2*, 27–30.

(91) Whitesides, G. M. *Nature* **2006**, *442*, 368–373.

(92) Temiz, Y.; Lovchik, R. D.; Kaigala, G. V.; Delamarche, E. *Microelectron. Eng.* **2014**, *132*, 156–175.

(93) Soo Ko, J.; Yoon, H. C.; Yang, H.; Pyo, H.-B.; Hyo Chung, K.; Jin Kim, S.; Tae Kim, Y. *Lab Chip* **2003**, *3*, 106–113.

(94) Chikkaveeraiah, B. V; Mani, V.; Patel, V.; Gutkind, J. S.; Rusling, J. F. *Biosens. Bioelectron.* **2011**, *26*, 4477–4483.

(95) Malhotra, R.; Patel, V.; Chikkaveeraiah, B. V; Munge, B. S.; Cheong, S. C.; Zain, R. B.; Abraham, M. T.; Dey, D. K.; Gutkind, J. S.; Rusling, J. F. *Anal. Chem.* **2012**, *84*, 6249–6255.

(96) Otieno, B. A.; Krause, C. E.; Latus, A.; Chikkaveeraiah, B. V.; Faria, R. C.; Rusling, J. F. *Biosens. Bioelectron.* **2014**, *53*, 268–274.

(97) Rusling, J. F. *Bioanalysis* **2010**, *2*, 847–850.

(98) Munge, B. S.; Dowd, R. S.; Krause, C. E.; Millord, L. N. *Electroanalysis* **2009**, *21*, 2241–2248.

Chapter Two

Inkjet-Printed Gold Nanoparticle Electrochemical Arrays on Plastic

2.1 Abstract

Thin film electronic devices hold enormous potential for the fabrication of low cost sensors that may be incorporated into next generation microfluidic devices. We employed a non-contact fabrication method of inkjet printing to produce gold nanoparticle (AuNP) electrochemical arrays on plastic, with a unit cost of only 20 cents per array. These arrays were fabricated from ink made of dodecane thiol-protected gold nanoparticles synthesized in-house and were soluble in toluene. This AuNP ink was then printed on to a flexible, heat resistant polyimide Kapton substrate.The inkjet-printed working electrodes had reproducible surface areas with RSD < 3%. These results demonstrated that an elegant, cheap, and simple technique for fabricating AuNP arrays by direct inkjet printing is capable of being incorporated into a next generation microfluidic device for the electrochemical detection of proteins.

2.2 Introduction

Thin film electronic devices hold enormous potential for the fabrication of low cost electrochemical sensors. These electronic devices are typically composed of a conductor, a dielectric, and a semiconductor in a multilayered structure.[1] Common methods in developing these thin-film electronic devices include chemical vapor

deposition (CVD),[2] photolithography,[3] screen-printing,[4] and stencil printing.[5] While each of these methods allows for well-defined electrode fabrication and insulation, they each require the creation of a master such as a custom-patterned screen, stencil, or mask for printing each new pattern.[6] Manufacturing these masters is time consuming and expensive which limits rapid prototyping and mass customization. Inkjet printing has the capability to circumvent these current limitations by offering the ability to rapidly produce patterns based on easily modifiable digital files.[6]

Herein, we describe a digital fabrication method for creating high-resolution conductive patterns on heat resistant polyimide dielectric sheets. To make printing the principal platform for patterning flexible conductors, inexpensive functional inks and substrates must be employed.[6] Nanoparticle inks have been used to print highly conductive tracks.[7,8] For these inks, electrical conductivity of the printed features is achieved by sintering nanoparticles such as silver, gold, and copper through either high temperature, laser pulsing, or microwave irradiation.[7,8] The substrates for these inks consequently must be highly durable and resistant to high temperature annealing.[7,8] Therefore, the heat resistant Kapton polyimide film was selected for the substrates of these high-resolution electrochemical sensors. For production of our ink gold nanoparticles were selected. These gold nanoparticles offer many promising features in producing highly conductive inks as they may be synthesized through a simple liquid-phase synthesis yielding nanoparticles that are easily dispersible in organic media.

The synthesis of our AuNPs followed most standard procedures today employing a reducing agent to solutions containing a metal salt, the metal ions are reduced and metallic solid particles are nucleated.[9,10,11] In our present study $AuCl_4^-$ was transferred

from an aqueous solution to toluene ($C_6H_5CH_3$) using tetraoctylammonium bromide ($N(C_8H_{17})_4$)as the phase transfer catalyst.[9,10,11] The organic phase was then separated and reduced with sodium borohydride in the presence of dodecanethiol ($C_{12}H_{25}SH$), the overall reaction is summarized below in two steps where the source of the electrons in BH_4^-.[9,10,11]

$$AuCl_4^- (aq) + N(C_8H_{17})_4^+ (C_6H_5CH_3) \rightarrow N(C_8H_{17})_4^+ AuCl_4^- (C_6H_5CH_3) \quad (1)$$

$$AuCl_4^- (C_6H_5CH_3) + C_{12}H_{25}SH\ (C_6H_5CH_3) + 3e^- \rightarrow$$

$$4Cl^-(aq)+(Au)(C_{12}H_{25}SH)\ (C_6H_5CH_3) \quad (2)$$

Following the synthesis of the AuNPs they were dispersed in organic media and printed using a piezoelectric inkjet printer.

Piezoelectic inkjet printing is a non-contact, high precision printing method with resolution of ≥ 20μm.[12,13,14] The resolutions of ink-jet printed patterns are controlled by several factors including the hydrodynamics of the jetted micro-droplets, and the volatility and viscosity of the constituents of the ink.[15] Therefore, careful attention was applied in production of these material inks. In this paper, we report the first direct inkjet fabrication and characterization of electrochemical arrays using 4nm nanoparticles and poly(amic acid) inks on heat resistant Kapton plastic.

2.3 Experimental

2.3.1 Chemicals and Materials

A Kapton FPPC film 127nm thick was purchased from American Durafilm. These large polymer sheets were washed with water and ethanol prior to use. Gold (III) chloride trihydrate, 1-dodecanethiol, tetraoctylammonium bromide, sodium borohydride, poly(amic acid) were purchased from Sigma-Aldrich.

2.3.2 Instrumentation

All electrochemical measurements were made using a CHI 1040A eight-channel potentiostat simultaneously for all eight electrodes at room temperature. All potentials are reported vs. a common saturated calomel reference (SCE) electrode, and cells employed a common platinum auxiliary electrode.

A Dimatix Materials Printer (ModelDMP-2800, FUJIFILM Dimatix, Inc. Santa Clara, CA) was used for inkjet printing. Dimatix 10pL, liquid crystal polymer printer cartridge were used for all printed inks (Model DMCLCP-11610). Printing patterns were made utilizing the Dimatix materials printer software. All printing patterns were developed using Microsoft Paint (Microsoft Inc. Redmond, WA) and imported using the Dimatix Materials printer with Dimatix Printer Controller software. Each pattern was printed with 15μm spacing between drops and using a custom printing waveform and each pattern was printed using a single jet for easy detection of clogs.

Atomic force microscopy (AFM) of gold nanoparticle arrays was done using a Digital Instruments Nanoscope IV scanning probe microscope, in tapping mode with

symmetric tip high-resolution TappingMode AFM probes (Veeco Metrology Inc., Model MPP-11100)

Scanning Electron Micrographs were taken on a Zeiss DSM 982 Gemini FE-SEM with a Schottky Emitter at an accelerating voltage range from 2 to 4 kV and a beam current of about 1 mA.

2.3.3 Gold Nanoparticle Synthesis and Ink formulation

Dodecane thiol-protected gold nanoparticles were synthesized as previously reported by Hostetler et al.[10] Briefly, 1.5g of tetraoctylammonium bromide was placed in a round-bottom flask containing 80mL toluene and 20mL water and stirred vigorously. 432mg of gold (III) chloride trihydrate was added to the solution and mixed for 5mins. The organic phase was separated and 43.8mL of 1-dodecane thiol was added and stirred for 10 min. 380mg sodium borohydride was dissolved in 25mL of water and quickly added to the vigorously stirring gold (III) chloride solution. The solution immediately turned dark in color and was then stirred for 3hours. Next, the organic phase was washed with several aliquots of water and toluene was removed by rotary evaporation under reduced pressure at 50^{o}C. The gold nanoparticles were dispersed in ethanol and filtered, after which they were washed with several aliquots of water followed by ethanol. The washed gold nanoparticles were covered and lowed to dry in air overnight prior to further use. Isolated particles on mica were analysed by AFM had an average diameter of 4.3 ± 0.8 nm (n=100) and were confirmed using transmission electron microscopy (TEM) shown below in Figure 2.1.

For TEM imaging 100 mg mL^{-1} solution of dodecanthiol gold nanoparticles was diluted to a final concentration of 2 mg mL^{-1}. The TEM sample was prepared by placing one drop of the final dispersion on a silica wafer and dried under vacuum. The average diameter was 4 ± 2 nm (Figure 2.1).

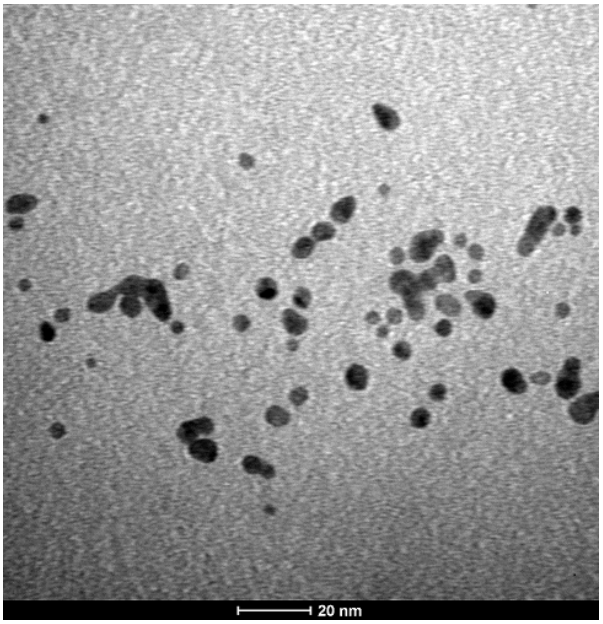

Figure 2.1 TEM image of dodecanethiol gold-nanoparticles with average diameters of 4 ± 2 nm on 20 nm scale bars.

The gold nanoparticle ink was prepared by dissolving dodecane thio-protected gold nanoparticles in toluene to a concentration of 100 mg mL^{-1}. The gold nanoparticle solution was filtered prior to use with a 0.2μm cutoff PTFE filter. 1.5mL of the gold

nanoparticle ink was injected into a liquid crystal Dimatix printer cartridge immediately prior to use.

Poly(amic acid) ink was prepared by diluting the 10% (m/m) poly(amic acid) solution in highly pure N-methyl-2-pyrrolidone (NMP) 1% (m/m). The solution was gently shaken to mix and the poly(amic acid) was injected into a liquid crystal Dimatix printer cartridge immediately prior to use.

2.3.4 Array Fabrication

For printing, clean 22 x 28cm polyimide films were placed in the Dimatix printer and heated to 35^{o}C and secured using the platen vacuum. The gold nanoparticle ink cartridges were placed in the Dimatix printer and visually checked using the high-speed drop watcher camera to ensure consistent ink droplet formation. The printer was aligned with the substrate. The pattern file was set to allow for printing multiple arrays in a single printing, with varying spacing between arrays. The gold nanoparticle ink was then printed onto the polyimide film. Following deposition of the gold nanoparticle ink onto the Kapton substrate, the arrays were heated to 200^{o}C for 3 min or until the films lightened slightly in color. The films were then briefly rinsed with water and returned to the printer for application of poly(amic acid) ink. The poly(amic acid) ink was placed in the printer and the arrays were aligned using the fiducial camera. Five layers of poly(amic acid) ink were printed over the array leads, leaving the working gold nanoparticle electrodes and electrical contacts uncovered. Following application of the poly(amic acid) solution to provide an insulating layer of polyimide on the leads. Surface area and reproducibility of the electrochemical arrays were estimated by cyclic voltammetry (CV) for a solution of

4mM potassium ferrocyanide in 100 mM KCl. Scan rates were varied from 100 to 10 mV s^{-1} (Figure 2.9).

2.4 Results

Ink made from dodecane thiol-protected gold nanoparticles (AuNPs) dissolved in toluene was adjusted in concentration to allow reproducible formation of conductive lines in a single printing to avoid clogging of the inkjets. AuNPs at 100 mg mL^{-1} in toluene produced stable inks that could print using the Dimatix printer for twenty- four hours without clogging the inkjets. However, storage of the ink within the cartridge over a period of a week was problematic due to slow evaporation of toluene and aggregation of the AuNPs.

1% polyamic acid by weight in N-methyl-2-pyrrolidone (NMP) having a kinematic viscosity of 4.28 ± 0.03 cP as measured by a capillary viscometer allowed for easy inkjet printing of an insulating film. The poly (amic acid) solution printed well using the custom waveform and printed continuously for 24 h without clogging. Furthermore, the poly (amic acid) cartridges were stable for a week when stored in a closed container and printed well following one week of storage.

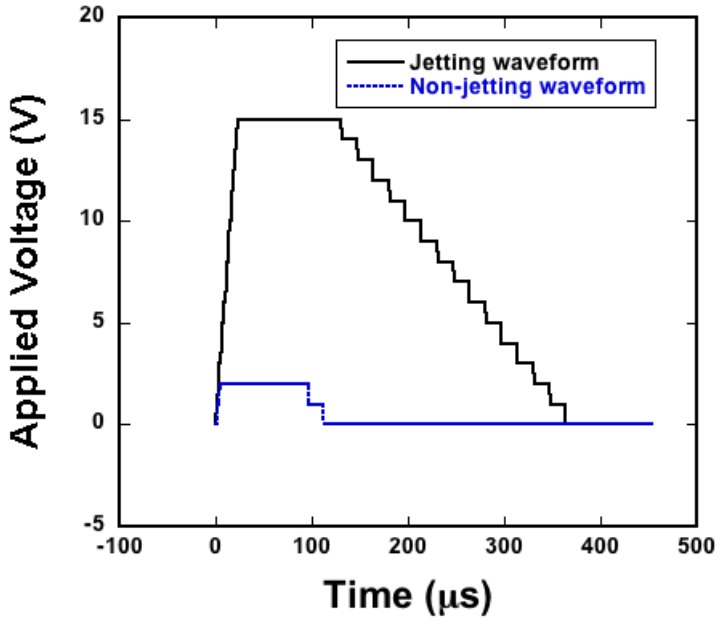

Figure 2.2 Jetting and Non-jetting waveforms used for printing both AuNP and poly (amic acid) inks (shown at 15 V). The two waveforms were consecutively applied based on the pattern to be printed. The non-jetting waveform helps to prevent bubbles forming in the jets while the jetting waveform applies a single drop of ink.

An optimized waveform for inkjet printing was employed, that consists of three steps; first, an increasing voltage period to fill the ink into the liquid crystal printer cartridges, second, a declining voltage period to dispense the fluid, and finally a segment that recovers its original shape without drawing air that could form bubbles shown above in Figure 2.2. This cycle helps to ensure that the cartridge is dispensing perfectly formed drops. The custom waveform maximum voltage for both non-jetting and jetting was adjusted prior too printing the patterns. Adjustments to the voltage settings were made by observing individual drops from the built in drop watch camera within the Dimatix

printer. All inks were printed reproducibly using this waveform with voltages applied in the 15-25 V range for jetting and 3-5 V for non-jetting waveform.

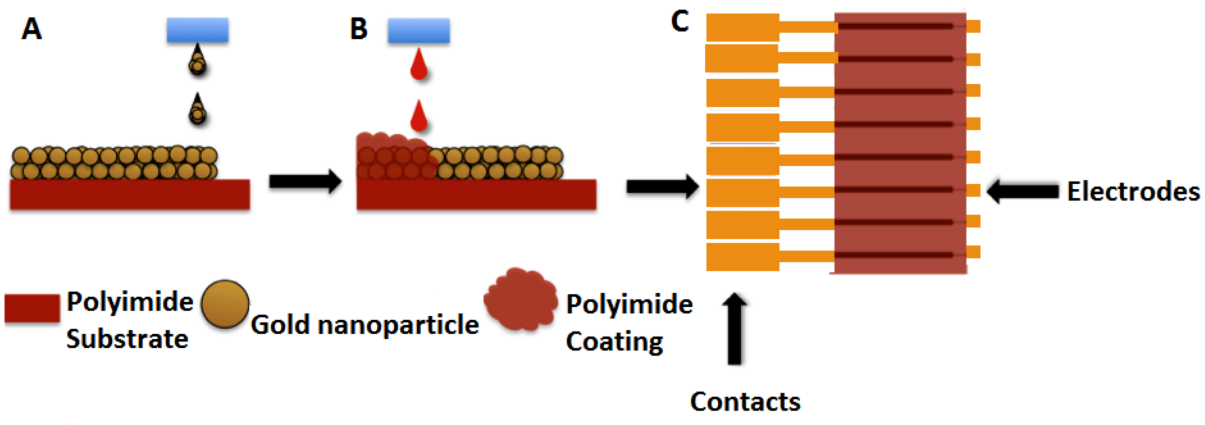

Scheme 2.1 Fabrication of AuNP arrays: **(A)** inkjet printing of the AuNP ink onto the substrate (Kapton); **(B)** inkjet printing of the poly (amic acid) to insulate the electrode leads; **(C)** the AuNP pattern (gold) overlaid with the poly (amic acid) printed pattern (orange).

Using the custom waveform, the gold nanoparticle ink was printed in an eight electrode array pattern (Scheme 2.1). The spacing between drops was set at 15 μm between each pixel, this spacing provides overlap as each drop spreads with an approximate 40μm diameter. The pattern was set to print a square working electrode of dimensions 465 x 465 μm. For each eight- electrode array, approximately 600 mg of gold was printed. When printed, the gold nanoparticle ink spread as expected, with the effect being most noticeable on the bottom of the electrode, which was the last portion of the array to be printed (Figure 2.3).

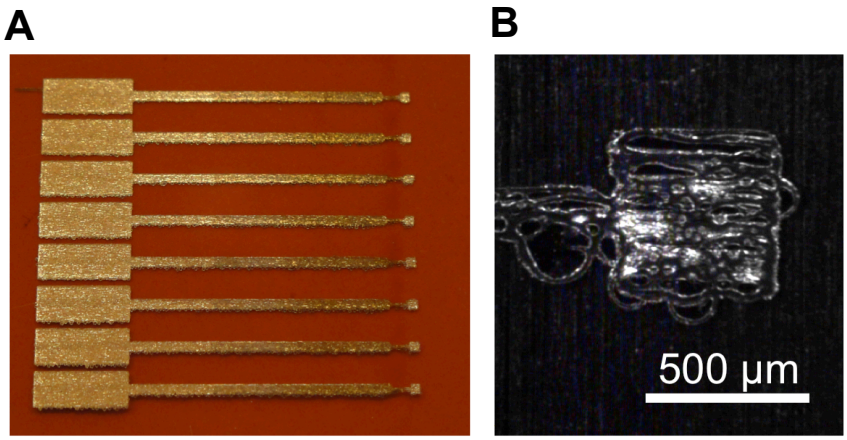

Figure 2.3 Photographs of the array: **(A)** printed AuNP array with the protective polyimide insulating film; **(B)** picture taken using the Dimatix printer's fiducial camera showing a typical single AuNP working electrode.

After spreading, the two-dimensional surface area of the arrays resulted in a geometric area of 0.299 ± 0.015 mm^2. Following gold nanoparticle printing, the arrays were sintered for ~ 3 min at 200^oC. The arrays slightly lightened in color marking the loss of the dodecane thiol layer and formation of percolation paths through the gold nanoparticle network.[16] After heating, the dry resistance of gold arrays from contact to working electrode was 20-25 ohms. Energy- Dispersive X-Ray spectroscopy confirmed the loss of the dodecanethiol layer. The elemental scan before sintering is shown below in Figure 2.4 with percentage of sulfur at 3.3%. The elemental scan after is shown in Figure 2.5 with a percentage of sulfur at 1.4% indicating a loss of ~43% once arrays are baked.

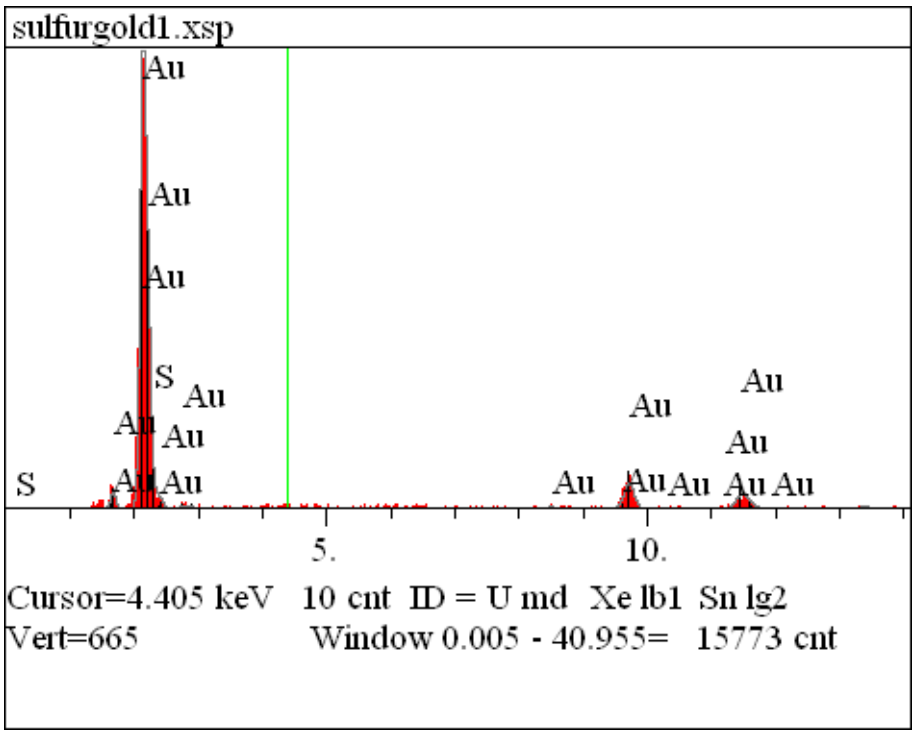

Elt.	Line	Atomic %	Conc	Units	
S	Ka	17.302	3.294	wt.%	
Au	La	82.698	96.706	wt.%	
		100.000	100.000	wt.%	Total

Figure 2.4 EDX pre-sintering elemental scan of the gold arrays.

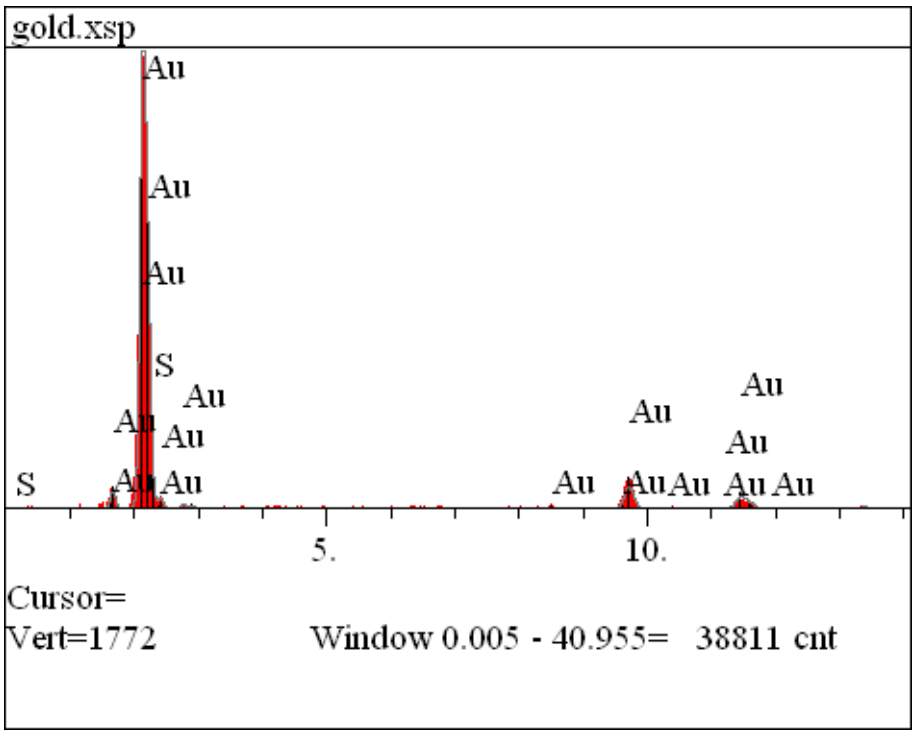

Elt.	Line	Atomic %	Conc	Units	
S	Ka	8.145	1.423	wt.%	
Au	La	91.855	98.577	wt.%	
		100.000	100.000	wt.%	Total

Figure 2.5 EDX post-sintering elemental scan of the gold arrays.

Field Emission Scanning Electron Microscopy, FESEM confirmed formation of percolated paths due to the loss of dodecanethiol layer. Scanning Electron Micrographs were taken on a Zeiss DSM 982 Gemini FE-SEM with a Schottky Emitter at an

accelerating voltage range from 2 to 4KV and a beam current of about 1mA. Printed dodecanethiol AuNPs before sintering is shown in Figure 2.6A indicating large gaps between the inkjet-printed scans that when heat treated at 200^{o}C for 15mins were removed dure to loss of the dodecanethiol groups forming the percolated paths as the Au cores coalesced as shown in Figure 6B and at the same magnification as Figure 2.6A. It seems as though there are cracks in Figure 6B but on further magnification we can see that they are just differences in the thickness of layers of the sintered gold Figure 2.6C.

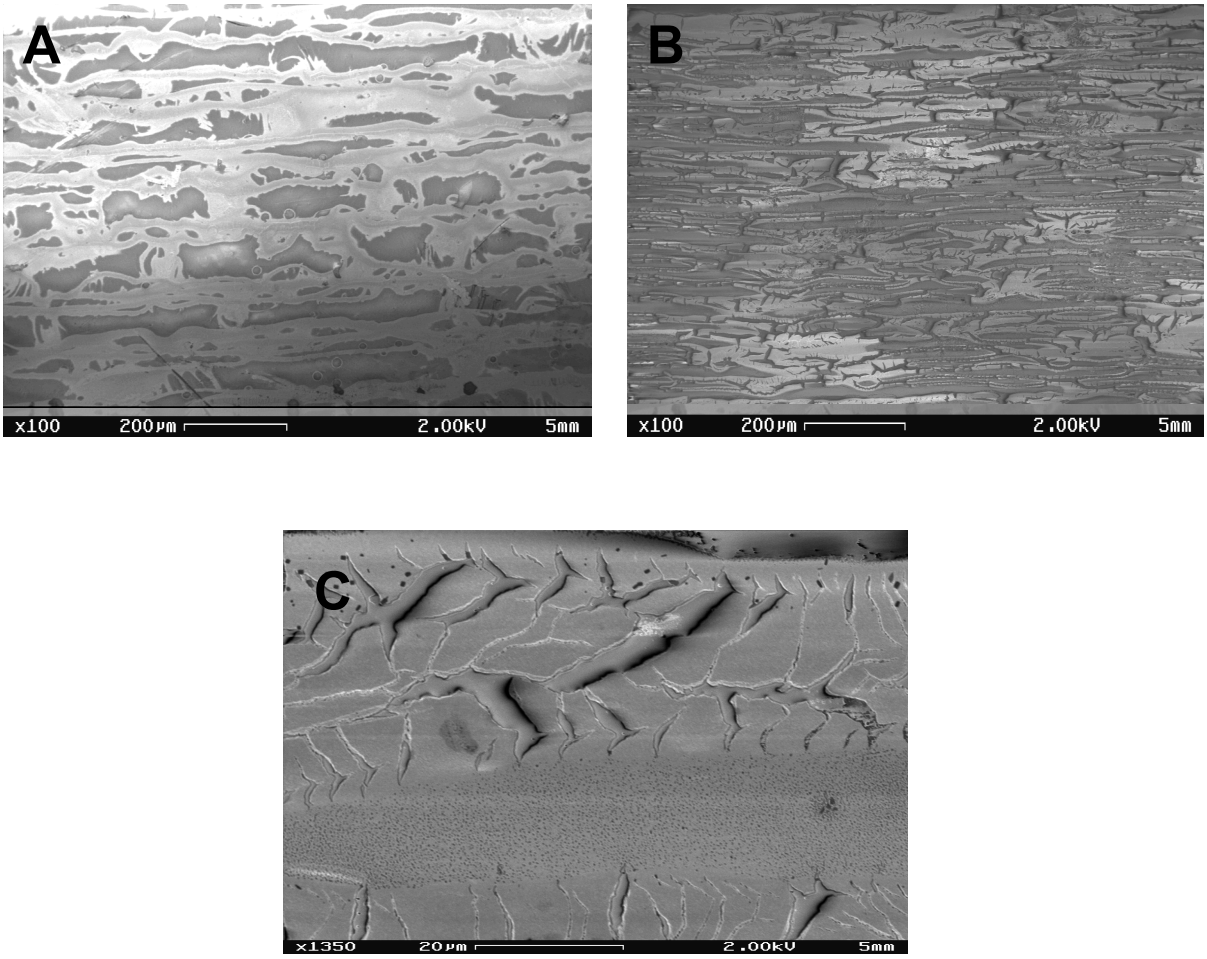

Figure 2.6 FESEM micrograph of an electrode on an array before sintering **(A)** and after **(B)** indicating that the Au cores coalesced, then a larger magnification **(C)** after sintering to demonstrate that it's not cracking but different thickness of films.

Poly (amic acid) ink was printed over the sintered gold nanoparticle arrays to insulate the leads. Poly (amic acid), when heated for 30 mins at 200^{o}C, dehydrates to form polyimide (Scheme 2), which adheres very strongly to the Kapton polyimide substrate.[17] Imidization of the poly (amic acid) essentially seals the old leads between the polyimide substrate and the newly formed polyimide coating. Due to the low concentration of poly (amic acid) in the poly (amic acid) ink, a total of five layers of ink

were required in the pattern shown in Scheme 2.1. Aligning the gold nanoparticle arrays for the application of the poly (amic acid) ink was difficult due to its low visibility. A test pattern consisting of several lines was printed to provide visualization and allow adjustment of the printing origin. Once aligned five layers of the poly (amic acid) ink were printed to ensure that the narrow leads were completely insulated. The imidiation process then formed a protective, insulating polyimide layer over the leads.

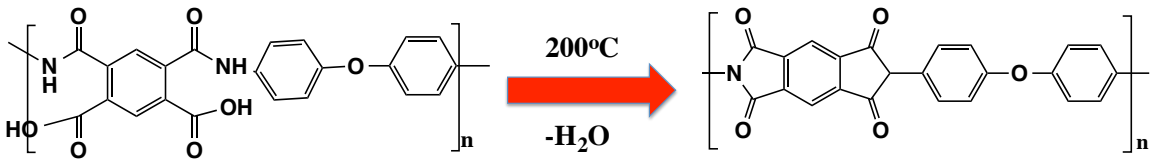

Scheme 2.2 Poly(amic acid) dehydration to give the corresponding polyimide.

The working electrodes of the gold nanoparticle arrays were clearly rough surfaces with well-defined borders as seen in Figure 2.2. Tapping-mode AFM Figure 2.7 images revealed a rough surface featuring larger hills and valleys superimposed on a smaller close packed particle landscape consistent with well defined individual AuNPs in a sintered network. The mean surface roughness was 21± 5nm for the sintered gold nanoparticle surface, confirming a rough nanostructured electrode surface suitable for fabrication of an immunosensor.

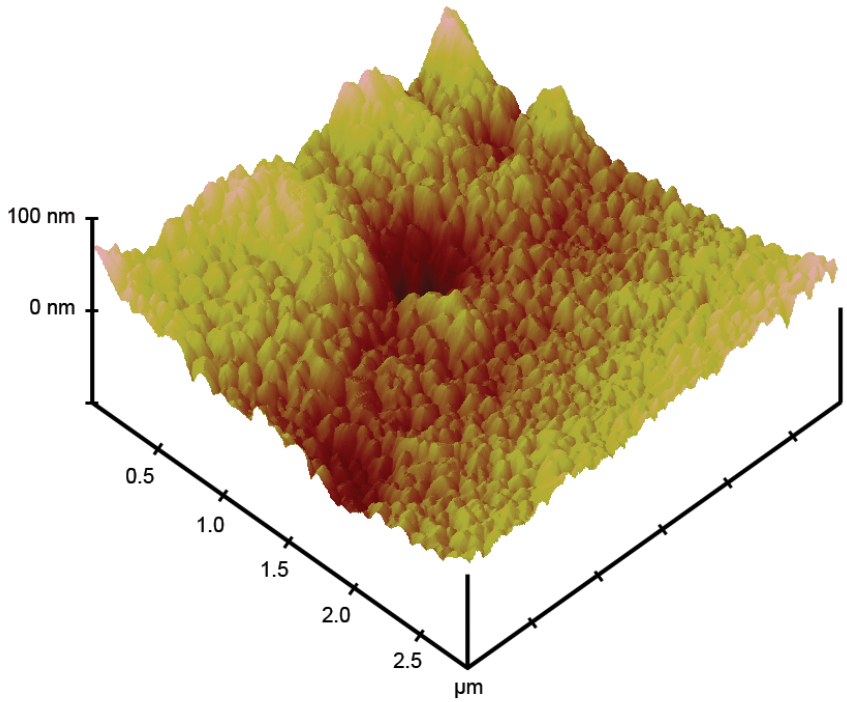

Figure 2.7 Tapping mode AFM of one of eight sintered working electrodes in an inkjet-printed gold nanoparticle array.

One of the major advantages of inkjet-printed arrays is the feasibility of large scale production using industrial inkjet printers. In this study, multiple arrays were printed in each printing run. An example is shown below in Figure 2.8 where 56 gold nanoparticle arrays were produced in a single printing.

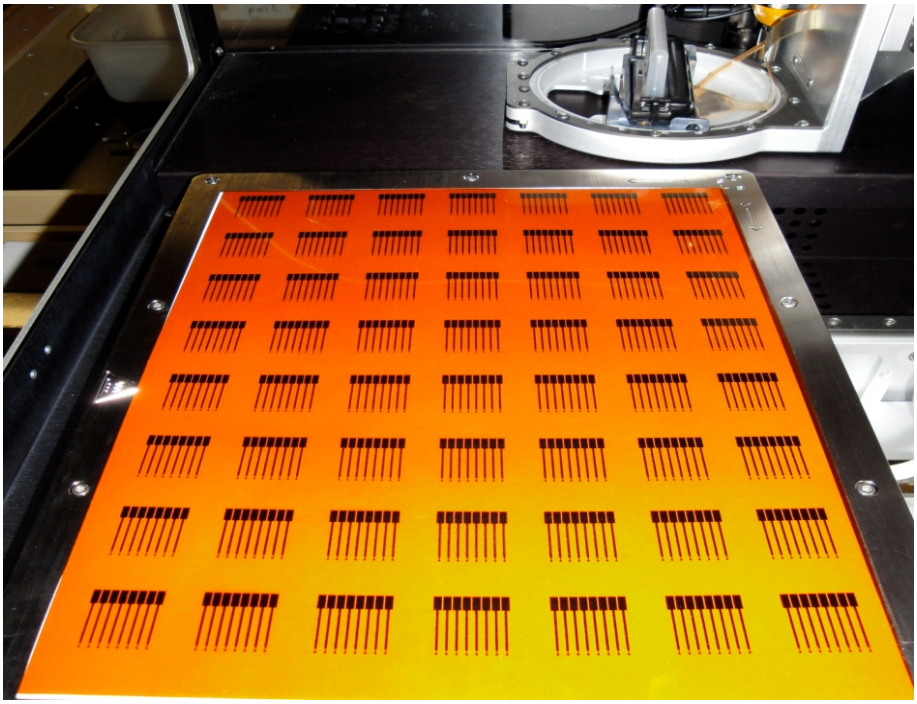

Figure 2.8 Kapton substrate after printing 56 eight-electrode AuNP arrays in a single run (shown within the Dimatix Materials Printer).

Following cleaning, the eight electrodes were scanned simultaneously by cyclic voltammetry in 1mM potassium ferricyanide solution and 100mM potassium chloride Figure 9. The electrode The electrochemical surface area of the arrays was determined, using the oxidation peak current, the Rangles-Sevick equation and the known diffusion coefficient of ferrocyanide to be 0.35 ± 0.01mm^2.[18] This area is 116% of the geometric surface area estimated by analysis of fiducial camera images. The working electrodes showed good reproducibility in electrochemical surface area with a relative standard deviation from electrode to electrode of < 3%, which is directly relevant to applications of the array.

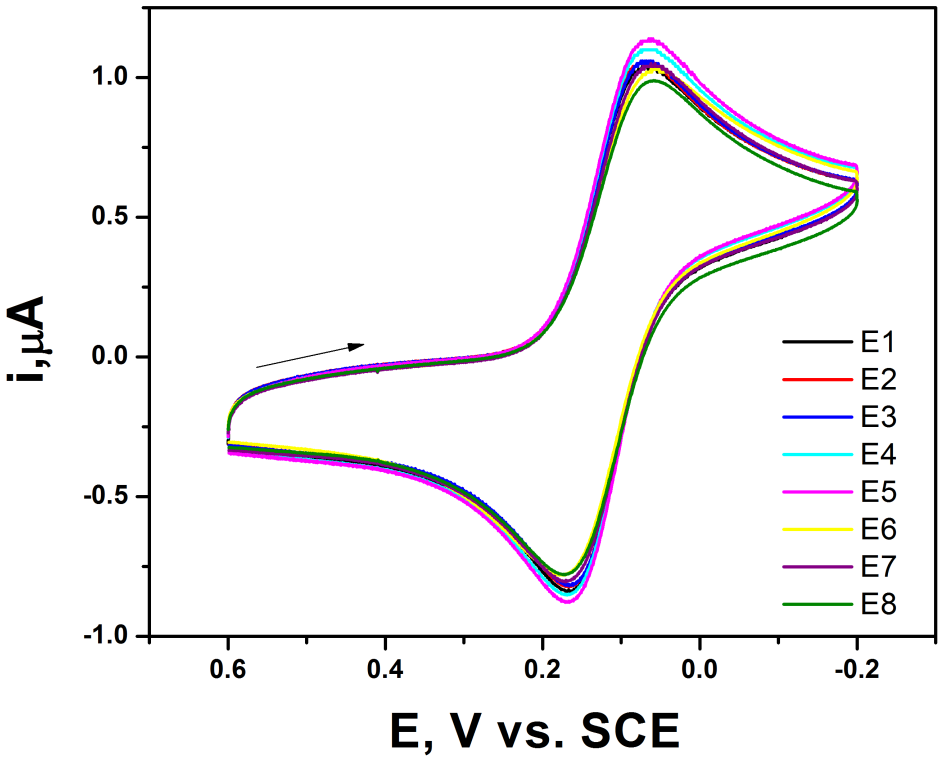

Figure 2.9 Simultaneous cyclic voltammograms of all eight array electrodes in 1 mM potassium ferricyanide and 100 mM potassium chloride at a scan rate of 100 mV s^{-1}.

2.5 Discussion

Inkjet-printed electronics hold enormous potential for the fabrication of low cost sensors and devices. A single array described here cost less than 0.2 cents in materials to produce. The non-contact fabrication of inkjet-printed arrays allowed for the simultaneous production of a large number of devices that were highly reproducible, conductive and easily adapted to fabrication of an immunosensor. This could easily be scaled up to print arrays in larger numbers at lower cost with and industrial-sized inkjet

printer. This ease of modification of the inkjet pattern is a major advantage of the printing technique. Patterns can be changed in a matter of minutes for prototype development. This advantage is clear when inkjet printing is compared to either screen-printing or chemical vapor deposition. While changes in screen-printed or CVD processes require the development of a new mask or screen, inkjet printed patterns can be simply modified using conventional artwork programs.

Thiol-protected AuNPs used in this work allowed development of highly stable ink formations that could be reproducibly printed on heat and chemically resistant Kapton plastic and sintered. These sintered gold nanoparticle networks had low resistance across the film and a nanostructured surface. The use of toluene as the solvent for the gold nanoparticles required a liquid crystal polymer cartridge but for industrial applications the inkjet reservoir could no doubt be designed to handle the solvent. Printing the poly (amic acid) insulating layer provided a well-defined, reproducible surface area with < 3% variation from electrode to electrode. Following the imidization of the poly(amic acid) solution the arrays were well protected with a stable and flexible coating.

2.6 Summary

The results above demonstrate an elegant, cheap, and simple technique for fabricating AuNP arrays by direct ink-jet printing. These printed AuNP arrays are readily adaptable to immunosensor applications as previously developed.[19,20,21,22] We are currently interfacing these eight-electrode arrays to microfluidic devices to provide better control over mass transport of mediator and peroxide to the electrode surface to eliminate current oscillations caused by stirring and improve signal/noise. Because the ink-jetted

pattern is easily modified, fast prototyping of patterns for use in microfluidic devices can be achieved.

2.7 References

(1) D, K.; SH, L.; S, J.; J, M. *Electrochem. Solid State Lett.* **2009**, *12*, H195–H197.

(2) Chen, Z.; Ren, W.; Gao, L.; Liu, B.; Pei, S.; Cheng, H.-M. *Nat. Mater.* **2011**, *10*, 424–428.

(3) Fourkas, J. T. *J. Phys. Chem. Lett.* **2010**, *1*, 1221–1227.

(4) Krebs, F. C.; Jørgensen, M.; Norrman, K.; Hagemann, O.; Alstrup, J.; Nielsen, T. D.; Fyenbo, J.; Larsen, K.; Kristensen, J. *Sol. Energy Mater. Sol. Cells* **2009**, *93*, 422–441.

(5) Siegel, A. C.; Phillips, S. T.; Dickey, M. D.; Lu, N.; Suo, Z.; Whitesides, G. M. *Adv. Funct. Mater.* **2010**, *20*, 28–35.

(6) Lessing, J.; Glavan, A. C.; Walker, S. B.; Keplinger, C.; Lewis, J. A.; Whitesides, G. M. *Adv. Mater.* **2014**, *26*, 4677–4682.

(7) Huang, D.; Liao, F.; Molesa, S.; Redinger, D.; Subramanian, V. *J. Electrochem. Soc.* **2003**, *150*, G412.

(8) Bieri, N. R.; Chung, J.; Haferl, S. E.; Poulikakos, D.; Grigoropoulos, C. P. *Appl. Phys. Lett.* **2003**, *82*, 3529.

(9) Brust, M.; Walker, M.; Bethell, D.; Schiffrin, D. J.; Whyman, R. *J. Chem. Soc. Chem. Commun.* **1994**, *7*, 801–802.

(10) Hostetler, M. J.; Wingate, J. E.; Zhong, C.-J.; Harris, J. E.; Vachet, R. W.; Clark, M. R.; Londono, J. D.; Green, S. J.; Stokes, J. J.; Wignall, G. D.; Glish, G. L.; Porter, M. D.; Evans, N. D.; Murray, R. W. *Langmuir* **1998**, *14*, 17–30.

(11) Yong, K.-T.; Swihart, M. T.; Ding, H.; Prasad, P. N. *Plasmonics* **2009**, *4*, 79–93.

(12) Tobjörk, D.; Österbacka, R. *Adv. Mater.* **2011**, *23*, 1935–1961.

(13) Sekitani, T.; Yokota, T.; Zschieschang, U.; Klauk, H.; Bauer, S.; Takeuchi, K.; Takamiya, M.; Sakurai, T.; Someya, T. *Science* **2009**, *326*, 1516–1519.

(14) Sele, C. W.; von Werne, T.; Friend, R. H.; Sirringhaus, H. *Adv. Mater.* **2005**, *17*, 997–1001.

(15) Singh, M.; Haverinen, H. M.; Dhagat, P.; Jabbour, G. E. *Adv. Mater.* **2010**, *22*, 673–685.

(16) Sivaramakrishnan, S.; Chia, P.-J.; Yeo, Y.-C.; Chua, L.-L.; Ho, P. K.-H. *Nat. Mater.* **2007**, *6*, 149–155.

(17) Oba, M. *J. Polym. Sci. Part A Polym. Chem.* **1996**, *34*, 651–658.

(18) Bard, A. J.; Faulkner, L. R. *Electrochemical Methods: Fundamentals and Applications*; Wiley, 2000; Vol. 6, p. 864.

(19) Chikkaveeraiah, B. V; Bhirde, A.; Malhotra, R.; Patel, V.; Gutkind, J. S.; Rusling, J. F. *Anal. Chem.* **2009**, *81*, 9129–9134.

(20) Chikkaveeraiah, B. V; Liu, H.; Mani, V.; Papadimitrakopoulos, F.; Rusling, J. F. *Electrochem. commun.* **2009**, *11*, 819–822.

(21) Chikkaveeraiah, B. V; Mani, V.; Patel, V.; Gutkind, J. S.; Rusling, J. F. *Biosens. Bioelectron.* **2011**, *26*, 4477–4483.

(22) Chikkaveeraiah, B. V; Bhirde, A. A.; Morgan, N. Y.; Eden, H. S.; Chen, X. *ACS Nano* **2012**, *6*, 6546–6561.

Chapter Three

Rapid Microfluidic Immunoassays of Cancer Biomarker Proteins using Disposable Inkjet-printed Gold Nanoparticle Arrays

3.1 Abstract

Conventional immunoassays often take many hours to complete, but more rapid methods are needed for point-of-care and surgical applications in cancer diagnostics. This paper describes a low-cost ink-jet printed sensor chip integrated into a simple microfluidic immunoarray for low sample volume detection of two cancer biomarker proteins in 8 min. Magnetic beads of 1 mm diam. re derivatized with ~300,000 enzyme labels and thousands of antibodies to capture the biomarker proteins from samples off-line to provide high sensitivity and ultralow detection limits (DL). For an assay time of 45mins, detection limits for interleukin (IL)-6 and IL-8 were as low 19 fg mL^{-1}. We decreased assay time by sacrificing high sensitivity, and obtained a clinically relevant DL of 5 pg mL^{-1} in 8 min. assays. Accuracy was demonstrated by determining IL-6 and IL-8 in conditioned media from head and neck squamous cell carcinoma (HNSCC) cells and comparing results to those obtained by standard single-protein ELISA. Results indicate that this immunoarray and protocol could be employed for rapid detection of a wide range of proteins.

3.2 Introduction

Despite recent advances in treatment, cancer remains a leading worldwide cause of human mortality. Current methods of cancer detection are often based on imaging technologies, such as magnetic resonance imaging (MRI), positron emission tomography (PET), and computed tomography (CT), which themselves have improved in performance using new contrast materials and can distinguish between different anatomical features.[1,2,3,4,5] However, these approaches rely on finding and imaging a tumor, giving limited information on the onset of cancer or quantification of cancerous cells.[1,2,3,4,5] Other techniques are based on cell morphology and microscopy which involve invasive biopsies to observe cancer cells in tissue.[6,7] These tests are not individually conclusive as biopsies can miss concentrations of cancer cells, especially at early stages of the disease.[6,7] Alternatively, specific biosensor arrays that rapidly measure multiple biomarker proteins in serum provide hope for future early cancer detection and monitoring.[8,9,10,11,12,13,14] Such sensitive detection schemes for a selective protein panel whose members are elevated at the onset of cancer are expected to greatly improve patient prognoses and treatment outcomes and may even lead to cancer prevention.[15] Immunosensor microarrays show great potential in targeting specific biomarkers especially when integrated with microfluidics.[15]

Interleukin 6 and 8 (IL-6 and IL-8) were chosen as test biomarkers in this study. These pro-inflammatory cytokines influence all stages of tumor development including initiation. Progression, and metastasis.[16,17] IL-6 and IL-8 have been used to detect and monitor head and neck squamous cell carcinoma (HNSCC) commonly referred to as oral cancer.[18,19] HNSCC has high mortality rates due to late diagnosis based on current

methods, mainly relying on visual identification of cancerous lesions.[20,21] Serum levels of IL-6 in patients with oral cancer are commonly ≥ 20 pg mL^{-1}, whereas healthy individuals are below 6 pg mL^{-1}.[22] Similarly, IL-8 serum levels in oral cancer patients are usually abover 20 pg mL^{-1} with concentrations below 13 pg mL^{-1} observed in healthy individuals.[23] A biosensor for IL-8 in serum was developed by Munge et. al.[24] with a detection limit of 1 fg mL^{-1} in ~1 hr assay time.[24] However, there is a need to rapidly measure multiple biomarker proteins in surgical applications to inform decisions such as defining surgical borders and metastasis and to detect and monitor recurrence.[25]

Effective point of care (POC) sensors must be inexpensive, rapid, adequately sensitive, and should require limited technical expertise and minimal sample volume.[8,9] A number of methods including fluorescence immunoassays,[26] PCR-based bar code labels,[27] radioimmunoassay,[28] two-dimensional (2D) electrophoresis,[29] and multidimensional liquid chromatography- mass spectrometry[30] have been used, but most are limited for POC protein measurements due to cost, assay time, or technical complexity. Recent approaches to decrease assay times include an Immuno-pillar chip [31] which gives immunoassay in 4 mins for C-reactive-protein using florescence detection.[31] Here, a 3D hydrogel format impeded removal of nonspecifically bound antibodies in wash steps, the assay yielded relatively high detection limits of 100 pg mL^{-1} for C-reactive-protein and ng mL^{-1} levels for α-fetoprotein and prostate specific antigen (PSA) in serum.[31,32]

We recently fabricated disposable inkjet-printed arrays form 4nm gold nanoparticles (AuNP) that costs less than $ 0.20/ array in materials.[33] Preliminary tests of these gold arrays without microfluidics achieved a detection limit of 20 pg mL^{-1} for IL-6.

[33] To facilitate rapid, semi-automated measurements of proteins in the present work, these AuNP arrays were integrated into a simple microfluidic device (Scheme 3.1), and protein analytes were captured for analysis with magnetic beads (MB) bioconjugated with hundreds of thousands of enzyme labels and secondary antibodies.[15]

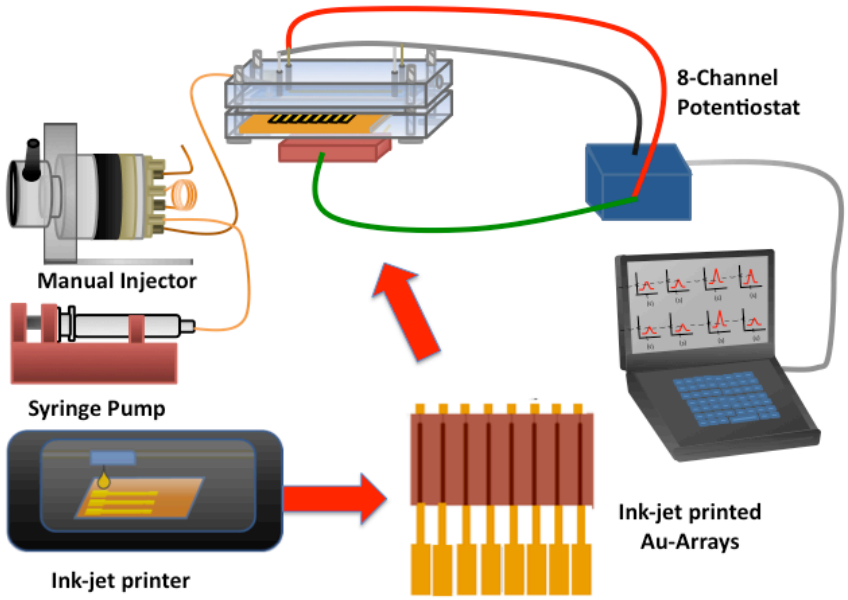

Scheme 3.1 Schematic representation of the disposable injet-printed array incorporated into a simple microfludic device.

We have also used sensor arrays made from commercial screen-printed carbon arrays decorated with 5nm AuNPs in a microfluidic system to achieve 1.25 hr assays with detection limits of 200 fg mL-1 for IL-6 and PSA in serum.[15] We later improved detection limits to 5-5- fg mL-1 for determining four oral cancer biomarker proteins in serum simultaneously in 50 min assays by using 400,000 horseradish peroxidase (HRP)

labels per bead.[18] The disadvantage here is that the disposable sensor arrays cost about $10/each and require manual deposition of AuNPs onto a polyion film on each sensor in the array. The advantage of the printed AuNP immunoarrays in this paper is that they are printed directly on thermostable plastic at low cost with automatic production of hundreds of arrays at a time using an inkjet materials printer. [33] Here we describe integration of this low-cost AuNP immunoarray into a microfluidic device to achieve clinically relevant DLs of ~5 pg mL^{-1} for IL-6 and IL-8 in 8mins.

3.3 Experimental

3.3.1 Chemicals and Materials

Kapton FPC film (127 mM thick) was purchased from American Durifilm. Lyophilized 99% bovine serum albumin (BSA), sterile-filtered bovine calf serum, gold (III) chloride trihydrate, 1-dodecane thiol, tetrocylammonium bromide, sodium borohydride, 3-Mercaptopropenoic acid (MPA), N-hydroxysulfoscuccinimide (NHSS), 1-Ethyl-3-[-3-dimethylaminopropyl] carbodimmide hydrochloride (EDC), poly(amic acid), Tween-20, and Hydroquinone (HQ) were purchased from Sigma-Aldrich. Hydrogen peroxide (H_2O_2, 30%) came from Fisher Scientific. The poly(dimethoxy)silane (PDMS) kit was purchased from Dow Corning. MyOne Tosylactivated beads (1 mm diameter, Dynabeads) and Streptavidin coupled magnetic beads (1 mm diameter, Dynabeads) were from Invitrogen. Immunoreagents (monoclonal primary antibodies, BSA, biotinylated secondary antibodies and biotinylated horseradish peroxidase (HRP)) were dissolved in pH 7.2 phosphate saline (PBS) buffer (5.9 mM Na_2HPO_4, 3.9 mM NaH_2PO_4, 2.7 mM KCl, 120 mM NaCl). 400 mM EDC and 100 mM NHSS were

dissolved in ultrapure water immediately before use. Monoclonial antihuman Interleukin-6 (IL-6) antibody (Ab_1) (clone no. 6708), biotinylated antihuman IL-6 antibody (biotin-Ab_2), recombinant human IL-6 (carrier-free), human IL-6 polyclonal (goat IgG) antibody(Ab_2), monoclonal antihuman interleukin-8 (IL-8) antibody(AB_1) (clone no. 6217), biotinylated antihuman IL-8 antibody(biotin-Ab_2), recombinant human IL-8 (carrier-free) were from R&D Systems, Inc. (Minneapolis, MN, USA).

3.3.2 Instrumentation

All electrochemical measurements were made using a CHI 1040A eight-channel potentiostat simultaneously for all eight electrodes at room temperature. The CHI 1040A was connected to the microfluidic array system and was used for amperometric detection. Single-potential amperometry was performed at optimal conditions for high sensitivity and low ratio signal/noise, -0.2 V vs. Ag/AgCl (0.14 M NaCl) reference with a solution flow of 100 μL min^{-1}. The microfluidic system was constructed as previously reported by Chikkaveeraiah et al.[15] It featured a molded, soft PDMS slab with a 1.5 mm wide rectangular channel that was placed on top of the electrode array. As before, the microfluidic channel was supported by two hard flat poly(methylmethacrylate) (PMMA) plates manufactured to fit on either side of the PDMS slab and bolted together (Figure 3.1A). The top PMMA plate contained female ports (4 mm diameter) for screwing in standard male plastic fittings (1.5 mm, up church) to hold 0.2 mm i.d. PEEK connecting tubing for an inlet and outlet (Figure 3.1A). The top PMMA also contained two holes 0.6 mm for Ag/AgCl and 0.2 mm diameter for Pt wire electrode. For the microfluidic system, a Harvard 70-4502 pump 11 elite model syringe pump was used. It was connected to the

inlet through a Rheodyne model 9725i injector valve with a sample loop of 100 mL through 0.2 mm i.d. tubing (Figure 3.1B).

A Dimatix Materials Printer (model DMP-2800, FUJIFILM Dimatix, Inc. Santa Clara, CA) was used for all inkjet printing as described previously by Jensen et al.[33]

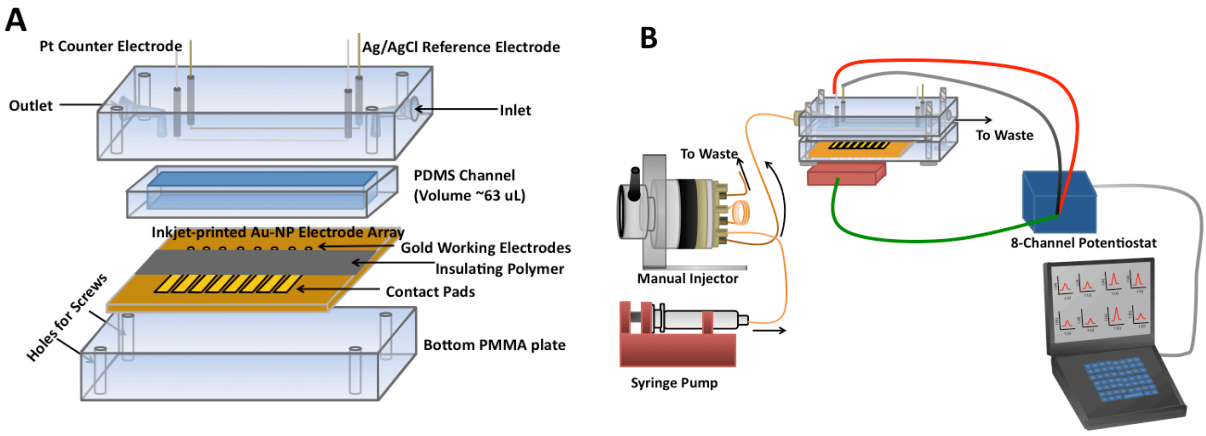

Figure 3.1 **(A)** The disposable ink-jet printed array incorporated into the microfluidic device consisting of soft PDMS channel and to PMMA plates, the top containing ports for both inlet and outlet for fluid to flow threw. The top PMMA also contains both the Pt counter and Ag/AgCl reference electrodes. **(B)** The experimental set up for the microfluidic device containing the 8-electrode potentiostat and computer readout.

3.3.3 Fabrication of gold electrode arrays

Gold arrays were fabricated as described previously by Jensen et al. using a Dimatrix Inkjet materials printer.[33] The gold nanoparticle ink was prepared, using toluene to a concentration of 100 mg mL^{-1} and filtered with a 0.2 μm cutoff PTFE filter and injected into a liquid crystal Dimatix printer cartridge immediately prior to use. [33] Once

the gold was printed, the arrays were then sintered for 15 mins at 200°C. [33] The arrays lightened in color indicating loss of the dodecane thiol layer and formation of percolated paths.[34] The poly(amic acid) ink was also prepared, as previously reported, [33] by diluting the 10% (m/m) poly(amic acid) solution in highly pure N-methyl-2-pyrrolidone (NMP) to 1% (m/m) and assed to a liquid crystal Dimatix printer cartridge immediately prior to use.

3.3.4 Preparation of magnetic Ab_2-tosyl or streptavidin magnetic beads (MB)-HRP conjugates

Ab_2-MB-HRP bioconjugates were prepared as previously described using either tosylactivated or streptavidin-coated magnetic beads (Figure 3.2).[17,18] As previously noted, an Invitrogen Dynal magnet was used to help complete all washing and separation steps required for conjugation of biomolecules to the magnetic beads. Briefly, either 2 mg of tosyl-MBs or 0.2 mg of streptavidin-MBs were combined with 3 mg HRP and 0.8 mg Ab_2 or 0.2 mg biotin-HRP and 0.8 mg biotin-Ab_2 in a microcentrifuge tube. The total volumes of the conjugation mixtures were ~580 μL for the tosyl-MBs (the bulk of which consisted of a mixture of 3 M ammonium phosphate buffer and 0.1 M sodium borate buffer) and ~200 μL for the streptavidin-MBs (beads were suspended in 0.1% BSA in phosphate buffer). The resulting mixtures were incubated at 37°C in an Invitrogen Dynabeads MX mixer for either 24 h (tosyl-MBs) or 25 mins (streptavidin-MBs). This incubation period facilitated conjugation of HRP and Ab_2 molecules to the bead surfaces. After conjugation, beads were washed with either PBS-T20 (tosyl-MBs) or 0.1% BSA in phosphate buffer (streptavidin-MBs) to remove excess, unbound HRP and Ab_2. Following washing, tosyl-MBs were suspended in 0.5% BSA in PBS and incubated for

an additional 18 h to remove any remaining unreacted tosyl moieties. After sufficient washing in 0.1% BSA in phosphate buffer, Ab_2-MB_{tosyl}-HRP and Ab_2-$MB_{streptavidin}$-HRP were separately suspended in 0.1% BSA in phosphate buffer at 3.2 mg MBs mL^{-1} and 1 mg MBs mL^{-1}, respectively, and stored at 4°C until further use. Both MB conjugates were stable for ~14 days.

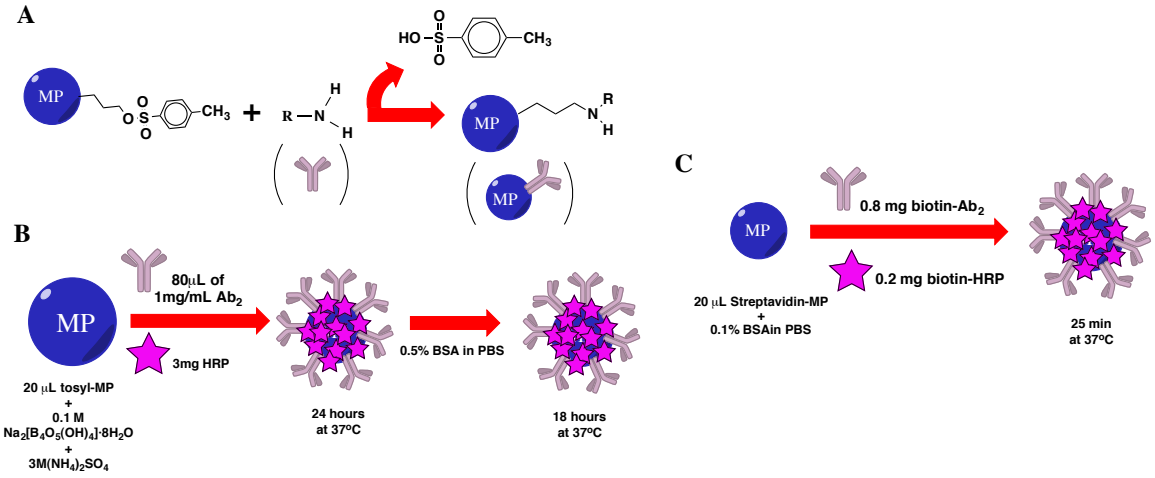

Figure 3.2 (A) The covalent attachment of antibodies to the tosyl functionalized magnetic particles. The tosyl groups act as good leaving groups for surface amine groups present on antibodies to attach. **(B)** The complete conjugation prep for both the attachment of antibodies as well as HRP enzyme labels using tosyl magnetic particles. **(C)** The complete conjugation prep for both the attachment of antibodies as well as HRP enzyme labes using streptavidin magnetic particles.

3.3.5 Off-line protein capture with tosyl or streptavidin magnetic beads

Previously reported procedures were followed to capture the antigen of interest (IL-6 or IL-8) from standard solutions that were prepared using undiluted calf serum. [15,18] Capture of antigen was performed using 60 μL of MBs for Ab_2-MB_{tosyl}-HRP or Ab_2-$MB_{streptavidin}$-HRP conjugates, respectively, in a microcentrifuge tube. Ab_2-MB-HRP conjugates were mixed with the antigen sample – and 60 μL of sample for either (for capture using Ab_2-MB_{tosyl}-HRP) or (for capture using Ab_2-$MB_{streptavidin}$-HRP). PBS containing 0.1% BSA was added to bring the total volume of the mixture to ~400 mL (for capture using Ab_2-MB_{tosyl}-HRP) or (for capture using Ab_2-$MB_{streptavidin}$-HRP). The resulting mixture was then vortexed, placed in a mixer, and incubated at 37^{o}C for 25 mins (for capture using Ab_2-MB_{tosyl}-HRP or Ab_2-$MB_{streptavidin}$-HRP) for shorter assay times this step was reduced down to 3mins. After this time, Ab_2-MB-HRP conjugates with captured antigen were washed twice with 0.1% BSA in PBS to remove any excess unbound antigen. Ab_2-MB_{tosyl}-HRP or Ab_2-$MB_{streptavidin}$-HRP conjugates with captured antigen were suspended in 0.1% BSA in PBS at concentrations of 1024 μg mL^{-1} MB_{tosyl} and 125 μg mL^{-1} $MB_{streptavidin}$, respectively, and used immediately in immunoassays.

3.3.6 Fabrication of the Immunosensor

Prior to forming the self-assembled monolayers (SAM) on the surface of the gold arrays with 3-mercaptopropionic acid (MPA), each of the gold arrays were cleaned in 0.18 M sulfuric acid applying 20 sweep segments between -0.2 V and 1.5 V at 100 mV s^{-1}. Once the gold arrays were cleaned, removing any excess oxide species, the arrays were rinsed with water, then ethanol, and finally submerged in 4 mM (MPA) in ethanol for 24

hours. Arrays were then washed with ethanol followed by water and dried with nitrogen gas.

The end carboxylic acids groups from SAM on the array surface were then activated by placing 1μL of 400 mM EDC and 100 mM NHSS on each electrode (8 electrodes) of the array. The array was then rinsed with water after 10 mins and primary antibody (Ab_1) was attached by amidization between the activated carboxylic groups of the SAM and the Ab_1 (stock solution of 100 μgmL^{-1}) and left overnight in the fridge at 20^oC. The following morning, arrays were washed with PBS T-20 followed by PBS. This was then preceded by addition of 2% BSA to block nonspecific binding (NSB) on the surface of each array for 1 hour. Once the blocking step was complete, the arrays were again washed with PBS T-20 followed by PBS. Arrays were then ready to be placed in the microfluidic device (Figure 3.1). The Ab_2-MB-HRP conjugate with off-line captured IL-6 or IL-8 were injected into the microfluidic channel at a flow rate of 100 $\mu Lmin^{-1}$. When the bioconjugate arrived in the channel, as evident by the red-brown MB color, flow was stopped and incubated for 15 mins on the sensor surface (for shorter assay times, this step was reduced to 3 mins). The last step was washing with 0.05%Tween-20 in PBS. Then detection was completed using 1 mM hydroquinone (HQ) that was passed through the microfluidic channel at 100 $\mu Lmin^{-1}$. The amperometric signal was generated at -0.2 V vs Ag/AgCl by injecting the mixture of 100 mM H_20_2 and 1 mM HQ in PBS.

3.3.7 Characterization of Array Surfaces After Modification by AFM

Tapping mode AFM images of the working electrode of the Au-arrays after cleaning in 0.18 M *sulfuric acid* revealed a mean surface roughness of 26 ± 2 nm (Figure

3.3A) which is comparable to that previously reported by Jensen *et. al.*[33] The morphology of the array after the immobilization of Ab_1 had a surface roughness of 13 ± 1 nm (Figure 3.3B). The globular features demonstrate the immobilization of Ab_1 on the surface with nearly full coverage across the electrode surface. After full immunoassay was performed with the introduction of BSA as well as the bioconjugate (Ab_2-MB-HRP), which resulted in filling the space between the primary antibodies, the surface roughness increased to 32 ± 2 nm with much larger globular features (Figure 3.3C). The much larger globular features further demonstrate the immobilization of the full immunoassay on the surface.

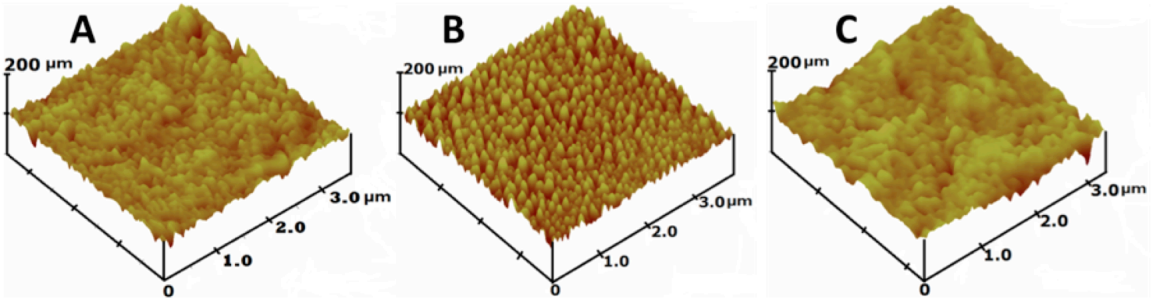

Figure 3.3 High resolution tapping mode AFM images of one of the eight sensor electrodes of **(A)** a bare AuNP array after cleaning in 0.18M H_2SO_4 , **(B)** AuNP array with Ab_1, and **(C)** AuNP array + Ab_1+ bioconjugate (Ab_2-MB-HRP).

3.4 Results and Discussion

3.4.1 Characterization of electrode arrays

Prior to each immunoassay, each of the gold arrays were cleaned in 0.18 M sulfuric acid, applying 20 sweep segments between 1.5 V and -0.2 V at 100 mVs^{-1}. It shows similar peaks to those found from bulk gold with formation of gold oxide at +1.2

V and reduction back to bulk gold occurring at 0.9 V shown in Figure 3.4A.[35] From these CVs, the active surface area was calculated following Trasatti et. al.[36] to be 0.42 (± 0.02) mm^2 for an individual array with RSD < 5%. This is comparable to the surface area calculated by Jensen et al of 0.35 ± 0.01 mm^2 in ferricyanide solution using the Randles-Sevcik equation.[33] However, the average surface area calculated over 20 arrays was found to be 0.46 ± 0.1 mm^2, giving an RSD of 22%. Therefore, each amperometric response was surface area corrected due to higher RSD in array-to-array reproducibility. To further assess the reproducibility of the array, amperometric signals were measured on all electrodes in the microfluidic device after injection of 100 mM $Fe(CN)_6^{3-/4-}$/ 0.1 M KCL. All eight electrodes of the array gave similar peak currents (Figure 3.4B), with average 2.3 (± 0.13) x 10^{-6} Acm^{-2} (RSD < 6%) demonstrating the minimum cross-talk between neighboring electrodes of the array.

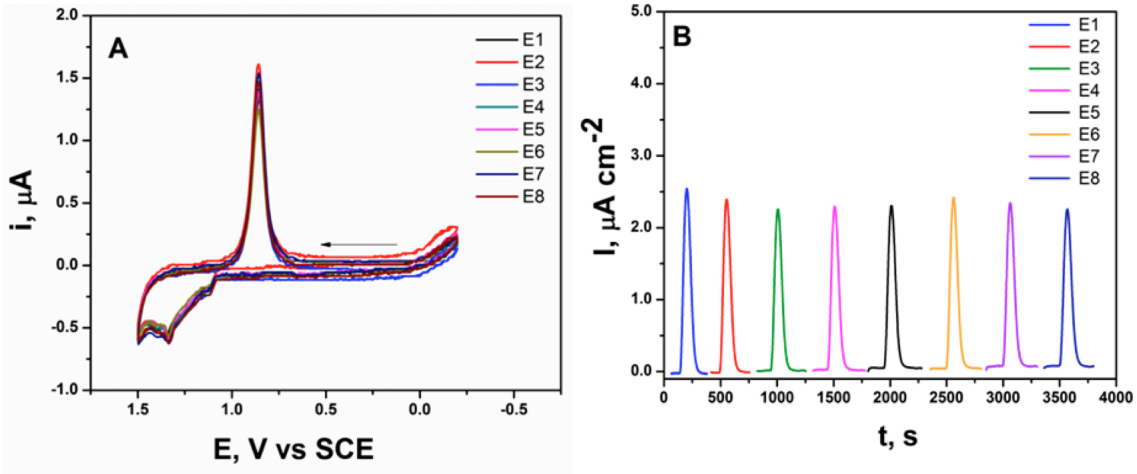

Figure 3.4 Array reproducibility: **(A)** CVs at 100 mV s^{-1} on 8-electrodes of the printed gold arrays in 0.18 M H_2S0_4. **(B)** Amperometric response at 0.1 V vs Ag/AgCl in the

microfluidic device after injection of 100 mL of 100 mM $Fe(CN)_6^{3-/4-}$ in 100 mM potassium chloride at 100 mL min^{-1}.

3.4.2 Immunoassay development

All sensor arrays prior to SAM of MPA were first cleaned by cycling in 0.18 M sulfuric acid to remove gold oxide from the surface. Immunoassay was then developed by covalently binding primary antibodies onto the SAM layers on each of the gold sensor surfaces. Using the off-line capture procedure as reported previously,[4,39] a single concentration of each analyte was used per array.

In order to control non-specific binding of the bioconjugates, 2% BSA was employed along with washing steps containing 0.05% T-20 and PBS. All assay parameters, including concentrations and incubation times, were optimized to obtain high sensitivity and low signal to noise. The analyte proteins were captured off-line by the heavily labeled antibody–equipped magnetic bead conjugates. Once captured, the bioconjugates were dispersed and then used to fill the sample loop and finally injected into the microfluidic chamber. The flow was stopped and 15 mins incubation was allowed to capture bioparticles by antibodies on the electrode surface. This was then followed by a wash with 0.05% T-20 in PBS.

Once the surface was washed, a mixture of 1 mM HQ mediator and 0.1 mM H_2O_2 was injected into the microfluidic device to generate the amperometric response. The amperometic response is generated by H_2O_2 activating HRP to the ferryloxy form, which is reduced by electron mediator HQ. Control experiments contained the full immunoassay procedure without antigens (IL-6 and IL-8). The total assay time was 45

mins, this was obtained by adding all times after antigen (IL-6 or IL-8) was added. This included the first incubation, in the off-line capture format that was 25 mins, the second incubation, where the conjugate was incubated on the surface of the array, reduced from 15 mins, along with wash steps and detection that took less than 4mins to perform.

Using the above procedures, peak current densities increased logarithmically from 156 fgmL^{-1} to 3,750 fg mL^{-1} with tosyl magnetic beads for IL-6 with a detection limit of 156 fgmL^{-1}, which yields a signal that is three times the average standard deviation above the signal exhibited by the control. Representative amperometric responses are shown in Figure 3.5A and corresponding calibration in Figure 3.5B, which confirmed the high sensitivity that the tosyl-MB conjugates could achieve.

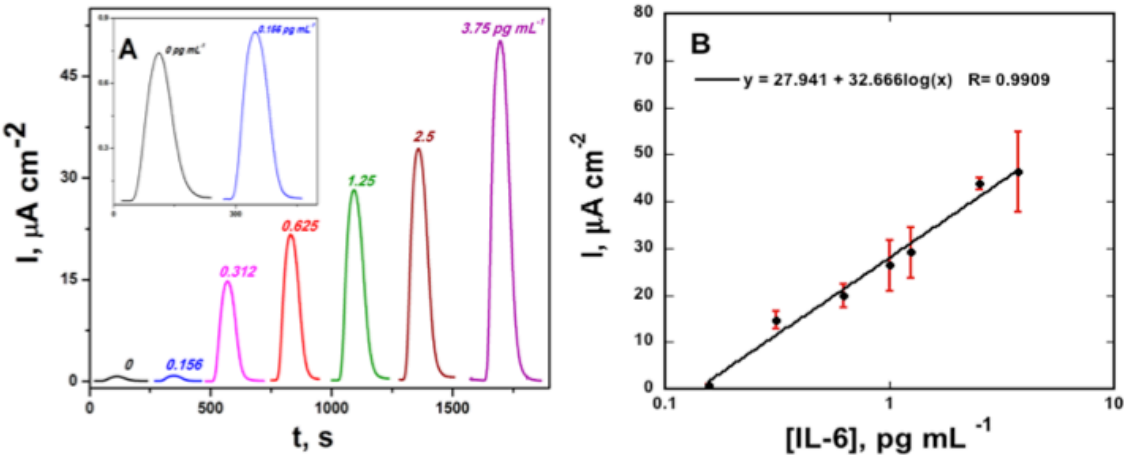

Figure 3.5 (A) Amperometric responses of IL-6 at -0.2 V developed by injecting 1 mM HQ and 0.1 mM H_2O_2 after capturing analyte -MB_{tosyl}-Ab_2-HRP bioconjugates on the electrodes in the microfluidic device. **(B)** Corresponding calibration curve y= 2.79x10^{-5} + 3.27x 10^{-5} log(x); R= 0.99.

The Ab_2-MB_{tosyl}-HRP conjugate preparation took approximately 42 hours; therefore, we decided to try streptavidin-coated magnetic particles with a total conjugate preparation time of 25 minutes in efforts to reduce conjugate preparation time. However, with a drastic reduction in preparation time, a decrease in sensitivity was observed in the calibration plot. The streptavidin magnetic beads ($MB_{streptavidin}$) containing IL-6, had peak current densities increasing logarithmically from 39 $fgmL^{-1}$ to 2500 $fgmL^{-1}$. The detection limit determined from three times the average standard deviation above the control was determined to be 78 $fgmL^{-1}$. Representative amperometric responses are shown in Figure 3.6A and corresponding calibration in Figure 3.6C. The slope of the calibration curve was able to demonstrate the slightly lower sensitivity that was achieved with the shorter $MB_{streptavidin}$ conjugate preparation.

We also obtained a calibration curve for IL-8 in undiluted serum similar to that of IL-6 with the $MB_{streptavidin}$. As before, we kept the concentration of primary antibody at 100 μgmL^{-1} and concentration for secondary antibody at 20 μgmL^{-1}. From these optimum concentrations of antibodies, a calibration plot was obtained. The peak current densities increased logarithmically from 19 $fgmL^{-1}$ to 5000 $fgmL^{-1}$ with streptavidin magnetic particles for IL-8 with a detection limit of 19 $fgmL^{-1}$. Representative amperometric responses are shown in Figure 3.6B and corresponding calibration in Figure 3.6C. The slopes of the calibration plots for both IL-6 and IL-8 indicated similar sensitivities for both biomarkers.

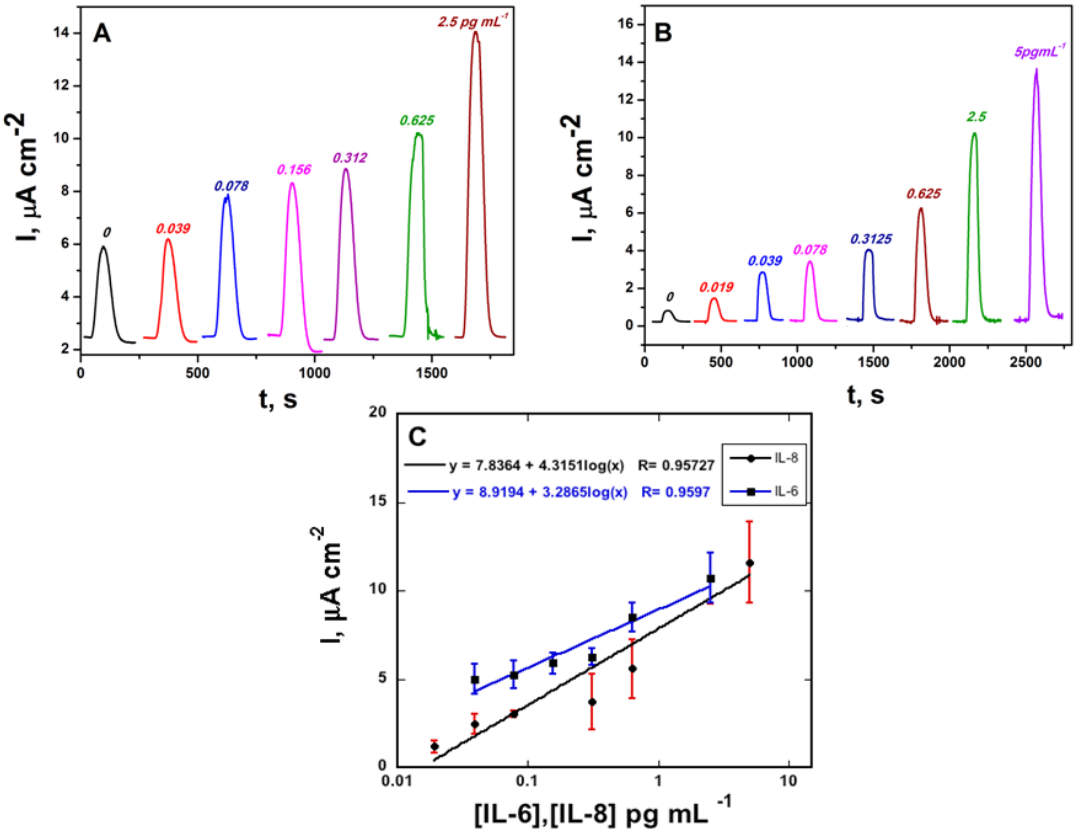

Figure 3.6 Amperometric responses of IL-6 **(A)** and IL-8 **(B)** at -0.2 V developed by injecting 1 mM HQ and 0.1 mM H_2O_2 after capturing analyte protein- Ab_2-$MB_{streptavidin}$-HRP conjugates on the electrodes in the microfluidic device. **(C)** Corresponding calibration curves for IL-6 (in blue), y= $8.91x10^{-6}$ + $3.29x\ 10^{-6}$ log(x); R= 0.96, and for IL-8 (in black) ,y= $7.84x10^{-6}$ + $4.31x\ 10^{-6}$ log(x); R=0.96.

3.4.3 Reducing Total Assay Time

Current methods of protein detection require long incubations leading to long assay times. Once we obtained calibration curves for really low concentrations of IL-8 and IL-6, we then wanted to try and reduce the entire assay time to below 10 minutes to further its ability to be used as a point-of-care sensor. In our assay procedures, total assay time was obtained by adding all times after antigen (IL-6 or IL-8) was added. Again, this included the first incubation, in the off-line capture format that was reduced from 25 mins to 10 mins, and finally down to 3 mins, the second incubation, where the conjugate was incubated on the surface of the array, reduced from 15 mins to 5 and finally to 3, along with wash steps and detection that was reduced and took less than 2 mins to perform. We kept a control, containing 0 $pgmL^{-1}$ of IL-6 , or IL-8 in serum , and sample, containing 20 $pgmL^{-1}$ (IL-6) or 10 $pgmL^{-1}$ (IL-8) for each of the selected assay times shown in Figure 3.7A (IL-6), and Figure 3.7B (IL-8). Therefore, the overall assay time from incubation of sample with Ab_2-MB-HRP to measurement including wash steps was 8 mins. By sacrificing detection limits to lower picogram levels rather than femtogram levels we are able reduce assay times down to 8 mins.

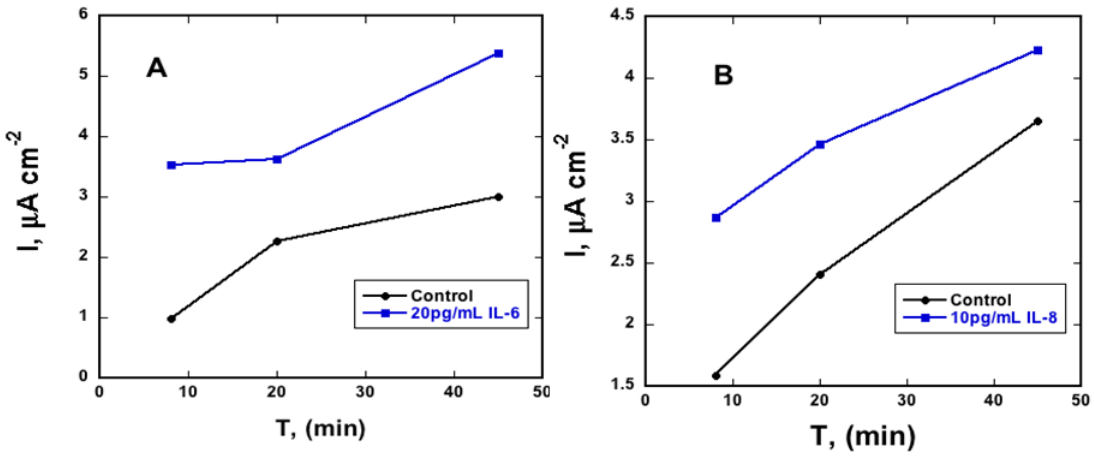

Figure 3.7 Optimization of assay time for Interleukin-6 reducing the time down to 45, 20, and 8 mins for (A) IL-6 and (B) IL-8.

To fully demonstrate the assay could be completed in 8 mins, we obtained calibration curves for both IL-6 and IL-8, keeping the concentration of both primary and secondary antibodies the same. From the calibration plot of both IL-6, and IL-8 we observed a detection limits of 5 $pgmL^{-1}$ which remains in the clinical range for both IL-8 and IL-6.[8,9] The peak current densities increased linearly from 5 $pgmL^{-1}$ to 200 $pgmL^{-1}$ for both cancer biomarkers. Representative amperometric responses for both IL-6 and IL-8 at 8 min assay times are shown in Figure 3.8A (IL-6) and Figure 3.8B (IL-8), along with corresponding calibration curves (Figure 3.8C). Calibration curves shown in Figure 3.7C confirm that high sensitivity can be achieved in spite of the short assay times.

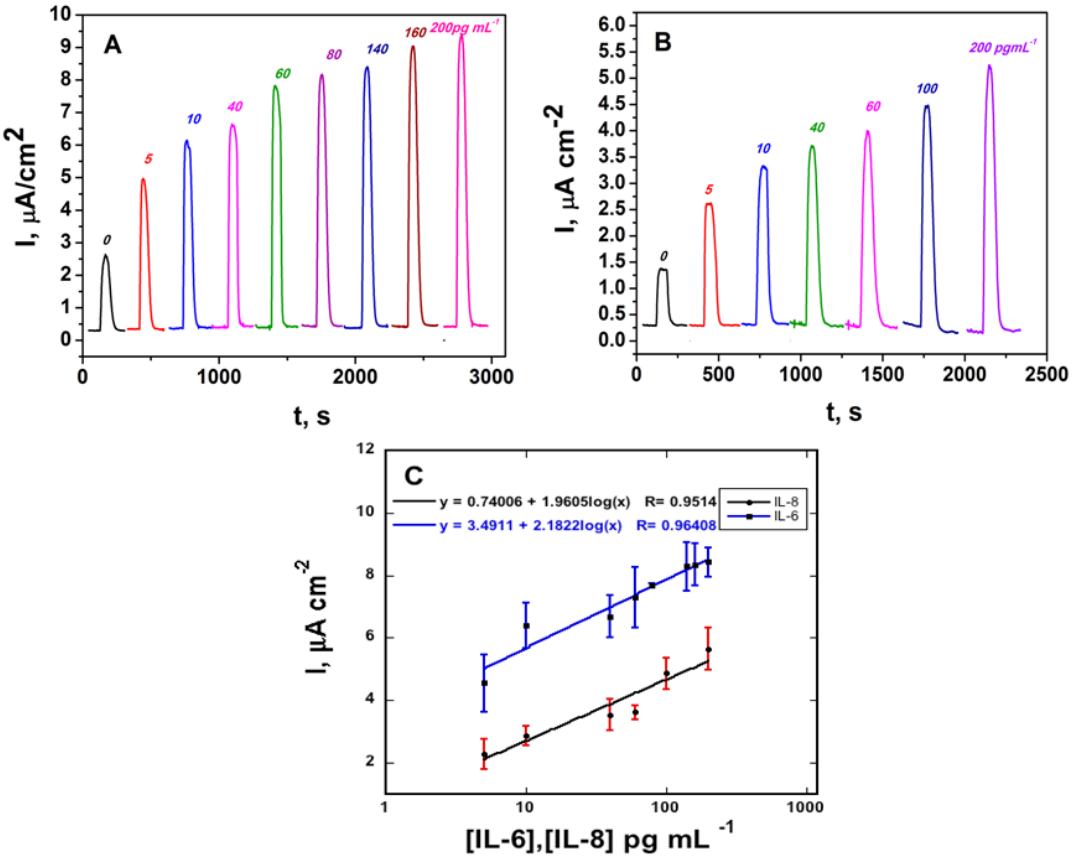

Figure 3.8 Amperometric responses of IL-6 **(A)** and IL-8 **(B)** at -0.2 V developed by injecting 1 mM HQ and 0.1 mM H_2O_2 after capturing analyte protein Ab_2-$MB_{streptavidin}$-HRP conjugates on the electrodes in the microfluidic device. **(C)** Corresponding calibration curves for IL-6 (in blue), y= $3.49x10^{-6}$ + $2.18x\ 10^{-6}$ log(x); R= 0.96, and for IL-8 (in black) ,y= $0.74\ x10^{-6}$ + $1.96x\ 10^{-6}$ log(x); R=0.95.

3.4.4 Assay Validation with Conditioned Media from Oral Cancer Cells

The electrochemical immunosensor was further validated by assaying oral cancer cell lines. We used secreted levels of human IL-6 and IL-8 in conditioned media from cell cultures to verify accuracy, due to ELISA requiring considerable human serum for replicate single protein assays. Excellent correlations were obtained between the immunoarray and ELISA results (Figure 3.9A, for IL-6 and Figure 3.9B for IL-8). All of the representative HNSCC cell lines used (HN12, HN13, and Cal 27) secreted large amounts (~1000 pgmL-1) of the biomarkers when compared to non-cancer counterparts (HaCaT) cells.

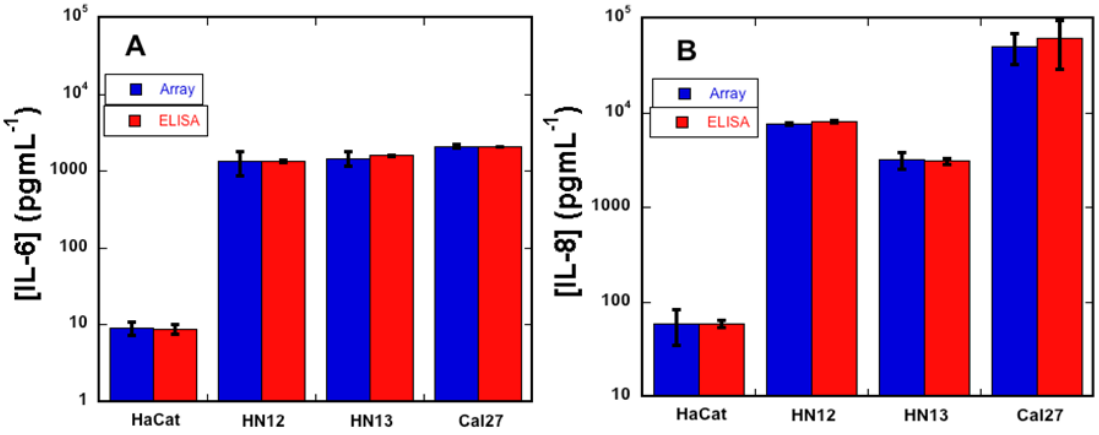

Figure 3.9 Comparison of immunoarray results with standard ELISA for conditioned media for cells (HaCaT, HN12, HN13, and Cal 27) for both IL-6 **(A)** and IL-8 **(B)**.

Total assay time remained at 8 min when detecting the oral cancer cell lines. Linear correlation plots for the immunoarray versus ELISA gave slopes close to 1.0 and intercepts within standard deviation of zero, confirming correlation (Figure 3.10).

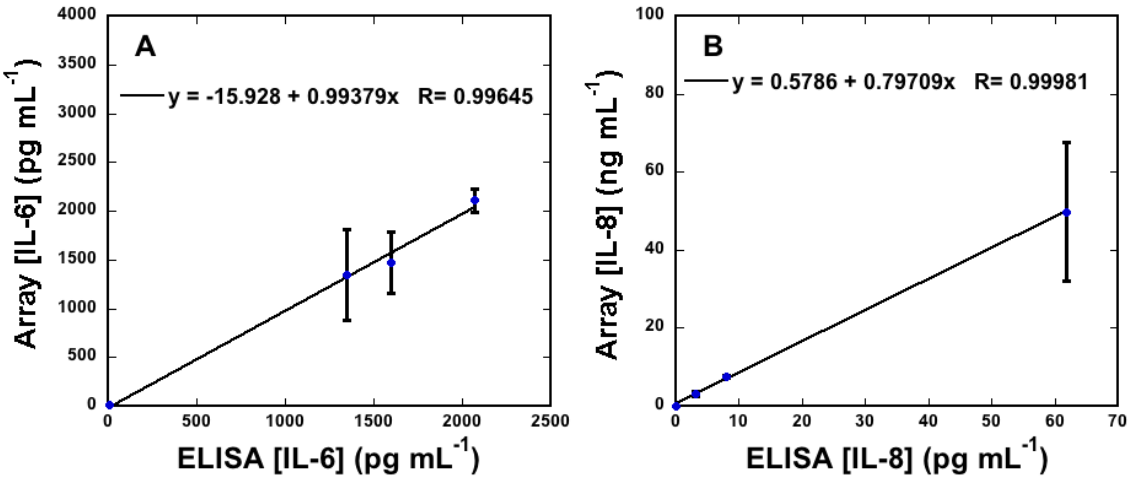

Figure 3.10 Correlation plots of immunoarray results with standard ELISA for conditioned media for cells (HaCaT, HN12, HN13, and Cal 27) for both IL-6 (A), and IL-8 (B).

3.5 Summary

Results described above demonstrate successful integration of a disposable, inkjet-printed AuNP immunoarray into a simple microfluidic device for multiple protein deteminations. Protocols involving off-line capture of proteins on heavily labeled magnetic beads for singal amplification can be optimized for either ultrasenstitive detection or rapid clinical assays in 5μL of serum. The AuNP immunoarray offers many promising features for rapid point-of-care applications, including, low cost, high

sensitivity, and multiplexing, but the current approach still requires moderate technical expertise. Operational features involving off-line capture, washing and reagent addition need to be simplified further, and we are currently addressing these issues in our laboratory.

3.6 References

(1) Weissleder, R. *Science* **2006**, *312*, 1168–1171.

(2) Czernin, J.; Allen-Auerbach, M.; Schelbert, H. R. *J. Nucl. Med.* **2007**, *48*, 78S – 88.

(3) Adams, S.; Baum, R. P.; Stuckensen, T.; Bitter, K.; Hör, G. *Eur. J. Nucl. Med. Mol. Imaging* **1998**, *25*, 1255–1260.

(4) Antoch, G.; Vogt, F. M.; Freudenberg, L. S.; Nazaradeh, F.; Goehde, S. C.; Barkhausen, J.; Dahmen, G.; Bockisch, A.; Debatin, J. F.; Ruehm, S. G. *JAMA* **2003**, *290*, 3199–3206.

(5) Schmidt, G. P.; Haug, A. R.; Schoenberg, S. O.; Reiser, M. F. *Eur. Radiol.* **2006**, *16*, 1216–1225.

(6) Ross, G. L.; Soutar, D. S.; Gordon MacDonald, D.; Shoaib, T.; Camilleri, I.; Roberton, A. G.; Sorensen, J. A.; Thomsen, J.; Grupe, P.; Alvarez, J.; Barbier, L.; Santamaria, J.; Poli, T.; Massarelli, O.; Sesenna, E.; Kovács, A. F.; Grünwald, F.; Barzan, L.; Sulfaro, S.; Alberti, F. *Ann. Surg. Oncol.* **2004**, *11*, 690–696.

(7) Kovács, A. F. *Br. J. Cancer* **2005**, *92*, 206–207; author reply 207–208.

(8) Rusling, J. F.; Kumar, C. V; Gutkind, J. S.; Patel, V. *Analyst* **2010**, *135*, 2496–2511.

(9) Rusling, J. F. *Chem. Rec.* **2012**, *12*, 164–176.

(10) Kulasingam, V.; Diamandis, E. P. *Nat. Clin. Pract. Oncol.* **2008**, *5*, 588–599.

(11) Ebert, M. P. A.; Korc, M.; Malfertheiner, P.; Röcken, C. *J. Proteome Res.* **2006**, *5*, 19–25.

(12) Tothill, I. E. *Semin. Cell Dev. Biol.* **2009**, *20*, 55–62.

(13) Hanash, S. M.; Pitteri, S. J.; Faca, V. M. *Nature* **2008**, *452*, 571–579.

(14) Wilson, D. S.; Nock, S. *Angew. Chem. Int. Ed. Engl.* **2003**, *42*, 494–500.

(15) Chikkaveeraiah, B. V; Mani, V.; Patel, V.; Gutkind, J. S.; Rusling, J. F. *Biosens. Bioelectron.* **2011**, *26*, 4477–4483.

(16) Waugh, D. J. J.; Wilson, C. *Clin. Cancer Res.* **2008**, *14*, 6735–6741.

(17) Grivennikov, S. I.; Karin, M. *Ann. Rheum. Dis.* **2011**, *70 Suppl 1*, i104–i108.

(18) Malhotra, R.; Patel, V.; Chikkaveeraiah, B. V; Munge, B. S.; Cheong, S. C.; Zain, R. B.; Abraham, M. T.; Dey, D. K.; Gutkind, J. S.; Rusling, J. F. *Anal. Chem.* **2012**, *84*, 6249–6255.

(19) Wei, F.; Patel, P.; Liao, W.; Chaudhry, K.; Zhang, L.; Arellano-Garcia, M.; Hu, S.; Elashoff, D.; Zhou, H.; Shukla, S.; Shah, F.; Ho, C.-M.; Wong, D. T. *Clin. Cancer Res.* **2009**, *15*, 4446–4452.

(20) Siegel, R.; Naishadham, D.; Jemal, A. *CA. Cancer J. Clin.* **2012***, 62*, 10–29.

(21) Horowitz, A. M.; Alfano, M. C. *J. Am. Dent. Assoc.* **2001**, *132 Suppl*, 5S – 6S.

(22) Riedel, F.; Zaiss, I.; Herzog, D.; Götte, K.; Naim, R.; Hörmann, K. *Anticancer Res.* **2005***, 25*, 2761–2765.

(23) Gokhale, A. S.; Haddad, R. I.; Cavacini, L. A.; Wirth, L.; Weeks, L.; Hallar, M.; Faucher, J.; Posner, M. R. *Oral Oncol.* **2005**, *41*, 70–76.

(24) Munge, B. S.; Coffey, A. L.; Doucette, J. M.; Somba, B. K.; Malhotra, R.; Patel, V.; Gutkind, J. S.; Rusling, J. F. *Angew. Chemie Int. Ed.* **2011**, *50*, 7915–7918.

(25) MASTERS, J. R. W. *Anticancer Res* **2007**, *27*, 1273–1276.

(26) *Topics in Fluorescence Spectroscopy*; Lakowicz, J. R., Ed.; Topics in Fluorescence Spectroscopy; Kluwer Academic Publishers: Boston, 2002; Vol. 4.

(27) Giljohann, D. A.; Mirkin, C. A. *Nature* **2009**, *462*, 461–464.

(28) Steiner, J. M.; Wilson, B. G.; Williams, D. A. *Can. J. Vet. Res.* **2004**, *68*, 309–314.

(29) Issaq, H.; Veenstra, T. *Biotechniques* **2008**, *44*, 697–698, 700.

(30) Aebersold, R.; Mann, M. *Nature* **2003**, *422*, 198–207.

(31) Ikami, M.; Kawakami, A.; Kakuta, M.; Okamoto, Y.; Kaji, N.; Tokeshi, M.; Baba, Y. *Lab Chip* **2010**, *10*, 3335–3340.

(32) Li, Z.; Konno, T.; Takai, M.; Ishihara, K. *Biosens. Bioelectron.* **2012**, *34*, 191–196.

(33) Jensen, G. C.; Krause, C. E.; Sotzing, G. a; Rusling, J. F. *Phys. Chem. Chem. Phys.* **2011**, *13*, 4888–4894.

(34) Sivaramakrishnan, S.; Chia, P.-J.; Yeo, Y.-C.; Chua, L.-L.; Ho, P. K.-H. *Nat. Mater.* **2007**, *6*, 149–155.

(35) Cadle, S. H.; Bruckenstein, S. *Anal. Chem.* **1974**, *46*, 16–20.

(36) Trasatti, S.; Petrii, O. A. *Pure Appl. Chem.* **1991**, *63*, 711–734.

Chapter Four

Ultrasensitive Microfluidic Array for Serum Pro-Inflammatory Cytokines and C-Reactive Protein to Assess Oral Mucositis Risk in Cancer Patients

4.1 Abstract

Oral mucositis is an inflammatory lesion of oral mucosa caused by high dose chemo- and/or radiation therapy. These oral lesions adversely impact clinical management of cancer patients, and can result in hospitalization, infection, and delay of therapy. There is need for novel technology to aid in predicting severity of oral mucositis and implementing personalized therapies. We describe here a semi-automated, modular microfluidic immunoarray optimized for ultrasensitive detection of pro-inflammatory cytokines involved in pathobiology of oral mucositis. These biomarkers include tumor necrosis factor (TNF-α), interleukin-6 (IL-6), interleukin-1β (IL-1β), and C-reactive protein (CRP). Using a modular microfluidic array device, protein analytes were captured from serum in a capture chamber by 1 μm magnetic beads coated with antibodies and enzyme labels. These beads are transported downstream to a detection chamber containing an 8-sensor array coated with glutathione-gold nanoparticles (GSH-AuNP) and a second set of antibodies to capture the beads with analyte proteins. Ultralow detection limits of 10-40 fg mL^{-1} in 5 μL serum were achieved for simultaneous detection of the four proteins in 30 min, for mass detection limit of 2.5-10 zeptomoles, or as few as

1500 molecules. Accuracy and diagnostic utility of the arrays was demonstrated by correlation of levels of the four biomarker proteins in serum from head and neck cancer patients with results from standard ELISA. This approach may lead to rapid, low-cost estimates of projected risk for severity of oral mucositis in cancer patients to enable improved therapeutic management. This general method can be adapted to other protein panels.

4.2 Introduction

High-dose chemotherapy or radiation utilized for treatment of cancer generates a complex inflammatory response in mucosal tissue called *mucositis*. The pathobiology is characterized by initial up-regulation of reactive oxygen species that can damage adjacent cells as well as cause activation of cell signaling pathways that escalate the mucosal injury.[1,2] At the clinical level, oral mucositis is a frequent and debilitating complication of cancer therapies.[1,2,3,4] This painful inflammation and ulceration of the oral mucosa can adversely affect patient's quality of life, threatens the efficacy of anticancer therapy, and increases healthcare costs.[1,2,3,4,5]

Given the clinical and health economic importance of mucositis, there has been an increasing trajectory of basic and clinical research directed to this cancer treatment toxicity over the past 15 years. This progress has led to the contemporary pathobiologic model that includes activation of transcription factor nuclear factor-κB (NF-κB) as a consequence of chemotherapy and radiotherapy that may contribute to the development of mucositis.[1,2,3,4,5,6,7] Among the many genes up-regulated by activation of NF-κB are those responsible for production of pro-inflammatory cytokines tumor necrosis factor α

(TNF-α), interleukin-6 (IL-6) and interleukin-1β (IL-1β). [1,2,3,4,5,6,7] Increased levels of these cytokines in tissues and peripheral blood coincide with non-hematological toxicity caused by radiation and chemotherapy and lead to tissue injury and cell apoptosis.[2,5,6] Measurements of NF-κB, TNF-α, IL-6 and IL-1β in the sera of rat models showed that concentrations of these proteins increase following the administration of chemotherapeutic agents.[3] In most cases, these elevations in serum concentrations occurred subsequent to histological changes associated with alimentary tract mucositis. Experimental models show that drug-induced inhibition of the production of pro-inflammatory cytokines TNF-α, IL-6 and IL-1β lessens the severity and frequency of mucositis.[1,2,5] High levels of C-reactive protein (CRP), another acute-phase protein over-expressed in response to inflammation, have also been detected in sera of patients with radiation-induced mucositis.[8,9]

Protein biomarkers in patient samples can be measured with enzyme-linked immunosorbent assays (ELISAs) or newer bead-based assays[10,11,12] with detection limits in the 1-10 pg mL^{-1} range. These technologies are limited for clinical and point-of-care use by cost, time and sample consumption.[13] Faster, low-cost, more sensitive, multiplexed methods are needed for measuring protein biomarkers to provide timely patient diagnostics.[10,13,14,15] For oral mucositis, such multiplexed biomarker measurement strategies could in the future enhance prediction of severity and frequency of mucositis based on personalized biomarker profiles at early stages of cancer treatment.

We recently developed a prototype microfluidic electrochemical immunoarray that is 10-100 times more sensitive and faster than traditional ELISA and bead-based assays using off-line capture of protein analytes.[16,17,18,19,20] Assay protocols employ

magnetic beads decorated with massive numbers of enzyme labels and antibodies to efficiently isolate target proteins from serum and greatly enhance sensitivity. Massively labeled magnetic beads, a modular microfluidic platform, and nanostructured sensor enable rapid, ultrasensitive, simultaneous detection of biomarker proteins in small-volume serum samples (~5 μL).[16,17,18,19,20] The off-line capture strategy was effectively used to measure IL-6 and prostate specific antigen (PSA) in serum samples from prostate cancer patients[16] and IL-6, IL-8, vascular endothelial growth factor (VEGF) and VEGF-C in sera of oral cancer patients.[17]

In the present paper, we adapt the analyte capture strategy to detect the panel of biomarkers associated with oral mucositis in serum samples using a semi-automated on-line capture format. This novel approach adds a protein capture chamber upstream of the 8-sensor detection chamber.[21] The modular microfluidic device first delivers the sample to this capture chamber, where enzyme-labeled magnetic beads equipped with antibodies capture each target protein. Then, the beads are washed under magnetic control and delivered to a nanostructured 8-sensor array decorated with a second set of antibodies that recognize and sort the magnetic bead-bound target proteins. After washing, the biomarker proteins are measured simultaneously by activation of enzyme labels and electrochemical detection. We report here the first true multiplexed application of this technology to simultaneous ultrasensitive detection of 4 proteins.

Target proteins TNF-α, IL-6, IL-1β and CRP were selected for their reported links to oral mucositis.[1,22] These pro-inflammatory cytokines play essential roles in the regulation of immune response to malignances.[23,24] Previous reports demonstrated markedly elevated serum levels of each of these proteins in patients with head and neck

(H&N) cancer compared to healthy controls.[24] Herein, we demonstrate that the four proteins can be measured accurately, quickly, and with high sensitivity using the novel on-line capture microfluidic immunoarray. Ultralow detection limits of 10-40 fg mL^{-1} were achieved for multiplex detection of the 4 oral mucositis biomarkers in 5 μL serum (2.5-10 zeptomoles). Accuracy was verified by agreement of ELISA values with microfluidic immunoassay results for spiked and unspiked serum samples from head and neck cancer patients undergoing radiation therapy.

4.3 Experimental

4.3.1 Antibodies and Proteins

Tumor Necrosis Factor (TNF-α) Duoset (catalog # DY210), Human C-Reactive Protein (CRP) Duoset (catalog # DY1707), and Interleukin-1β (IL-1β) Duoset (catalog # DY201) were from R&D systems, Inc. Human Interleukin-6 (IL-6) standard ELISA kit (catalog # 900-K16) was from PeproTech. Lyophilized 99% bovine serum albumin (BSA) and calf serum were from Sigma-Aldrich.

4.3.2 Chemicals

Screen-printed carbon arrays with 8 sensors (700 μm dia.) were from Kanichi Research, Ltd. L-Glutathione reduced (GSH, 99%), gold (III) chloride trihydrate ($HAuCl_4 \cdot 3H_2O$, 99.9%), sodium borohydride (99%), poly(diallyldimethylammonium chloride) (PDDA, MW 100,000-200,000, 20%), 1-(3-(Dimethylamino)propyl)-3-ethylcarbodiimide hydrochloride (EDC), N-hydroxysulfosuccinimide (NHSS), Tween-20,

hydroquinone (HQ, ≥ 99%), lyophilized 99% bovine serum albumin (BSA), and calf serum were from Sigma-Aldrich. Hydrogen peroxide (H_2O_2, 30%) was from Fisher. The polydimethylsiloxane (PDMS) kit was from Dow Corning. Buffer pH 7.4 phosphate saline (PBS) was 0.01 M in phosphate, 0.14 M NaCl, 2.7 mM KCl. Streptavidin-coated 1μm diameter magnetic beads (SA-MP) were from Life Technologies. All solutions were prepared with water purified by a Hydro water purification system to 18 MΩ•cm.

4.3.3 Human Serum Samples

Human serum samples were collected from patients undergoing high-dose radiation therapy for H&N cancer at the Neag Comprehensive Cancer Center, University of Connecticut Health Center (UCHC). The study protocol was IRB approved and written Informed Consent of participants was obtained prior to sample collection. All samples were stored at or below -80^{o}C until use. Serum samples were assayed directly and in selected cases spiked with biomarker proteins for validation tests.

4.3.4 Instrumentation

Amperometric measurements were made with a CHI 1040A eight-channel potentiostat at room temperature at conditions optimized for high sensitivity and low S/N, i. e. current was measured at all 8 sensors simultaneously with sensor electrodes held at -0.2 V vs. Ag/AgCl reference at solution flow rate 100 μL min^{-1}.

The online microfluidic device features a syringe pump (Harvard, no. 704504), injector valve (Rhedodyne, 9725i), capture chamber containing a tiny magnetic stir bar, a switching valve to change the direction of fluid flow, and a detection chamber that

housed sensors, reference and counter electrodes (Figure 4.1).[21] The capture chamber features a layer of molded, flexible PDMS, contained between two poly(methylmethacrylate) (PMMA) plates to form an oval cylindrical channel 1.5 mm wide and 100 ± 2 μL in volume that houses a tiny magnetic stir bar. The top PMMA plate featured two female ports (4 mm diameter) for screwing in standard male plastic fittings (1.5 mm i.d., Upchurch) to hold 0.2 mm i.d. PEEK connecting tubing for an inlet and outlet. The detection chamber (Figure 1B) features a layer of molded, flexible PDMS sandwiched between two PMMA plates to form a rectangular channel 1.5 mm wide and 2.8 cm long and 63 ± 2 μL in volume. The top PMMA plate again features the two female ports (4 mm diameter) and in addition is equipped with holes for Ag/AgCl reference electrode (0.6 mm dia.) and Pt counter electrode (0.2 mm dia.). The syringe pump was connected to two switch valves through a sample injector using 0.2 mm i.d. tubing. The two valves are used to either direct flow to waste or to the detection chamber.

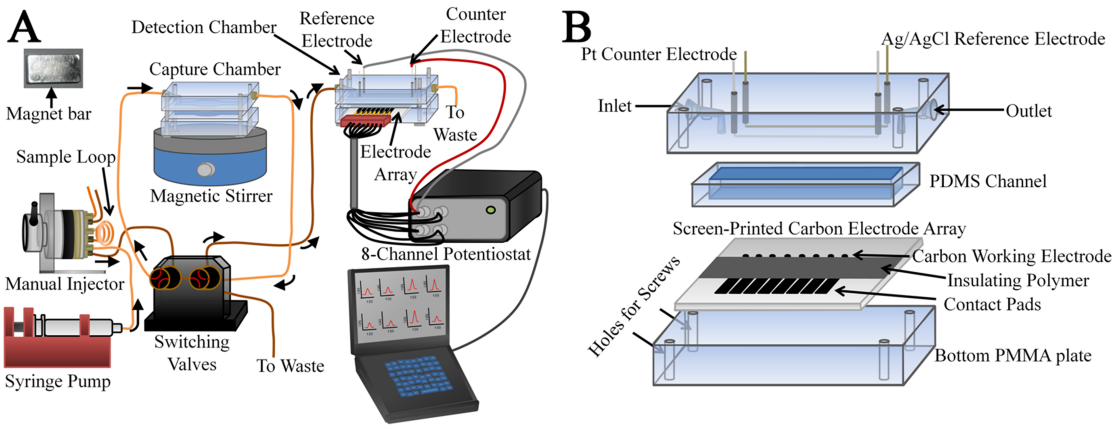

Figure 4.1 Illustrated representations of the **(A)** on-line capture setup featuring syringe pump, a manual injector, sample loop, capture chamber on-top a magnetic stirrer, switching valves, detection chamber, 8-channel potentiostat and computer read-out; **(B)** the detection chamber that is used to house the 8-electrode array and both the Pt counter and Ag/AgCl reference electrodes.

4.3.5 Array Fabrication

The carbon electrode arrays were coated with sequential layers of the polycation PDDA and 5 nm GSH-AuNPs using a layer-by-layer electrostatic adsorption technique as previously reported.[25] The surface carboxyl groups of the GSH-AuNPs were then activated by EDC and NHSS to attach the primary antibodies (Ab_1) to the arrays through amidization.[16,17] The electrode arrays were washed and incubated with 2% BSA in PBS for 1 hr to block non-specific binding (NSB). For electrochemical measurements, Ab_1-modified electrode array (Figure 4.2A) was positioned in a detection chamber, which consisted of a microfluidic channel with reference and counter wire electrodes (Figure

4.1B). A new AuNP-antibody array was inserted into the detection chamber for each assay.

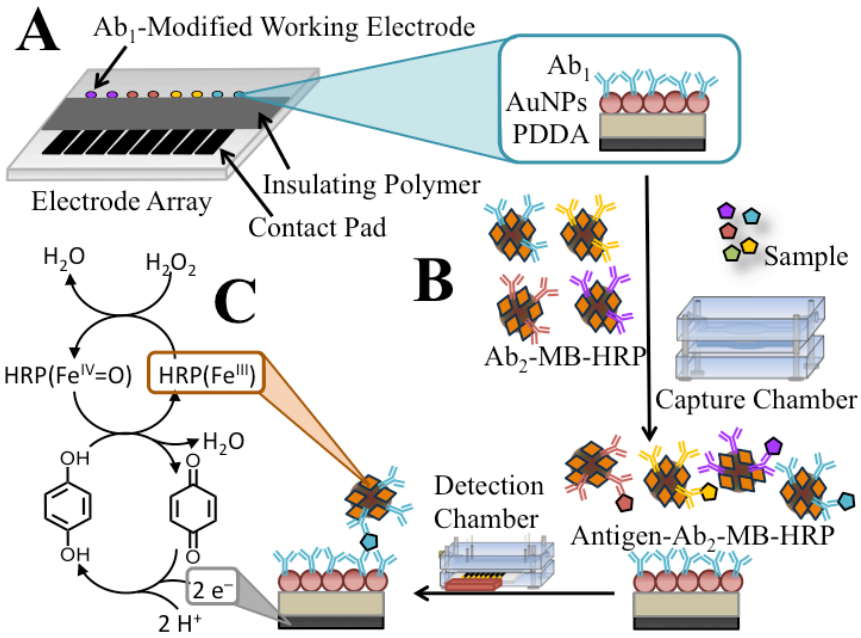

Figure 4.2 Immunoassay strategy for detection of the four protein analytes on **(A)** the Ab_1-modified electrode surface. **(B)** On-line capture of protein analytes onto the Ab_2-MP-HRP in the capture chamber to form protein-bead bioconjugates. **(C)** Amperometric signal generation by injecting a mixture of 1 mM HQ, electron mediator, and 0.1 mM H_2O_2 into the detection chamber.

4.3.6 Preparation of Ab_2-magnetic particle-HRP bioconjugates

Both biotinylated secondary antibodies (Ab_2) and biotinylated horseradish peroxidase (HRP) labels were attached to 1µm diameter streptavidin-coated superparamagnetic beads as previously reported.[17] Briefly, 10 µL of magnetic particles

(10 mg mL^{-1}) were washed three times with 0.1% BSA in PBS pH 7.4 and then reconstituted with 40 μL of 0.1% BSA in PBS pH 7.4. 40 μL of biotinylated-HRP (2.5 mg mL^{-1}) and 20 μL of the optimal concentration for biotinylated-Ab_2 (Figure 3), were simultaneously added to the magnetic bead particle dispersion. The reaction proceeded at 37°C for 25 mins for the conjugation to occur. Following the conjugation, the beads were magnetically separated using an Invitrogen DynaMag-spin magnet, and subsequently washed 3 times with 0.1% BSA in PBS pH 7.4 to remove any non-specifically bound Ab_2 and HRP. The conjugate was then reconstituted with 100 μL of 0.1% BSA in PBS and stored at 4°C. The number of Ab_2 per magnetic particle was estimated to be 40,000 (± 5,000) using a bicinchoninic acid assay (BCA) kit.[26] In addition the amounts of HRP per magnetic particle were estimated to be 300,000 (± 27,000) following the 2,2'-Azino-bis(3-Ethylbenzthiazoline-6-Sulfonic acid (ABTS) assay.

4.3.7 On-line capture of protein analytes

The microfluidic system was used in concert with Ab_2-MP-HRP detection beads and Ab_1-decorated sensor arrays (Figure 4.2). Briefly, 40 μL of Ab_2-MP-HRP (1 mg mL^{-1} MPs) was dispersed in 120 μL of 20 mM PBS pH 7.4, loaded into a 100 μL sample loop and injected at 100 μL min^{-1} into the capture chamber. Subsequently, biomarker protein standard (5 μL of protein analyte in 5-fold diluted in calf serum) or patient sample was loaded into the sample loop and injected into the chamber. For multiplex detection, a mixture of 20 μL of the Ab_2-MP-HRP bioconjugate for each analyte was dispersed in 80 μL of PBS, loaded into the 100 μL sample loop and injected into the reaction chamber, followed by injection of a mixture of the four analytes diluted in calf serum for standard

calibrations. Once the capture chamber was filled with sample, flow was stopped for 30 mins to facilitate analyte capture (Figure 4.2B). The protein-Ab_2-MP-HRP conjugates were then washed, dispersed in PBS-Tween-20 and a valve was switched to transport them into the detection chamber. When protein-Ab_2-MP-HRP conjugates filled the detection chamber, flow was stopped for 15 mins to capture the conjugate beads on the Ab_1 modified sensor surfaces. Buffer flow was then resumed to remove any unbound conjugate from the microfluidic channel.

The 8 sensors in the array and common Pt counter and Ag/AgCl reference electrodes were connected to a CHI 1040A multipotentiostat. To generate amperometric peaks, a mixture of 1 mM hydroquinone (HQ) mediator and 0.1 mM H_2O_2 was injected into the microfluidic device through the 100 μL sample loop to activate the HRP labels. Amperometric signals were measured via the multipotentiostat with the array potential at -0.2 V vs. Ag/AgCl (0.14 M NaCl).[21] HRP on antigen-Ab_2-MP-HRP beads is activated by hydrogen peroxide to give the oxidized ferryloxy form of HRP. The electron mediator (HQ) then reduces ferryloxy-HRP, regenerating HRP. The signal is developed by the reduction of oxidized mediator (benzoquinone) at the sensor surface (Figure 4.2C).

4.3.8 Effect of blocking agent

Background signals in our assays result from a combination of direct reduction of hydrogen peroxide and NSB of the labeled bioconjugate beads on the sensors. The BSA blocking agent was employed to prevent NSB of macromolecules in the sample that may interfere with the assay, and binding of labeled-Ab_2 on non-antigen sites on the sensor. In absence of BSA, signals arising from NSB generate large background currents that can

not be differentiated from those originating from antigen-antibody binding, and are not proportional to concentration of the antigen (Figure 4.3).

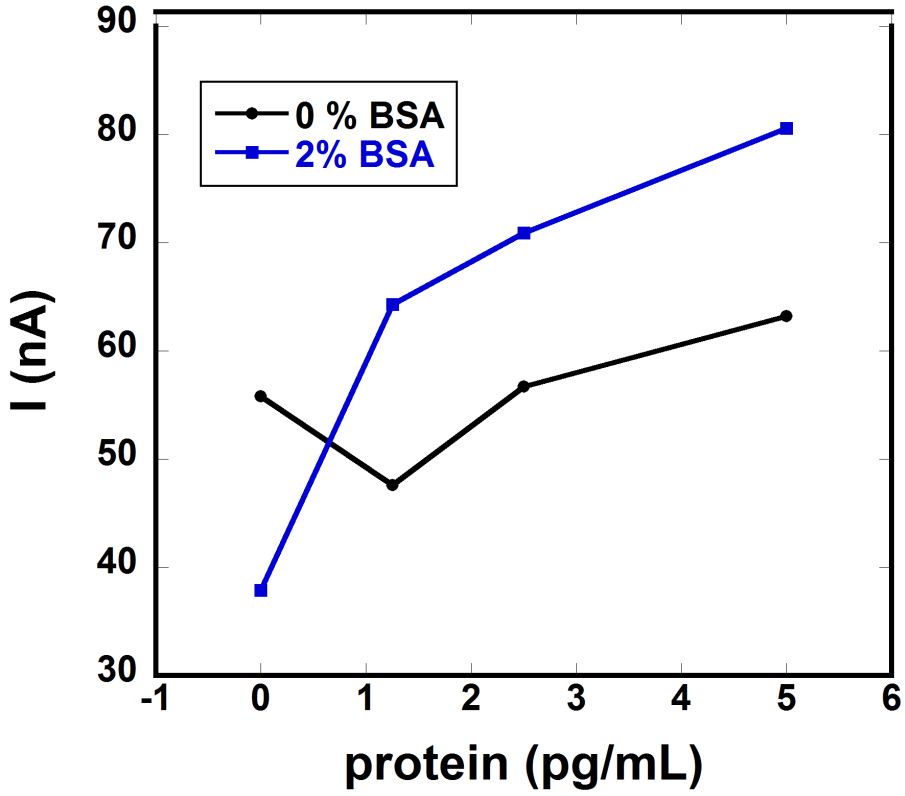

Figure 4.3 The Current response for sensors with/without 2% BSA blocking agent.

4.3.9 Optimization of Secondary Antibody

In order to establish optimal conditions for the immunoassay as well as to improve both the sensitivity and signal to noise ratio, secondary antibody concentrations were varied on the magnetic bead conjugates. Optimal secondary antibody concentrations were obtained using a consistent primary antibody (Ab_1) concentration of 100 μg/mL and employing standard concentrations of 0, 5, 10, and 50 pg mL^{-1} for IL-6, TNF-α, CRP, and IL-1β. The greatest signal difference between control and sample concentration

indicated the optimal secondary antibody concentration to be 9 μg mL^{-1} for IL-6, 20 μg mL^{-1} for TNF-α, 10 μg mL^{-1} for CRP, and 10 μg mL^{-1} for IL-1β (Figure 4.4).

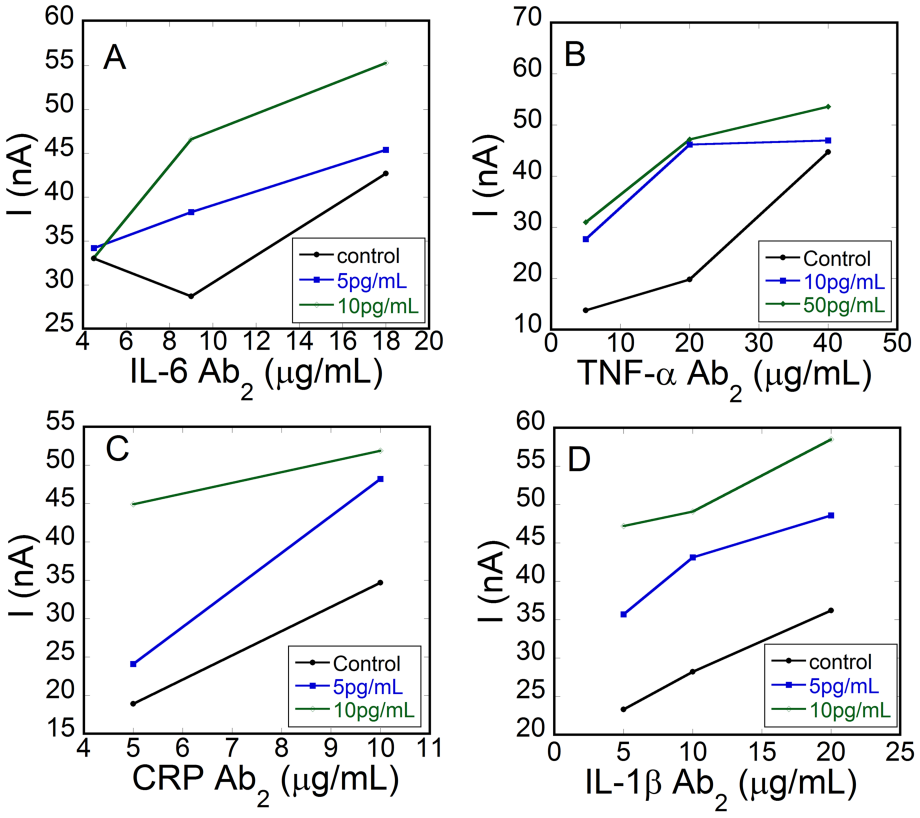

Figure 4.4 Optimization of secondary antibody (Ab_2) using a consistent primary antibody (Ab_1) concentration of 100 μg mL^{-1} and employing standard concentration of 0, 5,10, and 50 pg mL^{-1} for **(A)** IL-6, **(B)** TNF-α, **(C)** CRP, **(D)** IL-1β. Optimal concentrations were determined to be 9 μg mL^{-1} (IL-6), 20 μg mL^{-1} (TNF-α), 10 μg mL^{-1} (CRP), and 10 μg mL^{-1} (IL-1β).

4.3.10 Stability of Electrode Arrays modified with capture antibodies

The stability of the capture antibody modified arrays was investigated up to 9 days after modification and found to be stable with minimal change in the response (Figure 4.5).

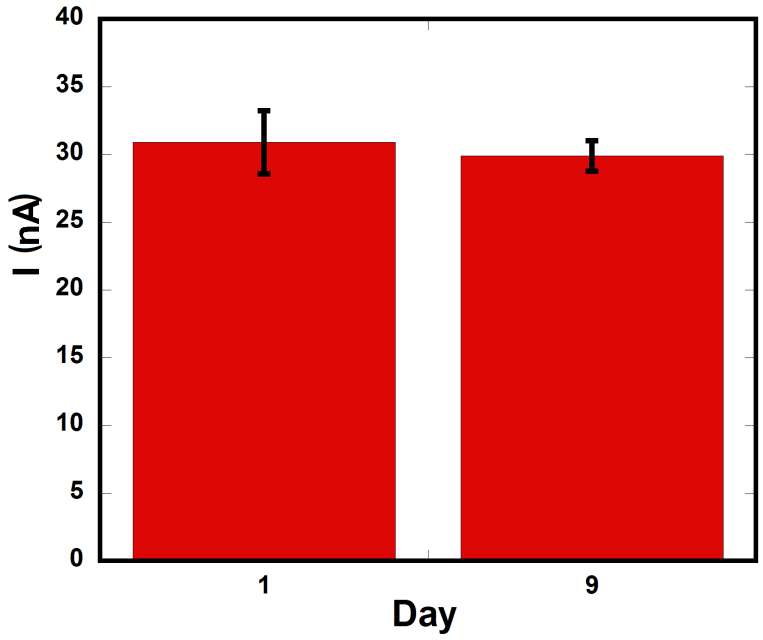

Figure 4.5 Stability of the array sensor (n=8 electrodes) modified with capture antibodies. Signal responses were measured at day 1 and day 9 with very little change.

4.3.11 Specificity of Multiplex Detection

Prior to multiplex detection, the specificity for each of the selected protein biomarkers was established on a single array for both a control, and sample (Figure 4.4). The control array featured full immunoassay procedures without protein analytes. The sample array consisted of a standard mixture of 18 fg mL^{-1} IL-6, 12 fg mL^{-1} TNF-α, 15 fg mL^{-1} CRP, and 22 fg mL^{-1} IL-1β. Current peaks for control is a combination of residual

non-specific binding from the bead conjugates (Ab_2-MP-HRP) and the direct reduction of hydrogen peroxide. Figure 4.6 demonstrates selective reproducible peaks with high signal/ noise ratios.

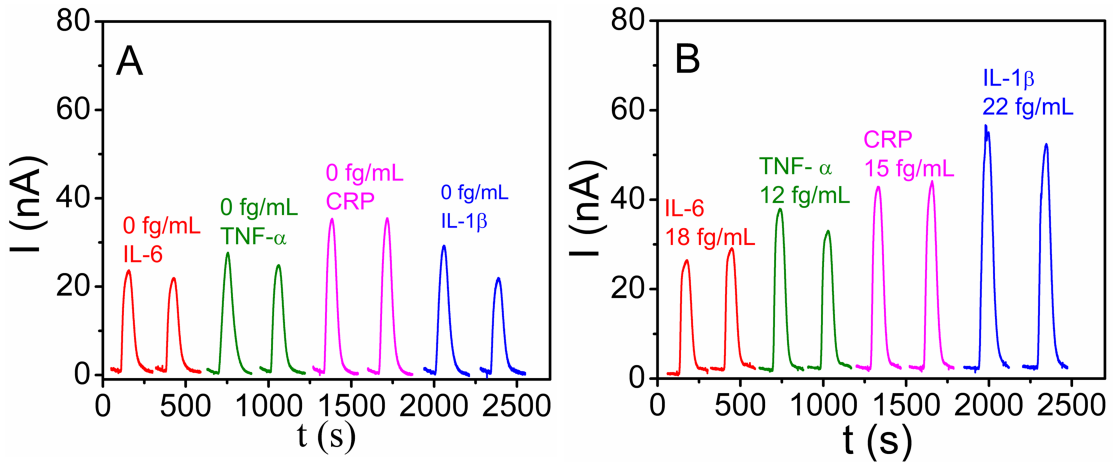

Figure 4.6 Duplicate responses measured simultaneously for (A) control mixture of 0 fg mL^{-1} for IL-6, TNF-α, CRP and IL-1β, and (B) standard mixture of 18 fg mL^{-1} IL-6, 12 fg mL^{-1} TNF-α, 15 fg mL^{-1} CRP, and 22 fg mL^{-1} IL-1β, illustrating reproducibility and selectivity.

4.4 Results

4.4.1 Single Protein Biomarker Detection

Assays were designed to accurately measure normal serum biomarker levels as well as levels in patients undergoing oral cancer therapy. Reported mean serum levels of healthy individuals for IL-6, IL-1β, and TNF-α are 10-30 pg mL^{-1}, and 30 μg mL^{-1} for

CRP.[24] Serum levels before radiation therapy in patients with oral cancer were reported to increase to 20-190 pg mL^{-1} for IL-6, IL-1β and TNF-α, and ≥30 μg mL^{-1} for CRP.[24]

The microfluidic array was first optimized separately for TNF-α, IL-6, IL-1β, and CRP in 5-fold diluted calf serum, a good surrogate for human serum.[27] Optimal surface concentrations of antibody on each Ab_2-MP-HRP conjugate were established prior to obtaining calibration curves by comparing amperomeic responses between analyte standards and controls (Figure 4.4). Control experiments featured the full immunoassay procedure without the protein analyte. Control signals result from a combination of direct reduction of hydrogen peroxide and NSB of the labeled bioconjugate beads on the sensors. To minimize NSB, 0.1% BSA was used in the preparation of the magnetic particle (MP) bioconjugates, while 2% BSA was incubated on sensors for 1 hr prior to incorporation into the microfluidic device. Further control of NSB was established by washing with PBS Tween-20 in both capture and detection chamber (See experimental).

Representative amperometric responses for single biomarker protein detection (Figure 4.7 A,C,E,G) show high sensitivity over at least 3 decades of concentration from pg mL^{-1} to the low fg mL^{-1} range. Amperometric signals were linear with respect to the log of biomarker concentration from fg mL^{-1} to low pg mL^{-1} standards with R^2 values of 0.98(±0.02) (Figure 4.7 B,D,F,H). Relative standard deviations (n=8) for single biomarkers were 8(±3)%. Detection limits measured as three times the standard deviation above that of the control were 11 fg mL^{-1} for IL-6, 6 fg mL^{-1} for TNF-α, 11 fg mL^{-1} for CRP, and 10 fg mL^{-1} for IL-1β.

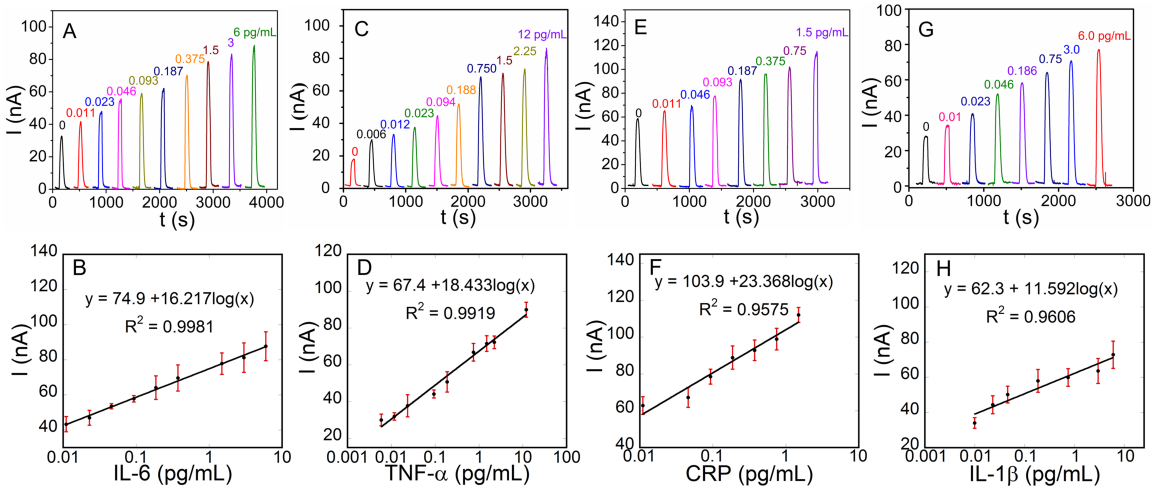

Figure 4.7 Immunoassay calibration peaks for individual biomarker proteins in 5-fold diluted calf serum for **(A)** IL-6, **(C)** TNF-α, **(E)** CRP and **(G)** IL-1β developed by injecting a mixture of 1 mM HQ and 0.1 mM H_2O_2 at -0.2 V vs. Ag/AgCl and the corresponding calibration plots for **(B)** IL-6, **(D)** TNF-α, **(F)** CRP and **(H)** IL-β.

4.4.2 Multiplex Detection of IL-6, TNF-α, CRP, and IL-1β.

Based on single protein biomarker detection described above, we progressed to simultaneous detection of all analyte proteins. Primary antibodies for each protein were attached to two of the 8-electrodes on the array. HRP-labeled magnetic beads with antibodies for IL-6, TNF-α, CRP, and IL-1β were combined, re-dispersed in PBS, and injected as a mixture into the reaction chamber, followed by injection of a mixture of the four protein standards. All steps including incubation, washing, transport to detection chamber and detection were done as described above for single proteins. Binding studies

related to the four protein analytes showed acceptably low cross-reactivity for all antibodies (Figure 4.6).

Representative amperometric responses for multiplexed detection (Figure 4.8 A,C,E,G), like those for single protein biomarker detection, demonstrate high sensitivity in the pg mL^{-1} to low fg mL^{-1} range. A linear relationship between amperometric signal and the log of biomarker concentration was found for fg mL^{-1} to low pg mL^{-1} standards with R2 values of 0.98 ($\pm$0.02) (Figure 4.8 B,D,F,G). Relative standard deviaitons were 6 ($\pm$3)%. Detection limits were 18 fg mL^{-1} for IL-6, 10 fg mL^{-1} for TNF-α, 15 fg mL^{-1} for CRP, and 40 fg mL^{-1} for IL-1β for multiplex detection. These detection limits were slightly larger than those found in single protein biomarker detection. However, the multiplexed detection limits are still 50-100 times lower than those typically obtained from standard ELISAs.

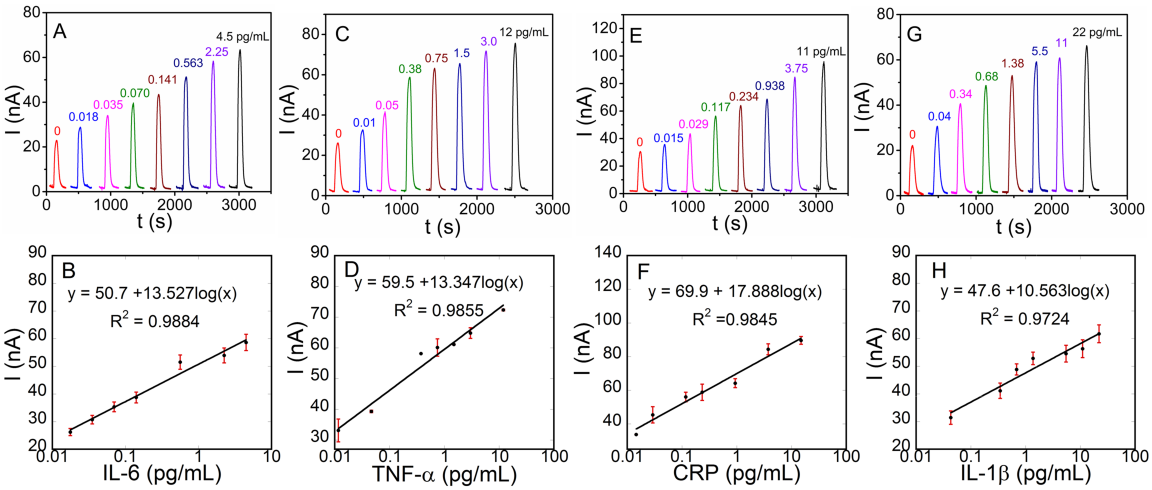

Figure 4.8 Amperometric responses for standard protein mixtures in 5-fold diluted calf serum for **(A)** IL-6, **(C)** TNF-α, **(E)** CRP, and **(G)** IL-1β, developed by injecting a mixture of 1 mM HQ and 0.1 mM H_2O_2 at -0.2 V vs. Ag/AgCl and the corresponding calibration plots for **(B)** IL-6, **(D)** TNF-α, **(F)** CRP, and **(H)** IL-β.

4.4.3 Assay validation with Human Serum Samples from H&N Cancer Patients

In order to validate accuracy, we used the microfluidic array to measure the levels of IL-6, TNF-α, and IL-1β simultaneously in ten serum samples from head and neck cancer patients undergoing radiation therapy. For patient samples CRP had to be measured separately due to its very high concentration in oral cancer patient serum.[25] For CRP, only 8 of the samples were analyzed as two of them had CRP levels well above our linear range after our standard dilution protocol, and amounts of sample were limited. In addition, CRP ELISA results were from a single sample run because of limited sample amounts. Serum samples collected on day 14 of radiation (1, 2, 3), day 35 of radiation (4,

5, 6, 7) and 21 days post-radiation (8, 9, 10) were used for these accuracy validation studies (Table 4.1).

Patient Samples	Visit	OMAS	WHO	Average Pain	Worst Pain
1	2	1.63	2	4	10
2	2	0.56	2	4	4
3	2	1.67	3	5	7
4	3	1.78	3	6	8
5	3	1	2	1	1
6	3	2.44	3	1	6
7	3	1.33	4	2	3
8	4	NA	NA	NA	NA
9	4	NA	NA	NA	NA
10	4	NA	NA	NA	NA

Table 4.1 Data on the human serum samples from H&N cancer patients undergoing radiation treatment. Visit 2 – Day 14 of radiation, Visit 3 – Day 35 of radiation, Visit 4 – 21 days post-radiation (no scales obtained at the visit). Oral Mucositis assessment scores (OMAS) showing site scoring of ulceration and erythema with maximum score of 5 (severe mucositis). World Health Organization (WHO) oral toxicity scale; 0 (no mucositis), 1 (erythema of oral mucosa and pain), 2 (Ulceration present, can eat solid foods), 3 (Ulceration present, diet limited to liquids) and 4 (Ulceration present, no alimentation possible). Pain scores (0-10 numerical scale); 0 (none) and 10 (most severe). Pain scores– average and worst pain experienced by the patient since the last visit (one score for the entire period of 1-5 days between visits).

Samples (5 μL) were diluted 30-fold in PBS prior to injection into the assay device to bring concentrations into the linear range of the calibrations. Several patient samples were spiked with different concentrations of standards to augment accuracy assessment and analytical recovery of the assay. By spiking the patient samples with 50, 100, 200, and 500 pg mL^{-1} of IL-6, TNF-α, and IL-1β standards, a wider range of concentrations of the proteins was obtained for more representative correlation plots vs. ELISA. Good correlation of our results with those obtained from standard single-protein ELISA measurements are illustrated using bar graphs (Figure 4.9).

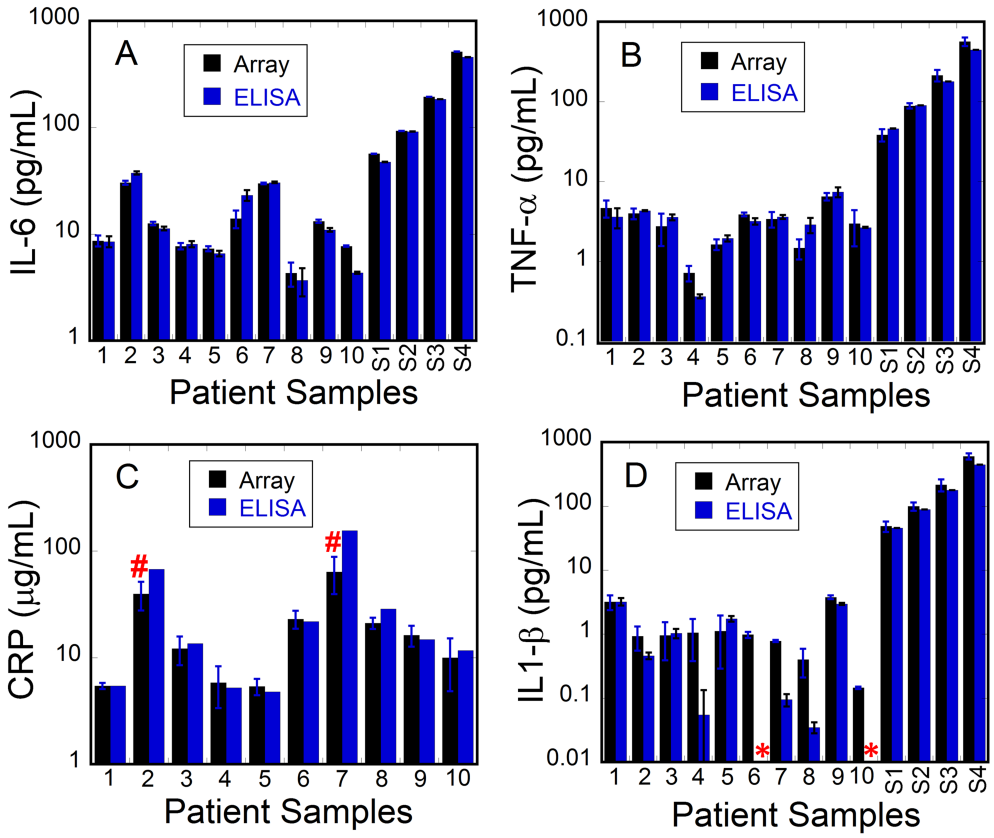

Figure 4.9 Immunoarray and ELISA assay results from serum samples of cancer patient serum for **(A)** IL-6, **(B)** TNF-α, **(C)** CRP, and **(D)** IL-1β. S1-S4 corresponds to patient samples spiked with 50, 100, 200, and 500 pg mL^{-1} respectively. (*) corresponds to values below the detection limits of ELISA and (#) corresponds to values above the dynamic range of the microfluidic immunoarray.

Correlation was also assessed by linear plots of our immunoarray results vs. single protein ELISAs. Strong correlation between two assays is indicated by slopes approaching 1.0 and intercepts near 0. For this small sample set (≤ 10), linear plots resulted in slopes and R^2-values close to 1 and intercepts near 0 for all target proteins

suggesting relatively good correlation for all the biomarker proteins (Figure 4.10, and Table 4.2). The correlation plot slope for CRP (0.78) is smaller than that of other proteins. This may be due to high levels of the protein in the μg mL^{-1} range requiring 1 million-fold serial dilutions that may generate volumetric errors, in addition to the fact that only one ELISA assay measurement for CRP was able to be obtained for each sample. Nevertheless, as with all target proteins, CRP microfluidic immunoassay results gave self-consistent values for individual samples that were similar to ELISA values for most of the samples (Figure 4.9).

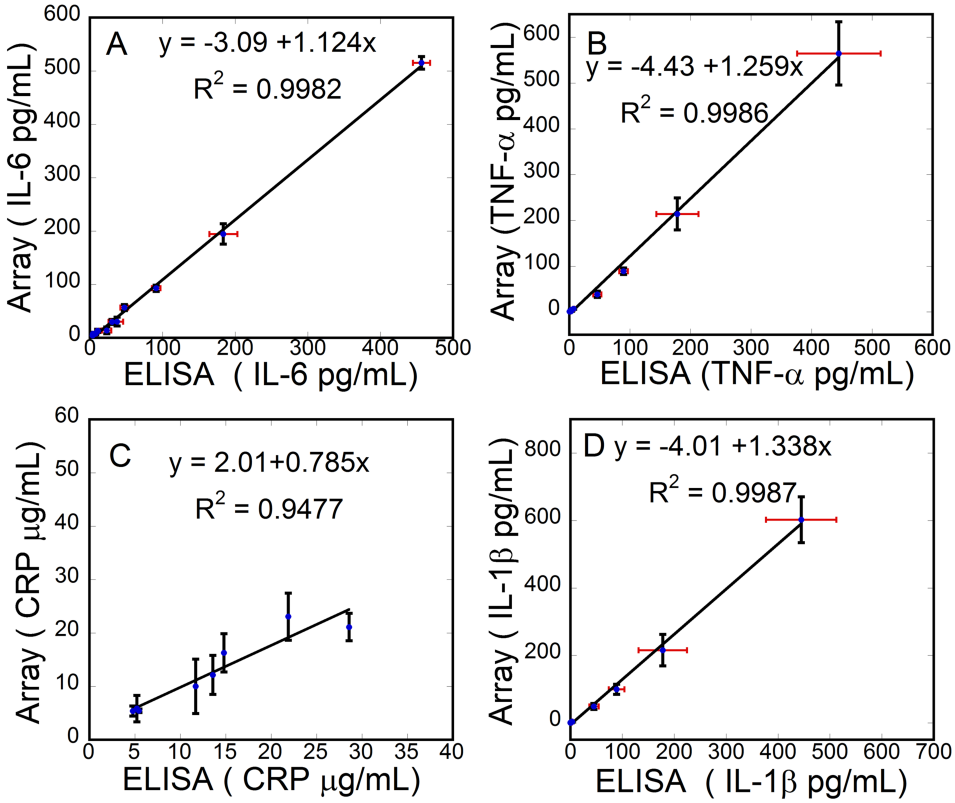

Figure 4.10 Linear correlation plots of immunoarray results against those from individual ELISAs for human serum samples from cancer patients for **(A)** IL-6, **(B)** TNF-α, **(C)** CRP, and **(D)** IL-1β. ELISA assays for CRP **(C)** represent a single trial.

Proteins	Slope	Intercept	R^2
IL-6	1.12 ± 0.014	-3.09 ± 1.84	0.998
TNF-α	1.26 ± 0.019	-4.43 ± 2.51	0.999
IL1-β	1.34 ± 0.022	-4.01 ± 3.09	0.999
CRP	0.78 ± 0.11	2.00 ± 1.67	0.948

Table 4.2 Slopes and intercepts of microfluidic immunoassay vs. ELISA correlation plots for the human serum samples from patients with H&N cancer.

4.5 Discussion

This study demonstrates the ability of the semi-automated microfluidic immunoassay to rapidly measure four relevant biomarkers for oral mucositis simultaneously. Massively labeled magnetic beads with 300,000 enzyme labels and 40,000 antibodies were employed to provide very high sensitivity. The presence of large quantities of antibodies on these beads ensures the capture of antigen proteins at concentrations much lower than those typically dictated by free antibody dissociation constants.[28,29] Detection limits of 10-40 fg mL^{-1} for 5 μL of serum (mass detection limits 2.5-10 zeptomoles) were achieved for multiplexed detection of the four proteins reaching levels far below those that can be achieved by commercial ELISA kits.[10,11,13] These detection limits are also superior to those offered by commercial multiplexed bead-based methods (Luminex, Roche, Horiba, Mesoscale Discovery, Bio-Rad) which typically range from 0.5-100 pg mL^{-1}. [10,11,13,30]

Sensitivities of immunoarray assays obtained from the slope of the calibration curves ranged from 4.18-7.07 μA mL [fg protein]$^{-1}$ cm^{-2} for multiplexed detection (Table 3). These sensitivities are comparable to those previously reported in the multiplex immunoarray detection of IL-6, IL-8, VEGF, and VEGF-C [17] without on-line sample capture. The microfluidic, on-line capture immunoarray offers an ultrasensitive, rapid, simple way to simultaneously detect panels of biomarker proteins in serum compared to commercial multiplexed bead based assays. The total assay time (30 min) and minimal sample volume requirements (5 μL) are additional factors highlighting the potential utility of these microfluidic arrays in the clinic.[10,31] Although we have optimized the present assays for ultrasensitive detection, parameters such as number of labels per bead and incubation time can be tailored for the exact clinical ranges to be measured in serum, as we have shown on an earlier version of the immunoarray without on-line capture.[19] Furthermore, the method is general and can be adapted to other small panels of protein, and even to protein biomarkers that may be present in much lower levels than in the samples analyzed here.

The overall accuracy of the assay in complex mixtures was determined by correlations between immunoarray results with those obtained by standard ELISAs for human patient serum levels. A clear advantage is the speed, sample size, and multiplicity of the immunoassays over ELISA, which requires 100 μL serum for each single protein assay.[10] The levels of the four protein biomarkers in the serum samples were comparable to those previously reported with IL-6, IL-1β and TNF-α in the pg mL^{-1} range while CRP was in μg mL^{-1} range.[24] In addition, the levels of the proteins in spiked samples demonstrate the analytical accuracy of the immunoassay with percentage recovery close

to 100%. The ability of the arrays to accurately detect individual biomarkers in serum that contains many hundreds of potentially interfering proteins demonstrates the assay's selectivity.

Preliminary correlation analysis of patient sample protein levels assayed in our work vs. standard metrics of oral mucositis severity suggested a strong correlation with IL-6, but results are inconclusive due to the limited number of samples. An ongoing related study by some of us (RVL, LAC, DEP) utilizing a wider range of samples established tentative correlations with IL-6 and CRP as biomarkers for oral mucositis (unpublished data).

Future plans include assessing larger cohorts of patient samples at varying stages of therapy. This approach may ultimately lead to accurate, low-cost, rapid estimates of projected risk of oral mucositis in cancer patients, enabling improved therapeutic management. For example, human keratinocyte growth factor-1 (palifermin) is recommended for the prevention of oral mucositis in patients receiving autologous stem cell transplants.[32] However, this treatment is expensive, requires intravenous infusion, and is typically not indicated for the patient projected to develop only mild clinical mucositis. The development of such biomarkers to accurately predict who will develop severe mucositis can enable such expensive interventions for mucositis to be selectively used in a cost-effective manner. In turn, this would facilitate optimal delivery of cancer therapy and improve patient prognosis.

4.6 References

(1) Sonis, S. T. *Nat. Rev. Cancer* **2004**, *4*, 277–284.

(2) Sonis, S. T. *J. Support. Oncol.* **2007**, *5*, 3–11.

(3) Logan, R. M.; Gibson, R. J.; Bowen, J. M.; Stringer, A. M.; Sonis, S. T.; Keefe, D. M. K. *Cancer Chemother. Pharmacol.* **2008**, *62*, 33–41.

(4) Peterson, D.; Srivastava, R.; Lalla, R. *Oral Dis.* **2013**.

(5) Sonis, S. T.; Elting, L. S.; Keefe, D.; Peterson, D. E.; Schubert, M.; Hauer-Jensen, M.; Bekele, B. N.; Raber-Durlacher, J.; Donnelly, J. P.; Rubenstein, E. B. *Cancer* **2004**, *100*, 1995–2025.

(6) Morales-Rojas, T.; Viera, N.; Morón-Medina, A.; Alvarez, C. J.; Alvarez, A. *Int. J. Paediatr. Dent.* **2012**, *22*, 191–196.

(7) Sonis, S. T.; Scherer, J.; Phelan, S.; Lucey, C. A.; Barron, J. E.; O'Donnell, K. E.; Brennan, R. J.; Pan, H.; Busse, P.; Haley, J. D. *Cell Prolif.* **2002**, *35 Suppl 1*, 93–102.

(8) Ki, Y.; Kim, W.; Nam, J.; Kim, D.; Park, D.; Kim, D. *Int. J. Radiat. Oncol. Biol. Phys.* **2009**, *75*, 393–398.

(9) Mohammed, F. F.; Poon, I.; Zhang, L.; Elliott, L.; Hodson, I. D.; Sagar, S. M.; Wright, J. *Head Neck* **2012**, *34*, 985–993.

(10) Rusling, J. F.; Kumar, C. V; Gutkind, J. S.; Patel, V. *Analyst* **2010**, *135*, 2496–2511.

(11) Apweiler, R.; Aslanidis, C.; Deufel, T.; Gerstner, A.; Hansen, J.; Hochstrasser, D.; Kellner, R.; Kubicek, M.; Lottspeich, F.; Maser, E.; Mewes, H.-W.; Meyer, H. E.; Müllner, S.; Mutter, W.; Neumaier, M.; Nollau, P.; Nothwang, H. G.; Ponten, F.; Radbruch, A.; Reinert, K.; Rothe, G.; Stockinger, H.; Tarnok, A.; Taussig, M. J.; Thiel, A.; Thiery, J.; Ueffing, M.; Valet, G.; Vandekerckhove, J.; Verhuven, W.; Wagener, C.; Wagner, O.; Schmitz, G. *Clin. Chem. Lab. Med.* **2009**, *47*, 724–744.

(12) Farrell, S.; Ronkainen-Matsuno, N. J.; Halsall, H. B.; Heineman, W. R. *Anal. Bioanal. Chem.* **2004**, *379*, 358–367.

(13) Rifai, N.; Watson, I. D.; Miller, W. G. *Clin. Chem.* **2012**, *58*, 1387–1388.

(14) Rusling, J. F. *Anal. Chem.* **2013**, *85*, 5304–5310.

(15) Ng, A. H. C.; Uddayasankar, U.; Wheeler, A. R. *Anal. Bioanal. Chem.* **2010**, *397*, 991–1007.

(16) Chikkaveeraiah, B. V; Mani, V.; Patel, V.; Gutkind, J. S.; Rusling, J. F. *Biosens. Bioelectron.* **2011**, *26*, 4477–4483.

(17) Malhotra, R.; Patel, V.; Chikkaveeraiah, B. V; Munge, B. S.; Cheong, S. C.; Zain, R. B.; Abraham, M. T.; Dey, D. K.; Gutkind, J. S.; Rusling, J. F. *Anal. Chem.* **2012**, *84*, 6249–6255.

(18) Rusling, J. F. *Chem. Rec.* **2012**, *12*, 164–176.

(19) Krause, C. E.; Otieno, B. A.; Latus, A.; Faria, R. C.; Patel, V.; Gutkind, J. S.; Rusling, J. F. *ChemistryOpen* **2013**, *2*, 141–145.

(20) Rusling, J. F.; Bishop, G. W.; Doan, N.; Papadimitrakopoulos, F. *J. Mater. Chem. B. Mater. Biol. Med.* **2014**, *2*.

(21) Otieno, B. A.; Krause, C. E.; Latus, A.; Chikkaveeraiah, B. V.; Faria, R. C.; Rusling, J. F. *Biosens. Bioelectron.* **2014**, *53*, 268–274.

(22) Peterson, D.; Keefe, D.; Sonis, S. **2012**.

(23) Brailo, V.; Vucicevic-Boras, V.; Lukac, J.; Biocina-Lukenda, D.; Zilic-Alajbeg, I.; Milenovic, A.; Balija, M. *Med. Oral Patol. Oral Cir. Bucal* **2012**, *17*, e10–e15.

(24) Jablonska, E.; Piotrowski, L.; Grabowska, Z. *Pathol. Oncol. Res.* **1997**, *3*, 126–129.

(25) Mani, V.; Chikkaveeraiah, B. V; Patel, V.; Gutkind, J. S.; Rusling, J. F. *ACS Nano* **2009**, *3*, 585–594.

(26) Smith, P. K.; Krohn, R. I.; Hermanson, G. T.; Mallia, A. K.; Gartner, F. H.; Provenzano, M. D.; Fujimoto, E. K.; Goeke, N. M.; Olson, B. J.; Klenk, D. C. *Anal. Biochem.* **1985**, *150*, 76–85.

(27) Yu, X.; Munge, B.; Patel, V.; Jensen, G.; Bhirde, A.; Gong, J. D.; Kim, S. N.; Gillespie, J.; Gutkind, J. S.; Papadimitrakopoulos, F.; Rusling, J. F. *J. Am. Chem. Soc.* **2006**, *128*, 11199–11205.

(28) Mani, V.; Wasalathanthri, D. P.; Joshi, A. A.; Kumar, C. V; Rusling, J. F. *Anal. Chem.* **2012**, *84*, 10485–10491.

(29) Chang, L.; Rissin, D. M.; Fournier, D. R.; Piech, T.; Patel, P. P.; Wilson, D. H.; Duffy, D. C. *J. Immunol. Methods* **2012**, *378*, 102–115.

(30) Chikkaveeraiah, B. V; Bhirde, A. A.; Morgan, N. Y.; Eden, H. S.; Chen, X. *ACS Nano* **2012**, *6*, 6546–6561.

(31) Gubala, V.; Harris, L. F.; Ricco, A. J.; Tan, M. X.; Williams, D. E. *Anal. Chem.* **2012**, *84*, 487–515.

(32) Lalla, R. V; Bowen, J.; Barasch, A.; Elting, L.; Epstein, J.; Keefe, D. M.; McGuire, D. B.; Migliorati, C.; Nicolatou-Galitis, O.; Peterson, D. E.; Raber-Durlacher, J. E.; Sonis, S. T.; Elad, S. *Cancer* **2014**, *120*, 1453–1461.